

Intelligent Energy Management System for a Hybrid Microgrid with Renewables and Battery Storage

Fuzzy Logic Approach



Prepared by:

Ntokozo Radebe

RDBNTO016

Prepared for:

A/Prof. Sunetra Chowdhury

Department of Electrical Engineering

University of Cape Town

May 23, 2025

Submitted to the Department of Electrical Engineering at the University of Cape Town in partial fulfilment of the academic requirements for a Bachelor of Science degree in Mechatronics Engineering

Keywords: Microgrid, Hybrid Microgrid, Intelligent Energy Management System

Declaration

1. I know that plagiarism is wrong. Plagiarism is to use another's work and pretend that it is one's own.
2. I have used the IEE convention for citation and referencing. Each contribution to, and quotation in, this report from the work(s) of other people has been attributed, and has been cited and referenced. Any section taken from an internet source has been referenced to that source.
3. This report is my own work, and is in my own words (except where I have attributed it to others).
4. I have not paid a third party to complete my work on my behalf. My use of artificial intelligence software has been limited to the following: [\[Appendix A\]](#)
5. I have not allowed and will not allow anyone to copy my work with the intention of passing it off as his or her own work.
6. I acknowledge that copying someone else's assignment or essay, or part of it, is wrong, and declare that this is my own work.

Word count: 20233



May 23, 2025

Ntokozo Radebe

Date

Acknowledgements

Let a desperate man go hunt. If he kills the elephant, his poverty ends. If the elephant kills him, his poverty ends.

—Pete Edochie

I would like to express my deepest gratitude to all those who have supported and guided me throughout this research journey. First and foremost, I extend my sincere appreciation to my supervisor, A/Prof Chowdhury, for her invaluable guidance, and insightful feedback. Her expertise and mentorship was instrumental in shaping this research. Your support has been a constant source of motivation. To my loving parents, Mr Thami Radebe and Mrs Kelebogile Radebe, thank you for your endless sacrifices, prayers, and unconditional love. Your belief in me has been my greatest strength. My brothers, Lesego and Thando, thank you for your constant encouragement and for always keeping me grounded. I am immensely grateful to my mentors, whose wisdom and advice have greatly influenced my academic and personal growth. My heartfelt thanks go to my dear friends, and soldiers, for their companionship, laughter, and moral support during both challenging and rewarding times. You have added value in academic journey and I am forever grateful. I extend my gratitude to acknowledge all individuals who contributed directly or indirectly to this research and academic journey at large. Your support has been invaluable, and I am truly grateful.

Abstract

This project investigates the development of an Intelligent Energy Management System (IEMS) for a hybrid microgrid integrating renewable energy sources (solar PV), a battery energy storage system (BESS), and the utility grid. A fuzzy logic controller (FLC) is proposed to manage power flow in both grid-connected and standalone modes while optimizing the use of renewable energy, reducing operational costs, and maintaining power quality. The system is modeled and simulated using MATLAB/Simulink. This report presents the literature framework, modeling methodology, and the proposed control architecture. The study aims to demonstrate that a fuzzy logic based EMS can provide a robust and computationally efficient solution for dynamic, multi-objective energy optimization in hybrid microgrid environments.

Abbreviations

EM Energy Management

EMS Energy Management System

IEMS Intelligent Energy Management System

FLC Fuzzy Logic Controller

PCC Point of Common Coupling

DER Distributed Energy Resources

PV Photo Voltaic

BESS Battery Energy Storage System

ESS Energy Storage System

AI Artificial Intelligent

ANN Artificial Neural Network

RL Reinforcement Learning

DL Deep Learning

ML Machine Learning

MPC Model Predictive Control

AC Alternating Current

DC Direct Current

RES Renewable Energy Sources

HRES Hybrid Renewable Energy Sources

MOGWO Multiobjective Gray Wolf Optimization Algorithm

SAGC South African Grid Code

SOC State of Charge

TOU Time Of Use

IEEE Institute of Electrical and Electronics Engineers

IEC International Electrotechnical Commission

Contents

List of Figures	ix
List of Tables	xi
1 Introduction	1
1.1 Background to the Study	1
1.2 Objectives of the Study	1
1.2.1 Problems to be Investigated	1
1.2.2 Purpose of the Study	1
1.3 Scope and Limitations	2
1.4 Plan of Development	2
2 Literature Review	3
2.1 Introduction	3
2.2 Fundamentals of Microgrids and Configurations	3
2.2.1 Definition and application of microgrids	3
2.2.2 Classification of microgrids and their applications	4
2.2.3 Definition and key components of hybrid microgrids	5
2.2.4 Role of renewable energy sources in hybrid microgrids	5
2.2.5 Importance of energy storage systems for stability and efficiency	6
2.3 Grid-connected and Standalone Microgrids	6
2.3.1 Grid-connected	6
2.3.2 Standalone	7
2.3.3 Challenges faced by grid-connected and standalone microgrids	7
2.4 Hybrid Microgrid Control	8
2.4.1 Centralized Control	9
2.4.2 Decentralized (Distributed) Control	9
2.4.3 Hierarchical Control	9
2.4.4 Impact of Control Strategies on EMS Performance	9
2.5 Energy Management Systems in Microgrids	10
2.5.1 EMS based on Classical Approaches	11
2.5.2 EMS based on Heuristic and Metaheuristic Approaches	12
2.5.3 EMS based on Intelligent Methods	13
2.5.4 Comparison of Energy Management System Approaches	14
2.6 Research-based EMS implementation in microgrid settings	14
2.6.1 Case 1: ANN based EMS	14
2.6.2 Case 2: FL based EMS	15
2.6.3 Case 3: DRL based EMS	15
2.6.4 Comparative Insights	15

2.7 Conclusion	15
3 Methodology	17
3.1 Introduction	17
3.2 Data Collection and Preparation	18
3.3 Software Selection	20
3.4 Mathematical Modeling and Sizing for a Test Microgrid	21
3.4.1 Solar PV Array	21
3.4.2 Battery Energy Storage System	21
3.4.3 Utility Grid	23
3.4.4 Energy Balance	24
3.4.5 Scenario	24
3.4.6 Sizing of The Test Microgrid Components	24
3.5 Development of Intelligent Energy Management System Design	27
3.5.1 Problem Formulation	27
3.5.2 Algorithm Flowchart Design	28
3.5.3 FLC Design	30
3.5.4 FLC Design for BESS Control	31
3.5.5 FLC Design for Operation Mode and Load Control	34
3.6 Simulation Model for Test Microgrid and IEMS	36
3.6.1 Simulation Model	36
3.6.2 Simulation Approach	38
3.6.3 Integration of Test Microgrid and IEMS	39
3.7 Case Study Development	40
3.7.1 Case 1: Base Model with no BESS and FLC	40
3.7.2 Case 2: Modified Base Case without FLC IEMS	40
3.7.3 Case 3: Operation Mode Selection on TOU with Varying Load	40
3.7.4 Case 4: Operation Mode Selection on TOU with Varying Load and Constant Load	40
4 Results and Analysis	42
4.1 Case 1: Base Case without FLC IEMS and Battery Storage	43
4.1.1 Objective	43
4.1.2 Simulation Setup	43
4.1.3 Power Flow Analysis	43
4.1.4 Power Quality Analysis	44
4.1.5 Energy Calculations	45
4.1.6 Evaluation of Base Case	46
4.2 Case 2: Modified Base Case without FLC IEMS	47
4.2.1 Objective	47
4.2.2 Simulation Setup	47
4.2.3 Power Flow Analysis	47
4.2.4 BESS SOC Dynamics	48
4.2.5 Power Quality Analysis	48
4.2.6 Energy Calculations	49
4.2.7 Evaluation of Modified Base Case	51

4.3	Case 3: Mode Selection on a TOU tariff with Varying Load	51
4.3.1	Objective	51
4.3.2	Simulation Setup	52
4.3.3	Power Flow Analysis	52
4.3.4	BESS SOC Dynamics	53
4.3.5	Power Quality Analysis	53
4.3.6	Energy Calculations	55
4.3.7	Evaluation of FLC IEMS and Summary of IEMS Function	56
4.4	Case 4: Operation Mode Selection on a TOU tariff with Varying Load and Constant Load	58
4.4.1	Objective	58
4.4.2	Simulation Setup	58
4.4.3	Power Flow Analysis	58
4.4.4	BESS SOC Dynamics	59
4.4.5	Power Quality Analysis	60
4.4.6	Energy Calculations	61
4.4.7	Evaluation of FLC IEMS Performance	62
5	Discussion	64
5.1	Summary of FLC IEMS Function	64
5.2	Comparative Performance Metrics	64
5.3	Limitations and Challenges	65
5.4	Achievement of IEMS Objectives	65
6	Conclusions	67
7	Recommendations	68
Bibliography		69
A AI Prompts Documentation		75
B Ethics Clearance		76
C Methodology Additional Content		77
C.1	Data Collections and Preparation	77
C.2	Microgrid Component Sizing	78
C.2.1	Load Data	78
C.2.2	Solar PV Data	78
C.3	FLC Design	79
C.3.1	Membership Function	79
D Results Additional Content		81
D.1	Cost of Energy Calculations	81
D.2	Case 4: Operation Mode Selection on a TOU tariff with Varying Load and Constant Load	81
E GA Table		84

List of Figures

2.1	Layout of a microgrid [1].	4
2.2	Classification of microgrids based on different characteristics [2].	4
2.3	Hybrid power supply microgrid [3].	5
2.4	Modes of operation on a microgrid [4].	7
2.5	Energy management system formulation for optimum operation of microgrid systems [5].	10
2.6	Control strategies for energy management systems in microgrids [5].	11
3.1	Overview of methodology steps.	17
3.2	Load profile.	18
3.3	Total PV generation and daily PV data.	18
3.4	Daily PV profile and irradiance.	19
3.5	IEMS proposed flowchart	29
3.6	High level structure of the fuzzy inference system [6, 7].	30
3.7	Fuzzy logic design for BESS action.	31
3.8	Input membership functions (shared with Mamdani FLC) and structure of the Sugeno FLC.	35
3.9	Utility grid simulation model.	36
3.10	Simulation models.	37
3.11	Simulation models.	37
3.12	Microgrid measurement signals.	38
3.13	Fuzzy logic simulink model.	38
3.14	Overall simulation steps and approach	38
3.15	Test microgrid with FLC integration.	39
3.16	Microgrid model with fuzzy logic.	39
4.1	Grid energy price TOU scheme.	42
4.2	Daily load profile.	42
4.3	Microgrid power profiles.	43
4.4	Microgrid frequency profile.	44
4.5	Load terminal voltage profile under varying PV generation conditions.	44
4.6	Energy profiles and calculations.	45
4.7	Grid power, TOU tariff, and utility grid cost profile.	46
4.8	Microgrid power flow profiles showing contributions from PV, BESS, grid, and loads.	47
4.9	BESS SOC profile.	48
4.10	Microgrid frequency profile.	49
4.11	Load terminal voltage profile.	49
4.12	Energy profiles and calculations for the base case.	50
4.13	Grid power, grid energy price and cost of energy profile.	51
4.14	Microgrid power profiles.	52
4.15	BESS SOC profile.	53

4.16 Microgrid frequency profile.	54
4.17 Microgrid voltage profile.	54
4.18 Energy profiles and calculations.	55
4.19 Grid power, grid energy price and cost of energy profile.	56
4.20 Power flow profiles for each microgrid component.	59
4.21 BESS SOC profile.	59
4.22 Microgrid frequency profile.	60
4.23 Load terminal voltage.	60
4.24 Energy profiles and calculations.	61
4.25 Load shed calculations.	61
4.26 Grid power, grid energy price and cost of energy profile.	62
5.1 Voltage profiles across case studies.	66
A.1 Snippet of the prompt used.	75
A.2 Snippet of the prompt used.	75
B.1 Ethics clearance outcome.	76
C.1 NASA data viewer website.	77
C.2 A triangular membership function.	80
D.1 Matlab function implementation for cost of energy calculations.	81
D.2 Cost of energy code snippet.	82
D.3 PCC and load switching signals.	82
D.4 Utility grid power profile ripples.	83
D.5 Total load and shed load profile.	83
D.6 Load shed calculations.	83

List of Tables

2.1	Consolidated advantages and limitations of microgrid control strategies	9
2.2	Consolidated comparison of classical approaches	12
2.3	Consolidated comparison of optimization approaches	12
2.4	Consolidated comparison of IEMS approaches	13
3.1	Technical Requirements for the IEMS for a hybrid microgrid with renewables and BESS	17
3.2	Comparison of Software Tools for EMS Development	20
3.3	BESS Type and chemistry	26
3.4	Defining fuzzy inputs	31
3.5	Defining fuzzy outputs	32
3.6	Fuzzy rules for BESS action	33
3.7	Optimized fuzzy rules for BESS action	34
3.8	Rules based on grid energy price, power balance, SOC, and commands	36
3.9	Optimized 6 rule Sugeno FLC	36
3.10	Case study evaluation summary	41
5.1	Performance comparison across case studies	64
C.1	Original load data from section 3.2	78
C.2	Original PV data from section 3.2	79
E.1	GA tracking table	84

Chapter 1

Introduction

1.1 Background to the Study

The global transition to sustainable and decentralized energy systems has required the development of innovative solutions for reliable and efficient power generation. In this context, microgrids, localized clusters of distributed energy resources (DERs), energy storage systems (ESS), and controllable loads have gained substantial traction as a viable alternative to conventional centralized grid systems. Hybrid microgrids, in particular, integrate renewable energy sources (RES) such as solar and wind with energy storage systems (ESS) and backup generators, enabling them to operate in both grid-connected and standalone modes. This flexibility enhances energy security, resilience, and environmental sustainability, particularly in remote or under-electrified areas.

Despite their benefits, hybrid microgrids present significant challenges in terms of energy management due to the variable nature of RES and the need for optimal coordination of diverse components, and the requirement to maintain system stability under fluctuating demand and supply conditions. These challenges require the implementation of advanced Energy Management Systems (EMS) capable of handling multi-objective optimization problems in real time. Traditional EMS approaches, while effective in some scenarios, often fall short in adaptability and computational efficiency. As such, intelligent EMS solutions, particularly those leveraging fuzzy logic offer a promising alternative. Fuzzy Logic Controller (FLC) provide a rule-based, with the intelligent fuzzy inference system, computationally efficient mechanism for handling uncertainty and non-linearity in energy systems, making them well suited for dynamic microgrid environments.

1.2 Objectives of the Study

1.2.1 Problems to be Investigated

This study investigates the following key challenges in the operation of hybrid microgrids:

- Managing energy flow and maintaining load balance during the intermittency of RES.
- Ensuring optimal utilization of renewable energy to reduce reliance on diesel generators.
- Minimizing energy costs in grid-connected scenarios by importing power from the utility grid when the electricity tariff is low.
- Maintaining voltage and frequency stability across all operational modes to ensure power quality.

1.2.2 Purpose of the Study

The purpose of this project is to design and simulate an intelligent energy management system for a hybrid microgrid incorporating RES, a diesel generator, battery storage, and the utility grid. The study adopts a fuzzy logic approach to optimize the performance of the EMS. The proposed system is evaluated on its ability to manage energy flow, ensure system stability, and reduce operational costs while maximizing the use of renewables.

1.3 Scope and Limitations

The scope of this study is limited to the modeling and simulation of a hybrid microgrid system using MATLAB/Simulink. The system components include a solar photovoltaic (PV) array, a battery energy storage system (BESS), and a utility grid interface. A fuzzy logic based EMS is designed to control power flow between these components under both grid-connected and standalone operating conditions. Real-world implementation and hardware testing are beyond the scope of this work. Additionally, the system is assessed under predefined load profiles and weather data, which may not capture the full variability of real-world scenarios. The sizing of components is influenced by the load and not fully optimized. Furthermore, due to project being time bound, only one intelligent algorithm was designed and tested, which constraints the depth of analysis and test that could be performed on the system.

1.4 Plan of Development

This report is organized into the following chapters:

- Chapter 2, literature review presents a detailed literature review on microgrid technologies, energy management strategies, control architectures, and the role of intelligent methods such as fuzzy logic in EMS design.
- Chapter 3, methodology outlines the methodology used to develop the hybrid microgrid model and the fuzzy logic-based EMS, including component sizing, mathematical modeling, and simulation procedures.
- Chapter 4, results and analysis analyzes the results and performance analysis of the proposed system under different operating scenarios.
- Chapter 5, discussions highlights the outcome of the results, and compares results across all cases and draw conclusions about the performance of the fuzzy logic IEMS.
- Chapter 6 and 7, conclusion and recommendations summarizes the key findings, draws conclusions based on the results, and offer recommendations for future work to improve the design of fuzzy logic controller for an intelligent energy management system.

state the limitations such as training, time, and expert knowledge of the system.

Chapter 2

Literature Review

2.1 Introduction

The increasing global demand for sustainable and efficient energy solutions has led to the widespread adoption of microgrids as a viable alternative to conventional power distribution systems. A microgrid concept is an innovative approach for integrating hybrid and renewable energy sources and energy storage systems into the utility grid, offer enhanced energy security, resilience, and cost-effectiveness [8]. However, managing these systems efficiently requires advanced energy management strategies that optimize power generation, storage, and consumption while ensuring stability and reliability.

This literature review explores the fundamental concepts, configurations, and control strategies of microgrids, with a particular focus on hybrid microgrid systems that integrate renewable energy sources with battery storage. The discussion includes a comparative analysis of energy management system (EMS) approaches, ranging from classical optimization techniques to intelligence based strategies. Additionally, case studies and real-world implementations are examined to highlight the practical applications and challenges associated with intelligent EMS in microgrids.

By analyzing existing research, this review aims to identify gaps in current methodologies and emerging trends in microgrid energy management. Furthermore, it outlines opportunities for future research, particularly in AI-driven EMS, to enhance cost-effectiveness, efficiency, and energy security in hybrid microgrid systems. The findings presented in this review contribute to the ongoing efforts to develop intelligent and adaptive energy management solutions that support the transition to a more sustainable and resilient energy infrastructure.

2.2 Fundamentals of Microgrids and Configurations

2.2.1 Definition and application of microgrids

Microgrids (MG) are a group of loads and distributed energy sources (DERs) that operate within specified electrical boundaries functioning as a single unit, often handling energy generation and distribution on a small scale [9]. A key characteristic of microgrids is their ability to maintain stable power supply by seamlessly disconnecting and reconnecting energy sources and loads with minimal disruption to the system [9]. This flexibility enables microgrids to effectively balance local energy supply and demand, additionally, enhancing energy resilience by ensuring a reliable power supply even during power outages of the main grid [9].

A microgrid consists of various components including power generation units, both renewable (solar and wind) and non-renewable (diesel generator), storage units (battery and supercapacitor), power electronic converters , energy consumption loads (linear and non-linear loads), and control unit, all operating within a network [9, 1]. These components are then connected to the utility grid at the point of common coupling (PCC) via a breaker which helps to operate the microgrid in both gird-connected and standalone mode [9, 1]. [Figure 2.1](#) shows a layout of a microgrid components.

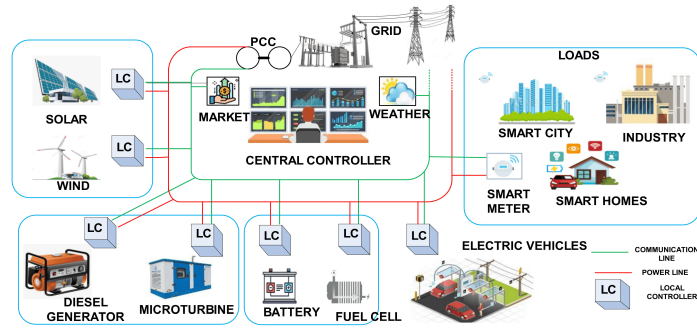


Figure 2.1: Layout of a microgrid [1].

2.2.2 Classification of microgrids and their applications

The authors in [9] present the classification of microgrids according to various criteria including operating modes, power capacity, type, source, and scenario [9]. Figure 2.2 illustrates the overall classification of microgrids based on various characteristics, ranging from size, source type, mode of operation and the scenario.

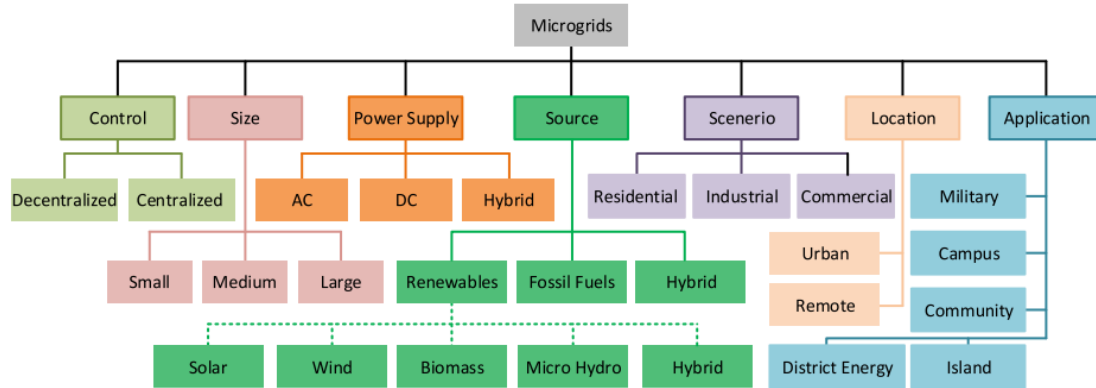


Figure 2.2: Classification of microgrids based on different characteristics [2].

The term hybrid in the microgrid literature can refer to three distinct categories in microgrid classification. In the context of power supply classification, hybrid describes a microgrid that incorporates both AC and DC buses and components [9]. This contrasts with purely AC microgrids, which have traditionally dominated power distribution systems, or purely DC microgrids, which have gained attention for their compatibility with renewable sources and modern electronic loads. Hybrid AC/DC architectures aim to leverage the advantages of both systems while minimizing conversion losses [10].

In terms of operational mode, hybrid refers to microgrids capable of operating in both grid-connected and standalone modes. Unlike microgrids designed exclusively for grid-tied operation or those built specifically for isolated operation, hybrid mode microgrids incorporate control systems and power electronics that allow seamless transition between these states, enhancing resilience while maintaining the benefits of grid connection [9].

In the classification of microgrid in the basis of source, hybrid indicates the integration of multiple types of energy resources. While some microgrids may rely on a single generation technology (solar only or wind only systems), hybrid resource microgrids combine different renewable sources such as solar, wind, biomass, and BESS, often with conventional generation and energy storage systems, to overcome the intermittency limitations of individual renewable technologies [2].

The term highlights the importance of precise terminology when discussing microgrid configurations and

emphasizes the need for clear specification when referencing hybrid aspects in energy management system design. In the context of this project, it will refer to the two categories, namely the hybrid mode of operation, and source.

2.2.3 Definition and key components of hybrid microgrids

Hybrid microgrids, which integrate renewable energy sources (RESs) with diesel generator sets and energy storage technologies, play a crucial role in delivering clean and cost-effective electricity to remote locations with limited or no access to reliable utility power systems [11]. These hybrid systems can incorporate multiple parallel distributed energy resources (DERs) capable of operating in both standalone and grid-connected modes [11]. The advantages of such configurations include enhanced environmental performance, increased system resiliency, and improved reliability, furthermore, hybrid microgrids ensure an uninterrupted power supply for critical loads while optimizing customer satisfaction by offering autonomy, safety, and security at a reduced operational cost [11].

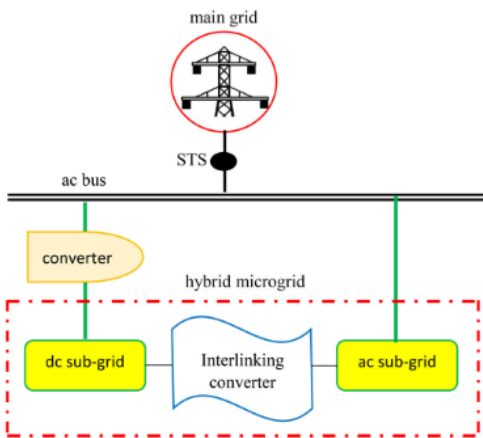


Figure 2.3: Hybrid power supply microgrid [3].

Shahgholian et al. [3] summarizes that a flexible microgrid must be capable of importing and exporting energy into and from the grid while regulating active and reactive power flows through effective energy storage management [3]. The configuration of a hybrid microgrid integrates a static transfer switch (STS) to establish a connection with the main grid [3]. As illustrated in Figure 2.3, the power exchange between the microgrid and the utility grid is regulated by a power electronic converter interface [3]. The flow of power is determined by the balance between energy generation and consumption [3]. Hybrid microgrids are designed to improve overall network efficiency by minimizing power conversion stages, improving reliability, reducing interfacing components, and lowering energy costs [9, 3].

2.2.4 Role of renewable energy sources in hybrid microgrids

Renewable energy sources (RES) contribute significantly to supplying some of the world's energy demands. 'According to the IEA forecast, renewable energy is expected to grow by approximately 2400 GW between 2022 and 2027' [2, p. 3]. Adding to that, the authors in [12] mention, 'Renewable energies will account for over 50% of electricity production worldwide by 2025' [12, p. 1].

Renewable energy sources, particularly solar and wind power, play a crucial role in hybrid microgrids by addressing the challenges of energy sustainability and mitigating the intermittency issues inherent to individual renewable sources [13]. The integration of solar and wind power in hybrid renewable energy systems (HRES)

enhances the overall reliability and stability of energy generation. These systems can significantly contribute to grid stability by managing frequency and voltage fluctuations caused by the intermittent nature of standalone renewable sources. Surplus energy can be injected into the grid during peak demand periods, enhancing grid stability and reducing congestion [13]. It is therefore evident that the deployment of HRES, incorporating solar and wind power, holds immense potential to reshape the global energy landscape. By providing a more consistent and reliable energy supply, these systems support the transition towards cleaner energy and contribute to the mitigation of climate change impacts. The integration of renewable energy sources in hybrid microgrids is essential for achieving a sustainable and efficient energy future.

2.2.5 Importance of energy storage systems for stability and efficiency

The importance and functionality of the Energy Storage System (ESS) in a microgrid architecture is discussed in the study by [11]. The authors in [11] explain that the ESS is crucial for the efficient operation of a microgrid. It ensures that excess energy produced can be stored and used when needed, thus balancing supply and demand. By providing peak shaving, the ESS reduces the strain on the grid during high demand periods, which can lower grid connection costs and alleviate technical constraints [11]. Additionally, the ESS stores energy produced during favorable conditions, preventing waste and reducing costs associated with energy introduction to the main grid. Effective management of energy fluxes through a controller is essential to maximize these benefits, and the research aims to develop optimal algorithms for this purpose [11]. Rai et. al[14] proposes that to limit renewable energy intermittent and grid instability, future research should work on innovative approaches for integrating ESS into microgrids [14]. The innovative approaches can be in the field of advanced ESS management systems, alternative storage technologies, and optimizing sizing and location as mentioned by [14].

The integration of Renewable Energy Sources (RES) such as solar and wind power with Energy Storage Systems (ESS) is vital for advancing sustainable energy solutions. RES address energy sustainability challenges and reduce climate impacts, while ESS enhance grid stability by storing excess energy, balancing supply and demand, and managing intermittency issues. Together, they create reliable and efficient hybrid microgrid systems, supporting the transition to cleaner energy and reshaping the global energy landscape.

2.3 Grid-connected and Standalone Microgrids

The topology of a microgrid is essential for determining its efficiency, stability, and ability to integrate with other energy systems. Interconnection and operation mode influence the overall performance of a microgrid. Microgrids can operate in two modes, namely, grid-connected mode and standalone mode:

2.3.1 Grid-connected

In this mode, the microgrid follows utility rules and manage power flow without being the main power supplier. This approach ensures continuous and stable electric power system operation [15]. Additionally, in this mode, the microgrid can export excess power to the main grid or draw power from it as needed. Consequently, microgrids must have the capability to control fluctuations in active and reactive power flows while monitoring the state of energy storage systems [15, 16]. As a result, in the grid-connected mode, the microgrid is synchronized with the primary electrical grid, establishing a directional energy exchange [15, 17, 18]. The grid-connected microgrid setup enhances system stability and demand management by using the primary grid as a backup during fluctuations in local generation or demand [17].

2.3.2 Standalone

In standalone operation, the microgrid functions autonomously and must have sufficient power capability to meet the total load demand, ensuring reliability and security of local loads. During standalone transition, disturbances may occur that require individual feeders to operate separately, leading to inaccurate power sharing due to unbalanced feeder impedances [15]. Local loads within the microgrid are sensitive to voltage variations, necessitating adequate local generation to maintain stable operation [15]. To achieve successful standalone operation, the microgrid scheduling of distributed generators must ensure enough local generation to meet the demands of sensitive loads, while these loads rely on the utility supply [15, 19]. This setup provides significant advantages to the microgrid concept, offering greater flexibility in handling disturbances and emergency conditions, thereby enhancing system reliability and ensuring the security of local loads [15]. Benefits of standalone mode operation include mitigating overload issues in the electric supply stem, minimizing operating and energy costs, resolving power quality problems, and facilitating maintenance operations on power system components without disrupting the service to end-user [15, 19, 20].

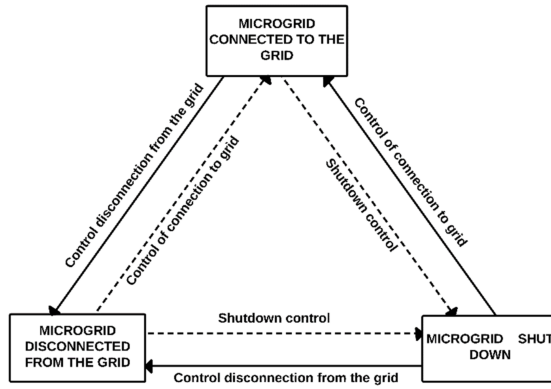


Figure 2.4: Modes of operation on a microgrid [4].

Contrary to what was mentioned in [15, 16, 17, 18, 19], the authors in [4] review that there are three modes of operation for microgrids to ensure stability, cost-efficiency and security [4]. The first mode is connected to the electrical power system (EPS), which enhances stability and reduces electricity costs. The second mode is disconnected from the EPS, allowing the microgrid to operate independently and supply loads in emergency or standalone mode. The third mode is microgrid shutdown, activated as a security measure to prevent damage to network elements. These modes are controlled by three mechanisms: disconnection from the EPS, connection to the EPS, and shutdown control, as illustrated in Figure 2.4. As proposed by [4], understanding these operation modes and their control mechanisms is crucial for managing microgrids effectively, ensuring optimal performance, cost savings, and protection of the microgrid infrastructure.

2.3.3 Challenges faced by grid-connected and standalone microgrids

Microgrids present technical challenges despite having many advantages compared to conventional utility grids [9]. Pravat et al. [9] describes the challenge of transitioning from grid-connected to standalone mode, that in case of any fault or grid failure, the microgrid must be capable to switch from grid-connected to standalone mode without affecting its stability[9].

Further to the challenge presented by [9], [21] describes a similar challenge and propose a solution. An key advantage of standalone microgrid is the ability to use renewable energy sources in areas where traditional power transmission is difficult, hence voltage and frequency management become a main issue due to the standalone

mode lacking the stability provided by the utility grid [21]. The solution to this challenge is by using an ESS along with an isolation inverter controller scheme, as the integrated control addresses the need for voltage and frequency regulation, enhancing energy storage efficiency and power quality control in a standalone microgrid [21].

Additionally, Andishgar et al. [22] investigates the microgrid stability during standalone mode, examining the impact of different loading environments on system performance. The study proposes an active damping controller with virtual resistance to enhance stability [22]. Furthermore, it demonstrates the effectiveness of frequency control using an internal oscillator and voltage feedback-based signals to regulate standalone mode voltage in Voltage Source Converters (VSCs) [22]. These strategies play a crucial role in mitigating instability issues when transitioning from grid-connected to standalone operation [22].

Uddin et al. [2] explains an operational issue in microgrids having to do with system security [2]. To keep the system secure, contingency planning and emergency actions (such as demand-side management, load shedding, standalone, or unit shutdown) are needed. [2] further explains that under contingency scenarios, generation should be rescheduled economically to accommodate system loading and load-end voltage/frequency, consequently, system security should be maintained in a microgrid through emergency operations and contingency planning, such as load shedding, distributed source management, standalone, and unit shutdown [2].

For the grid-connected mode, the literature identifies virtual inertia deficiency in power electronic interfaces and uncontrolled power flow fluctuations at the PCC as primary concerns. However, this analysis is underexplored, missing critical issues like grid synchronization complexities, economic dispatch coordination, and bidirectional power flow management. The focus on virtual inertia represents only one aspect of broader grid integration challenges.

In standalone mode, voltage and frequency regulation without utility grid stability emerges as the most critical challenge, alongside power balance management and system stability under variable loading conditions. The literature proposes control solutions including ESS integration, virtual resistance damping, and internal oscillator frequency control. However, there's overemphasis on control systems while neglecting energy storage economics, renewable intermittency management beyond basic storage, and load prioritization strategies during generation shortfalls.

The presented approach is predominantly reactive, focusing on emergency actions like load shedding and generation rescheduling. This lacks proactive strategies such as predictive analytics and preventive control measures, while missing coverage of communication failures and cyber-physical security threats.

The literature demonstrates a fragmented approach, treating challenges as isolated technical problems rather than interconnected system-level issues. While proposed solutions (virtual resistance damping, BESS integration) address specific technical concerns, there's insufficient discussion of comparative effectiveness, implementation costs, and real-world validation.

2.4 Hybrid Microgrid Control

Effective energy management in hybrid microgrids requires robust control strategies to maintain system stability, optimize power distribution, and enhance overall efficiency. To ensure stable voltage and frequency synchronization with the utility grid during fault conditions, various control strategies have been applied to both AC and DC microgrids independently [23]. Moreover, control strategies influence EMS by determining how power sources,

ESS, and loads interact under varying operational conditions [23]. The three main control architectures, centralized, decentralized, and hierarchical play crucial roles in EMS implementation. [5].

2.4.1 Centralized Control

Centralized control uses a single central controller with a high-performance computing and a secure communication infrastructure to manage various components of the system such as RESs and ESSs, ensuring optimal energy dispatch and real-time coordination of RESs and ESSs and loads [5].

2.4.2 Decentralized (Distributed) Control

Decentralized control distributes decision-making among local controllers, which use local measurements such as frequency and voltage values to elect the leader entity, and can share information with neighbors [5]. Each local controller operates individually on a microgrid component without the central control [5].

2.4.3 Hierarchical Control

Hierarchical control integrates centralized and decentralized strategies, offering a structured approach for EMS operation through three levels: primary level regulating voltage and frequency stability, ensuring real-time energy balancing; secondary level correcting deviations from optimal operating conditions and enhancing power quality; last tertiary level managing energy market participation, ensuring cost-effective energy dispatch and optimized grid interaction [5, 24]

Table 2.1 consolidates the microgrid control architectures, advantages and limitations.

Table 2.1: Consolidated advantages and limitations of microgrid control strategies.

Control	Application	Advantages	Limitations	Ref.
Centralized	Small size microgrids	<ul style="list-style-type: none"> Strong controllability and real-time observability of the whole microgrid Simple system supervision and wide control of the whole grid 	<ul style="list-style-type: none"> Failure of central controller affects the entire system High communication infrastructure costs Lacks scalability, and may not efficiently support plug-and-play functionalities 	[5, 24]
Decentralized	Battery storage system	<ul style="list-style-type: none"> Distributed processing improves reliability High redundancy and fault tolerance Improved privacy and minimized computational demands 	<ul style="list-style-type: none"> Incomplete information about microgrid status Requires effective synchronization and strong communication to achieve synchronicity Challenges in global optimization and synchronization among distributed entities, such as limited information exchange, load dependency issues, and harmonics 	[5, 24]
Hierarchical	Complex modern system	<ul style="list-style-type: none"> Combines previous control structures, optimal decision is possible Voltage and current are regulated locally by the source converters Ensures synchronous generators maintain consistent frequency across the grid, enhancing controller coordination Efficiently dispatches operational constraints across different levels, reducing processing time 	<ul style="list-style-type: none"> Requires advanced coordination mechanisms Fewer computational burdens, but increased system complexity Distributed generators are tasked with voltage regulation and frequency control, adding complexity to operational coordination 	[5, 24]

2.4.4 Impact of Control Strategies on EMS Performance

The choice of control strategy significantly affects EMS efficiency, reliability, and adaptability. Centralized control is optimal for small microgrids requiring high precision but lacks scalability. Decentralized control enhances

resilience and scalability but may lead to suboptimal global energy coordination. Hierarchical control provides a balanced approach, enabling EMS to operate efficiently across different layers of microgrid management.

Future EMS advancements will integrate artificial intelligence (AI) and machine learning (ML) into these control frameworks, improving adaptability, predictive maintenance, and self-healing capabilities in microgrid operations.

2.5 Energy Management Systems in Microgrids

In the evolving landscape of energy systems, EMS play a pivotal role in ensuring optimal operation and sustainability. According to the International Electrotechnical Commission (IEC) standard 61970, an EMS is defined as “a computer system comprising a software platform providing basic support services and a set of applications providing the functionality needed for the effective operation of electrical generation and transmission facilities to assure adequate security of energy supply at minimum cost” [23]. This definition underscores the role of EMS in enhancing grid stability and optimizing the integration of renewable energy sources. In hybrid AC/DC microgrids, EMS is particularly crucial for balancing power flow between photovoltaic (PV) and wind energy systems, reducing operational costs, and ensuring sustainable energy utilization [23, 25]. As renewable energy adoption increases, EMS will become an essential component in achieving energy efficiency and reliability in modern power networks [23].

Simulation-based energy management (EM) employs a variety of methodologies, such as commercial software solutions, traditional techniques, rule-based systems, optimization algorithms, artificial intelligence (AI) approaches, and hybrid methods [24]. These strategies are used to model, analyze, and optimize EM processes across different contexts, providing valuable insights into system behavior, performance, and efficiency [24]. Commercial software applications play a crucial role in energy management by offering functionalities like control strategies, simulation and technical analysis, economic optimization, and multi-objective optimization [24].

Similar to what [23] and [24] proposed, when one or more energy sources in a microgrid system are deployed, there is a need for efficient control strategies for managing energy flow [5]. As a result the development of energy management systems is required. Elmouatamid et. al [5] mentions that optimization techniques are needed to achieve different energy management system objectives and satisfy multiple constraints, as illustrated in Figure 2.5.

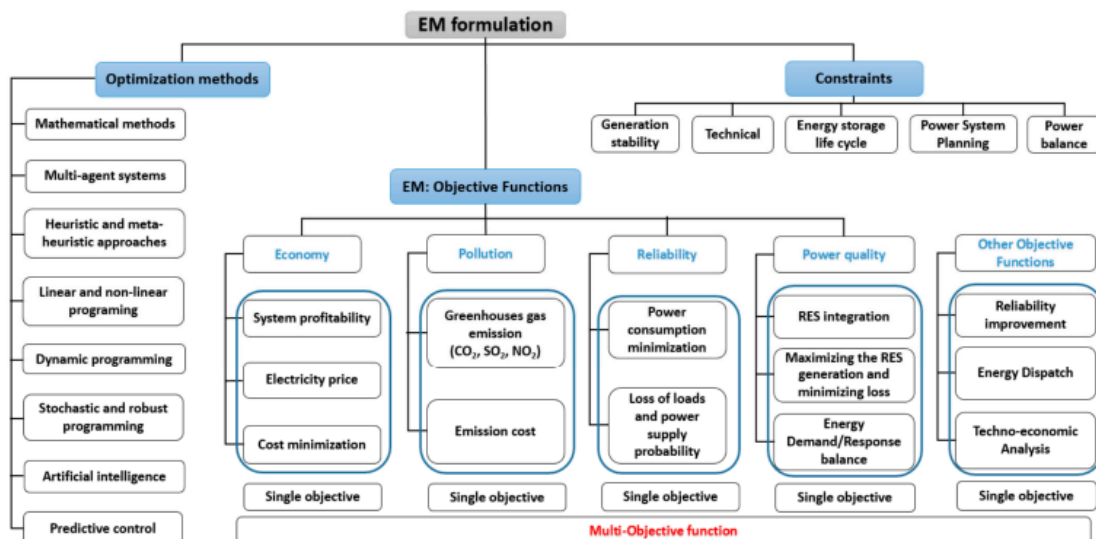


Figure 2.5: Energy management system formulation for optimum operation of microgrid systems [5].

The deployment of energy management control strategies specifies the main objective functions, which could be related to the operational cost, pollution, reliability, and power quality, for instance, the main aim of using economic objective functions is to minimize the electricity price [5]. This relates to the project scope of achieving cost-effectiveness in the operation of microgrids under grid-connected and standalone mode of operation.

DC microgrids improve energy efficiency by reducing power conversion stages and integrating power electronics interfaces effectively. According to [26], these systems minimize power losses and simplify converter control structures, leading to improved overall efficiency. By enabling direct power transfer between energy sources, storage systems, and loads, DC microgrids reduce complexity while optimizing performance [26]. However, challenges such as frequency and reactive power control persist, requiring advanced management strategies. To maintain system stability and ensure energy balance, an EMS is necessary [26]. The EMS plays a crucial role in evaluating power balance and regulating energy fluctuations, thereby enhancing the reliability and efficiency of DC microgrids, as a result a proper EMS is essential for energy system management, monitoring, and control purposes [26].

In addition to what [26] proposed, the authors in [5] conducted extensive research on microgrid control, considering various system topologies, structures, and operational modes, for instance, optimization and control techniques should address the variability of RES by ensuring a stable power supply to consumers while maintaining the storage system, electricity costs, and occupant comfort within acceptable operating conditions [5]. Figure 2.6 illustrates a proposed classification of commonly used microgrid control methods.

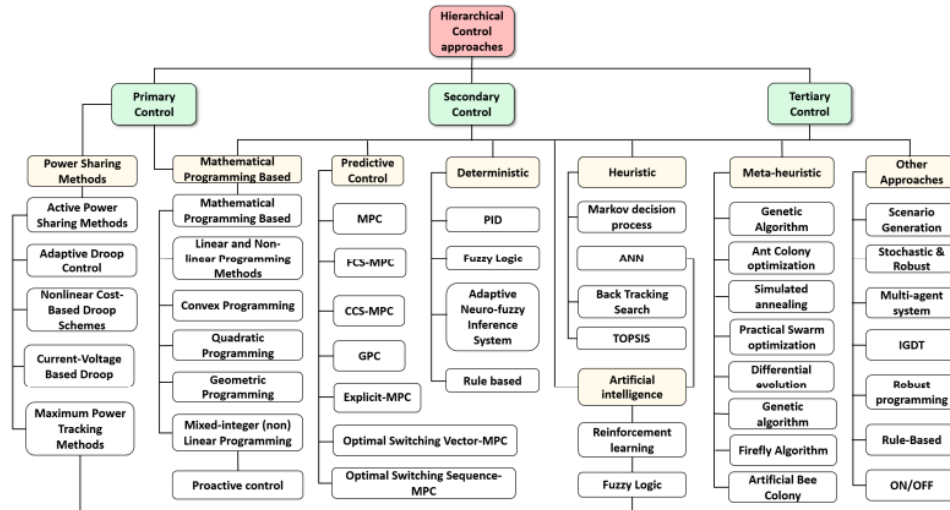


Figure 2.6: Control strategies for energy management systems in microgrids [5].

This section will discuss the main three relevant energy management approaches:

2.5.1 EMS based on Classical Approaches

Classical approaches in EMS for microgrids are efficient for controlling microgrid systems according to specified objectives and constraints [5]. In microgrids, continuous variables such as power generation or exchange with the grid form non-integer values, whereas the state of microgrid components such as grid-connected/standalone mode and ESS charging/discharging states, among other states, can be formulated as binary or integer variables [27]. These classical methods are powerful tools for system analysis and optimization, making them suitable for managing distributed generation and microgrid systems [5]. The classical approaches mainly concentrate on optimizing the energy resources and transmission with the mother grid [28].

Table 2.2 presents the consolidates descriptions, applications, advantages and disadvantages of the Classical EMS algorithms (control approach).

Table 2.2: Consolidated comparison of classical approaches.

Approach	Description	Application	Advantage	Disadvantage
Rule based [29]	<ul style="list-style-type: none"> Optimizes the operation of a grid-connected microgrid. It follows if-then-else rules to assign values to binary variables in the hybrid model of the microgrid, such as the ON/OFF status of generators and the charging/discharging modes of batteries 	<ul style="list-style-type: none"> Enhancing the energy management of a grid-connected microgrid comprised of renewable energy sources, loads, and ESS 	<ul style="list-style-type: none"> Ensures no performance loss by offering a sizable decrease in computation time 	<ul style="list-style-type: none"> Rule based lack adaptability to changing conditions and might not provide optimum solutions; they are limited by the complexity of capturing all system dynamics and interactions
Non-Linear Programming Method (NLP) [30]	<ul style="list-style-type: none"> An advanced optimization technique used to manage and control the energy flow within a microgrid 	<ul style="list-style-type: none"> Minimization of the system losses in the DC microgrid 	<ul style="list-style-type: none"> Minimizes both distribution and converter losses for better system performance 	<ul style="list-style-type: none"> NLP can be computationally expensive and may not always guarantee finding the global optimum
Mixed Integer Programming (MIP) [31]	<ul style="list-style-type: none"> This method coordinates networked microgrids, Distributed Energy Resources (DERs), and controllable loads that interface directly with utilities in a distributed manner 	<ul style="list-style-type: none"> Aimed at distributed energy management for modern distribution systems embedded in networked microgrids 	<ul style="list-style-type: none"> Minimizes total system operating costs Encourages active participation from all participants while preserving their autonomy 	<ul style="list-style-type: none"> Requires handling the inherent intermittency and uncertainty of loads and renewable sources under the proposed distributed framework.

2.5.2 EMS based on Heuristic and Metaheuristic Approaches

Heuristic and metaheuristic approaches, widely applied in telecommunications and transportation, are increasingly used in microgrid EMS. Heuristic optimization employs exploratory methods to solve optimization problems efficiently within reasonable timeframes, though without guaranteeing optimal solutions [5]. Metaheuristic approaches are efficient and popular for microgrid control and energy management, often combined with other control methods to enhance performance [5]. These approaches utilize randomization and local search procedures for optimization and global search pathways [32]. Most optimization algorithms are population-based, maintaining entire solution sets where each solution represents a distinct search space point, continuously updated toward near-optimal solutions [32]. **Table 2.3** presents a comparative analysis of commonly used optimization approaches in microgrid EMS.

Table 2.3: Consolidated comparison of optimization approaches.

Approach	Description	Objective	Benefits	Setbacks
Particle swarm optimization (PSO) [21, 32]	<ul style="list-style-type: none"> Uses the characteristics and movement of a group of bird or fish to search for food, identifies the optimal solution to a formulated problem through iterative process; Significantly reducing energy costs and emissions into the environment 	<ul style="list-style-type: none"> Power and comfort level optimization <ul style="list-style-type: none"> Optimize energy prices, and energy transfer to the utility grid 	<ul style="list-style-type: none"> Requires fewer parameters to adjust Simple execution with higher efficiency and fast convergence Hard to define the initial design parameters 	<ul style="list-style-type: none"> Can converge prematurely <ul style="list-style-type: none"> PSO can limit its ability to find the best solutions in the microgrid applications with highly nonlinear and multi-objective objectives

Ant colony optimization (ACO) [32]	<ul style="list-style-type: none"> Inspired by the behavior of ants, which use pheromone trails for communication and to identify the most frequently traveled paths, often leading to optimal solutions. 	<ul style="list-style-type: none"> Energy consumption optimization 	<ul style="list-style-type: none"> Adaptability to changes in new solutions 	<ul style="list-style-type: none"> Requires in-depth theoretical understanding and complex mathematical modeling, which can complicate implementation and analysis Probability distribution changes by iteration
Artificial bee colony (ABC) [32]	<ul style="list-style-type: none"> Based on the natural foraging act of honey bees, can be integrated with other optimization techniques to develop a hybrid system 	<ul style="list-style-type: none"> Energy efficiency 	<ul style="list-style-type: none"> Needs a few control parameters Has both exploration and exploitation capability 	<ul style="list-style-type: none"> Search space is limited by initial solutions
Genetic algorithm (GA) [21, 32]	<ul style="list-style-type: none"> GA concentrates exclusively on the global search 	<ul style="list-style-type: none"> Electricity bill and the end-user comfort optimization 	<ul style="list-style-type: none"> Easy implementation Performs a parallel search into multiple regions 	<ul style="list-style-type: none"> Slow convergence speed It cannot always deliver optimal or high quality solutions, especially in complex or highly constrained problem spaces
Multiobjective Gray Wolf Optimization Algorithm (MOGWO) [33, 34]	<ul style="list-style-type: none"> Inspired by the social behavior of wolves, used to optimize the technical goals including the loss and voltage indices 	<ul style="list-style-type: none"> Location and size of multi-distributed generation units in the microgrid 	<ul style="list-style-type: none"> Generation of quality solutions with a competitive computational effort 	<ul style="list-style-type: none"> The algorithm can be computationally intensive, especially for large-scale systems with many objectives and constraints

2.5.3 EMS based on Intelligent Methods

Intelligent methods, such as artificial neural networks, are considered stochastic methods used to solve optimization problems involving random variables [5]. Despite the efficiency of these methods, real-time and predictive control approaches are still required for intelligent energy management in smart microgrid systems [5]. Intelligent methods demonstrate strong computational intelligence, allowing it to predict complex and non-linear systems effectively [32].

Table 2.4 presents the consolidated descriptions, applications, advantages and disadvantages of the Intelligent EMS algorithms (control approach).

Table 2.4: Consolidated comparison of IEMS approaches.

Approach	Description	Application	Advantage	Disadvantage
Artificial neural network (ANN) [5, 32, 35]	<ul style="list-style-type: none"> A type of information processing system that seeks to mimic the human brain by simulating nonlinear processes A multi-dimensional information space that can learn information patterns, and exhibits strong computation intelligent which can predict any complex and non-linear system 	<ul style="list-style-type: none"> Distributed power generation units Multiple microgrid system interconnection Controls the bidirectional converter to protect the battery against over-charging and over-discharging Used for energy consumption minimization 	<ul style="list-style-type: none"> Can control, optimize and identify system's parameters in online or offline applications Solve problems with nonlinear data approaches in large-scale systems in microgrid Self-learning controller 	<ul style="list-style-type: none"> Complexity of the model structure; response time is slow The model is difficult to interpret and validate experimentally due to its complex and opaque internal structure (black box nature)

Reinforcement Learning (RL) [36]	<ul style="list-style-type: none"> Optimization based using two distinct components; the first strategy reduces the voltage distribution of the point of common coupling (PCC) Second strategy is based on a current control scheme and optimizes distributed resource power quality concerns 	<ul style="list-style-type: none"> It manages uncertainties by looking at real-time data with online energy management systems 	<ul style="list-style-type: none"> Flexibility and potential for adaptation to uncertainty 	<ul style="list-style-type: none"> Requires extensive training and computational resources May face challenges in defining reward functions and convergence in complex grid environments
Fuzzy Logic (FL) [35]	<ul style="list-style-type: none"> Based on fuzzy-logic reasoning technique that aims to generate the best possible buffer zone between 0 and 1 	<ul style="list-style-type: none"> Bi-directional DC-DC converter control 	<ul style="list-style-type: none"> Variations in the parameters have no or rare effect on the performance and operation 	<ul style="list-style-type: none"> The controlling progress is slow Creation require complicated rules
Sliding Mode Control (SMC) [35]	<ul style="list-style-type: none"> Efficient controller for DC-DC power converters control Operated as switching devices with ON and OFF 	<ul style="list-style-type: none"> Regulate the Bi-directional Buck-Boost converter for microgrid control and energy management 	<ul style="list-style-type: none"> Consistent performance during transients and fluctuation states Minimization of total harmonic distortion 	<ul style="list-style-type: none"> Discrete implementation of the Chattering Phenomenon Procedure for creating a complex design
Model-Based Predictive Control (MPC) [32]	<ul style="list-style-type: none"> Based on the optimal control actions of a dynamical system by predicting the future behavior of a system based on a mathematical model 	<ul style="list-style-type: none"> Electrical photovoltaic energy curtailment 	<ul style="list-style-type: none"> Has improved transient response It can control multiple variables within the boundary 	<ul style="list-style-type: none"> High computational load and algorithm complexity High number of control parameters

2.5.4 Comparison of Energy Management System Approaches

Selecting an EMS approach is crucial for ensuring the reliable and stable operation of a microgrid system. The choice of EM depends on various characteristics of the deployed system, such as topologies, operation modes, and structure. It is important to note that deploying one method does not imply that other methods are unreliable. The primary concern is to identify the utility of the chosen method based on the studied constraints and the fixed objectives of the control strategy [5].

The review by [5], [35], [32], compared conventional and intelligent controllers based on their classification, characteristics, structure, advantages, and disadvantages. Based on the strong connection between these studies, it reveals that intelligent controllers, such as FL, ANN, and MPC are more effective than conventional controllers. These intelligent controllers excel in terms of accuracy, robustness, generalization performance, transient response, and steady-state and dynamic performance.

2.6 Research-based EMS implementation in microgrid settings

This section discusses the case studies in which various intelligent methods have been applied to EMS. Furthermore, this section will discuss the drawbacks of the implemented intelligent methods on EMS, and moreover criticize the case studies.

2.6.1 Case 1: ANN based EMS

Findings in [26] demonstrated an EMS based control technique utilized to maintain voltage stability and power balance in DC microgrids by keeping the DC-bus voltage within the suitable range. The benefit of ANN was to accomplish peak shaving and offer direct prediction of approximating future demand forecasts under

defined assumptions and regulate the energy management system to ensure DC BUS and frequency stability. Its shortcoming was that the ANN required extensive training dataset.

2.6.2 Case 2: FL based EMS

Findings in [37] demonstrated A FLC based EMS was designed to cope with a multi-objective problem with the goal to increase the microgrid performance in terms of efficiency, operating costs, and lifespan of the HESS. The benefit of implementing FL algorithm is that it showed a low computational cost, with fuzzy rules simplifying the complex decision making. The FLC shortcoming was its limited predictability, it relies on current and predicted power balance but lacked long-term forecasting precision.

2.6.3 Case 3: DRL based EMS

The study in [38] proposed the deep reinforcement learning algorithms were implemented to the energy management system designed to coordinate among the different flexible sources by defining the priority resources, direct demand control signals, and electricity prices. DRL-based EMS showed the benefits of avoiding the need for explicit system modeling, reducing maintenance costs, and ultimately maximized gross energy profit by optimizing local generation, storage, and demand response. The shortcoming of the DL algorithm was that it required extensive hyperparameter tuning and suffered from high dimensional action spaces, as a result, policy based methods such as reinforcement showed slow convergence and instability.

2.6.4 Comparative Insights

The three case studies highlight distinct intelligent control strategies, ANN, FL, and DRL for a microgrid energy management system, each with unique strengths and limitations. The ANN based EMS excels in demand forecasting and voltage stabilization, making it ideal for systems with predictable loads, but its reliance on extensive training data and lack of interpretability limit its adaptability to dynamic conditions. In contrast, the FL based EMS offers a low computational cost solution for multi-objective optimization, balancing efficiency, cost, and HESS lifespan, though its heuristic nature restricts long-term forecasting precision. Meanwhile, the DRL based EMS stands out in dynamic environments by maximizing economic profit through adaptive learning without requiring explicit system modeling, yet its slow convergence and sensitivity to hyperparameters pose significant deployment challenges.

To address these limitations, hybrid approaches could be beneficial. Combining FL's rule-based robustness with ANN's predictive capabilities could enhance both short-term control and long-term planning, while DRL could focus on optimizing economic outcomes in fluctuating markets. Additionally, integrating lightweight forecasting models with FL and simplifying DRL's action spaces could mitigate their respective weaknesses. Future work should emphasize real-world validation and benchmarking against traditional methods to assess practical viability. Ultimately, a hierarchical EMS structure leveraging FL for real-time control, ANN for forecasting, and DRL for economic optimization could provide a balanced, resilient solution for a modern microgrid energy management system.

2.7 Conclusion

The literature review has examined the fundamentals of microgrid configurations, control strategies, and EMS, highlighting their significance in modern power systems. Microgrids, particularly hybrid configurations integrating renewable energy sources and energy storage systems, offer promising solutions for enhancing energy efficiency,

reliability, and sustainability. However, challenges persist in optimizing energy management, ensuring stability during grid transitions, and improving cost-effectiveness.

A comparative analysis of EMS approaches has shown that traditional optimization techniques, such as classical, heuristic, and metaheuristic methods, provide effective solutions but often lack adaptability to dynamic energy environments. In contrast, artificial intelligence-driven EMS has emerged as a promising alternative, offering enhanced predictive capabilities, real-time optimization, and adaptive control mechanisms. Studies reviewed indicate that intelligent based EMS, including neural networks and reinforcement learning, can significantly improve energy distribution efficiency and system reliability in hybrid microgrids.

Identified research gaps include the need for more robust IEMS that can handle uncertainties in renewable energy generation and demand fluctuations. Furthermore, integration of smart grid technologies and real-time data processing remains an area requiring further exploration. Emerging trends indicate a shift toward decentralized and autonomous energy management solutions, which leverage machine learning and IoT-based control systems to enhance microgrid operations.

Future research should focus on developing AI-enhanced EMS capable of real-time decision making, optimizing cost and energy efficiency while ensuring grid stability. Additionally, experimental validation of intelligent EMS strategies through real-world microgrid implementations will be crucial in bridging the gap between theoretical advancements and practical deployment.

Overall, this review underscores the importance of intelligent EMS in advancing hybrid microgrid technology. As energy systems transition toward more decentralized and resilient infrastructures, innovative control strategies and AI-driven EMS will play a critical role in ensuring sustainable and efficient energy management in the future.

Chapter 3

Methodology

3.1 Introduction

This chapter presents the systematic methodology used to design and evaluate a test microgrid integrated with an Intelligent Energy Management System (IEMS). The process follows a structured, sequential approach, as depicted in [Figure 3.1](#), to ensure the microgrid adheres to the predefined technical requirements outlined in [Table 3.1](#).

The methodology begins with the identification of technical requirements, followed by data collection to inform the design process. Next, a suitable software simulation tool is selected to model and size the microgrid components, including the load, solar photovoltaic (PV) system, battery energy storage system (BESS), and the utility grid. Subsequently, the IEMS is developed, with an emphasis on problem formulation, algorithm design, and the implementation of the IEMS.

The chapter also details the simulation procedures and the integration of the microgrid with the FLC IEMS. Finally, it presents case studies to validate system performance across four case scenarios.

[Figure 3.1](#) provides an illustration of the summarized sequential design method followed to design the test microgrid and IEMS.



Figure 3.1: Overview of methodology steps.

[Table 3.1](#) provides the technical requirements identification that the design process was guided by.

Table 3.1: Technical Requirements for the IEMS for a hybrid microgrid with renewables and BESS

Technical Requirement	Explanation
TR01	Microgrid total power generation should not exceed 1 MW
TR02	Ensure the MG utilize renewable resources and energy storage and integrate with the utility grid
TR03	Ensure the MG is hybrid by including a frequency stabilizing component for standalone mode of operation
TR04	Design the intelligent EMS to minimize cost of energy from the grid during grid-connected mode of operation
TR05	Design the intelligent EMS to maximize the utilization of renewable energy sources during standalone mode of operation
TR06	Design the intelligent EMS to maintain the power quality at load terminals at all times

3.2 Data Collection and Preparation

The load profile data was obtained from the [Eskom demand side](#) website spanning from 30 March 2025 00:00:00 to 04 April 2025 23:00:00, and the data were open source. The study utilized the period on 01 April 2025 from 00:00 to 23:00. The load data obtained represented the total contracted demand for the whole country ranging from 20000 to 30000 MW as seen in [Figure 3.2](#). A scale factor of 10^{-3} was used to convert the load demand from MW to kW, to satisfy TR01 from [Table 3.1](#) and hence a daily profile as illustrated in [Figure 3.2b](#) was obtained.

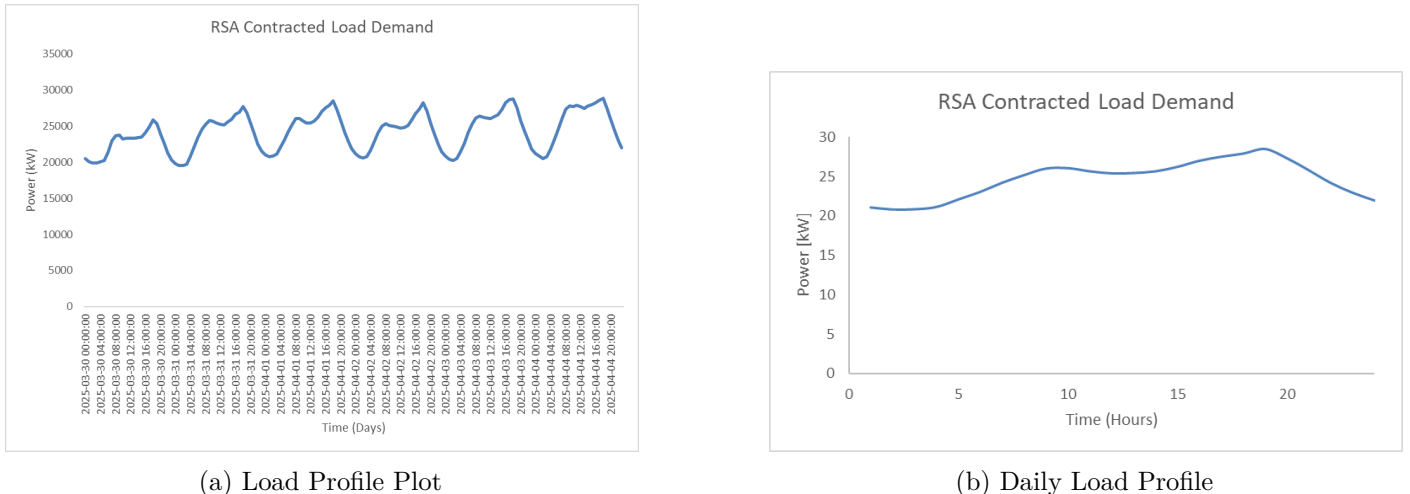


Figure 3.2: Load profile.

The solar PV generation data was obtained from [Eskom renewables site](#) and the data was open source. The solar PV generation represents the total solar PV generated country wide and ranges from 0 to 1800 MW spanning from 00:00 01 April 2025 to 23:00 11 May 2025 as seen in [Figure 3.3a](#). Similar to the load data, a scale factor of 10^{-3} was used to convert the load demand from MW to kW, to satisfy TR01 from [Table 3.1](#). The selected period was 01 April 2025 from 00:00 to 23:00, as a result the daily solar PV profile was obtained as seen in [Figure 3.3b](#).

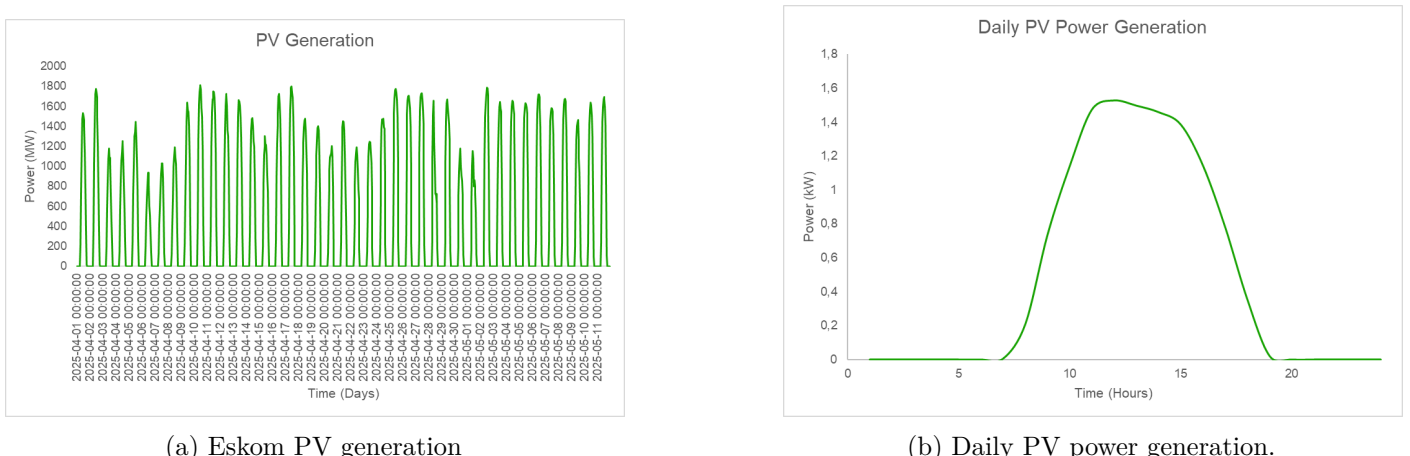


Figure 3.3: Total PV generation and daily PV data.

The [NASA data viewer](#) was used to obtain weather data including temperature and irradiance in South Africa

spanning a period of 00:00 01 April 2024 to 23:00 04 April 2024¹. An assumption was made to assume the weather for 2024 would match the weather data for 2025, and the weather conditions were for a clear sky with no clouds. The website was open source. The location of choice was Loeriesfontein, situated at Northern Cape. The irradiance was expressed in Wh/m^2 , since the data was sampled hourly, each value already representsd the accumulated energy in W/m^2 over the past hour. Therefore, no division was needed as the values were effectively in W/m^2 when interpreted as an average over that hour. Figure 3.4 illustrates the relationship between the generated PV power and irradiance.

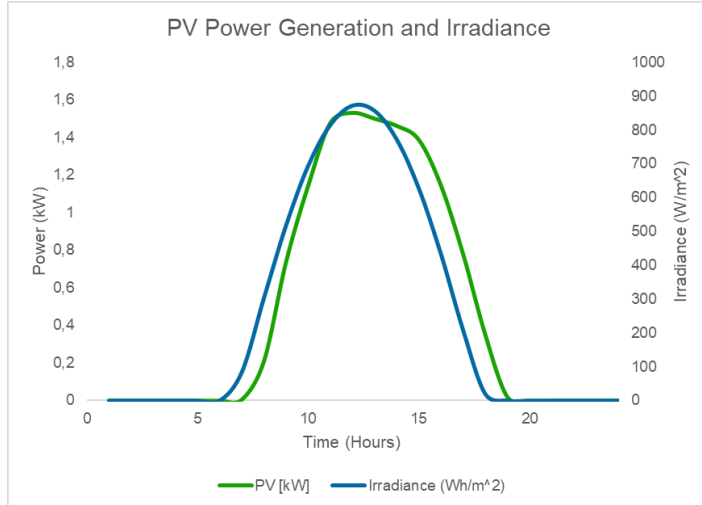


Figure 3.4: Daily PV profile and irradiance.

The grid energy price was obtained from [39, p. 11], open source. The type of consumer selected was Miniflex, an Eskom electricity tariff designed for urban customers with a National Maximum Demand (NMD) between 23 kVA to 5 MVA to align with TR01 from Table 3.1. The tariff used was the Non-Local Authority Time of Use (ToU) tariff for a transmission zone of 900 km and and, and a voltage of <500 V [39]. The season of choice was low demand season from September to May with the following tariff:

- Peak: R2.3044/kWh
- Standard: R1.59/kWh
- Off peak: R1.0137/kWh

The selected ToU periods were influenced by [39, p. 47], and were defined as follows:

- Peak periods: 06:00 to 10:00 and 18:00 to 22:00
- Standard periods: 10:00 to 18:00
- Off peak periods: 00:00 to 06:00 and 22:00 to 20:00

¹Data for April 2025 is not available, hence 2024 data on the same period as solar generation data was selected.

3.3 Software Selection

The list of simulation software programs to select from were PowerFactory, HomerPRO, Python and MATLAB. Critical factors for selecting software programs were considered, including the system's complexity, the library of energy sources and loads, and the level of control and monitoring required.

Table 3.2 provides a consolidated information of the 4 software tools:

Table 3.2: Comparison of Software Tools for EMS Development

Criteria	MATLAB Simulink	HomerPro	PowerFactory (DIgSILENT)	Python
Main Strength	Algorithm development, dynamic simulation, control design	Economic analysis and system sizing	Grid-level load flow, fault analysis	High flexibility in algorithm design and data processing
Customization	High (user-defined algorithms, scripting, control logic)	Low (fixed workflow and models)	Moderate (scripting via DPL, but limited flexibility for control algorithms)	Very High (open-source libraries allow full customization)
Suitable for EMS?	Yes, especially for real-time or intelligent EMS	No, it is mainly for off-grid economic planning	Limited, it lacks flexibility for AI-based EMS	Yes, especially for data-driven or AI-based EMS, but lacks built-in power system modeling tools
Learning Curve	Moderate to High	Low	High	High (requires strong programming knowledge and integration skills)
Data Visualization & Analysis	Excellent, integrated plots, scopes, and dashboards	Moderate	Good, but less interactive than MATLAB	Excellent, but requires manual setup using libraries like matplotlib or Plotly

MATLAB Simulink was selected as the simulation platform of choice for developing the IEMS due to its integrated environment, robust toolboxes, and flexibility in modeling both control logic and dynamic energy flows. Compared to Python, which is highly customizable and offers powerful data analysis and AI libraries, MATLAB provided a more seamless workflow for system level simulation, particularly in hybrid microgrids where both algorithm design and physical modeling must be integrated. Although Python supported machine learning and fuzzy logic through libraries such as Scikit-learn and scikit-fuzzy, it lacked native block-based modeling for power systems and required significant effort to integrate various components manually [40]. In contrast, MATLAB Simulink offered drag-and-drop modeling, built-in support for renewable energy components, and real-time simulation capabilities, making it the most suitable and efficient platform for prototyping, testing, and validating intelligent EMS strategies.

While HomerPro excelled in preliminary design and feasibility assessment, it does not support detailed control design or real-time simulations [41]. PowerFactory was robust for grid related studies but was not built for custom energy management algorithm development or intelligent control [42]. Thus, MATLAB Simulink stood out for its ability to handle EMS development that required custom logic, simulation of hybrid sources, and dynamic performance evaluation. Several studies, including [43] utilized MATLAB to simulate and analyze the performance of EMS under different scenarios and control strategies.

Contribution to Result Analysis

Matlab Simulink supports detailed data analysis through built-in tools such as:

- Time-series visualization

- Signal logging and scope-based monitoring
- Statistical and machine learning toolboxes for performance evaluation

This facilitated precise performance tracking of EMS decisions, energy flows, state of charge dynamics, and renewable power availability in different scenarios. It also allowed integration of optimization and decision-making algorithms, making the analysis of results more comprehensive [44].

Impact of Software Limitations on Accuracy of Results

Although MATLAB Simulink was powerful, certain limitations could influence the results:

- Real-world deployment constraints such as communication delays, hardware incompatibilities, and cost aspects are not inherently modeled unless explicitly integrated.
- High-fidelity grid simulations may require co-simulation with tools like PowerFactory for voltage stability or protection studies.

However, these limitations did not critically affect the accuracy or validity of the results for EMS algorithm validation, as the focus was on decision-making logic and energy balancing strategies rather than deep electrical phenomena. Where necessary, MATLAB can be extended or interfaced with external simulators such as Python to bridge these gaps.

3.4 Mathematical Modeling and Sizing for a Test Microgrid

This section introduces the mathematical modeling and design steps followed to develop a test microgrid and the load. The mathematical models also applied in the MATLAB Simulink components.

3.4.1 Solar PV Array

Solar radiation is converted into electrical energy in photovoltaic (PV) panels where light photons striking the PV panel cause electrons in the substrate material to become more active, then steered away from the panel to produce DC [45].

As characterized by [12], the power output from the PV panel (P_{PV-out}) is given in Equation 3.1:

$$P_{pv} [\text{W}] = N_{pv} \times G \times A \times \eta \times [1 + \alpha(T_c - T_r)] \quad (3.1)$$

where P_{pv} is the output power, N_{pv} is the number of panels, G solar irradiance in W/m^2 , α is the voltage temperature coefficient of power expressed as $-3.7 \times 10^{-3} \text{ }^\circ\text{C}^{-1}$, T_r is the reference temperature at standard test condition (STC) expressed as 25°C and T_c is the cell temperature in $^\circ\text{C}$ [12, 46].

3.4.2 Battery Energy Storage System

The carrying capacity of the BESS determined in Equation 3.2 [47]:

$$BESS_{cap} [\text{kWh}] = \frac{AD \times E_{Load}}{\eta_{inv} \times \eta_{BESS} \times DOD} \quad (3.2)$$

where E_{Load} is the energy demand of the load, η_{inv} is the battery inverter efficiency, η_{BESS} is the battery efficiency, DOD is the depth of discharge, and autonomy days, AD , reflect the number of days the BES can

supply the load without depleting its charge [47].

When there is an overabundance of energy generated, it is stored in the BESS to be utilized at a later stage, and the power output of the BESS is modeled as [12]:

$$P_{BESS}(t) [\text{W}] = P_{pv}(t) - \frac{P_L(t)}{\eta_{\text{Inv}}} \begin{cases} P_{BESS}(t) < 0, \text{energy generation deficit} \\ P_{BESS}(t) > 0, \text{energy generation exceeds power demand} \\ P_{BESS}(t) = 0, \text{power generated equals load power demand} \end{cases} \quad (3.3)$$

where P_{BESS} , P_L and η_{Inv} are battery power, load power, and inverter efficiency respectively [12].

The state of charge (SOC) of the BESS is a key factor influencing its performance and indicating its current capacity [12]. The SOC has two modes, charging mode which occurs when the BESS absorbs excess power from the grid or renewable sources, and discharging mode which happens when the BESS supplies power due to insufficient renewable generation to meet demand [12]. The modes are modeled in Equation 3.4 and Equation 3.5 [12]:

Charging mode: $P_{pv}(t) > P_L(t)$

$$E_{BESS}(t) [\text{Wh}] = E_{bat}(t-1) \times (1 - \sigma) + [P_{pv}(t) - \frac{P_L(t)}{\eta_{\text{Inv}}}] \times \Delta t \times \eta_{\text{ch}} \quad (3.4)$$

Discharging mode: $P_{pv}(t) < P_L(t)$

$$E_{BESS}(t) [\text{Wh}] = E_{BESS}(t-1) \times (1 - \sigma) + [\frac{P_L(t)}{\eta_{\text{Inv}}} - P_{pv}(t)] \times \frac{\Delta t}{\eta_{\text{disch}}} \quad (3.5)$$

where $E_{BESS}(t-1)$ represents the energy stored in the BESS at the previous time in Watt-hour (Wh), σ is the self-discharge rate per hour, $\eta_{\text{ch/disch}}$ denotes the efficiency of the BESS in charge and discharge mode, and η_{Inv} is the inverter efficiency [12].

Bilal et. al [47] mentioned that the BESS can fulfil the demand as long as the state of charge is above SOC_{min} . A surplus of energy produced charges the BESS till it hits the SOC_{max} [47]. Thus the maximum SOC is equivalent to the BESS's total capacity (B_{BES}) as shown in Equation 3.6 [47]:

$$BESS_{cap} [\text{Ah}] = \frac{N_{BESS}}{N_{BESS_sr}} \times BESS_{cap_s} (\text{Ah}) \quad (3.6)$$

Additionally, the maximum allowable depth of discharge (DOD) is expressed as a percentage [47]. Since it is not feasible to completely deplete the BES, the DOD value represents the maximum extent to which the BES can be discharged, thus, minimum capacity required by for the BES is determined in Equation 3.7 [47]:

$$E_{BESS_min} [\text{Wh}] = (1 - DOD) \times E_{BESS_max} \quad (3.7)$$

Since battery storage are used to increase the reliability of the power supply, the capacity of the storage unit should be between the maximum and minimum values at any given time t [45]. The limits to be adhered are formulated in Equation 3.8 and Equation 3.9 [45]:

$$0 \leq P_i^{\text{CB, DB, min}}(t) \leq P_i^{\text{CB, DB, max}}(t) \quad (3.8)$$

$$E_{BESS\ min} \leq E_{BESS} \leq E_{BESS\ max} \quad (3.9)$$

where $P_i^{\text{CB}, \text{DB}, \min}$ and $P_i^{\text{CB}, \text{DB}, \max}$ is the minimum and maximum battery power respectively. $E_{BESS\ min}$ and $E_{BESS\ max}$ is the minimum and maximum energy stored in the battery respectively [45].

Modeling load balancing is important considering during an on grid-connected mode, the BESS contributes to load leveling, and on standalone mode, it ensures a stable energy supply during periods of zero PV generation [13]. The equations [Equation 3.10](#) and [Equation 3.11](#) [13] model these cases:

$$\text{Power balance for off-grid scenario: } P_{PV,t} + P_{BESS,t} = P_{load} [\text{W}] \quad (3.10)$$

$$\text{Power balance for on-grid scenario: } P_{PV,t} + P_{BESS,t} + P_{grid} = P_{load} [\text{W}] \quad (3.11)$$

$$\text{State of Charge of the battery: } SOC(t) [\%] = SOC(t - \Delta t) + P_{BT,t} \cdot \frac{\Delta t}{E_{BESS,max}} \quad (3.12)$$

where $E_{BESS,max}$ is the maximum energy storage capacity of the battery [13].

$$\text{Power charged/discharged by the BT for off-grid: } P_{BESS} [\text{W}] = \eta_{BESS} \cdot \eta_{Inv} \cdot (P_{PV} - P_{load}) \quad (3.13)$$

$$\text{Energy balance for on-grid scenario: } P_{BESS} [\text{W}] = \eta_{BESS} \cdot \eta_{Inv} \cdot (P_{PV} + P_{grid} - P_{load}) \quad (3.14)$$

3.4.3 Utility Grid

The utility grid is modeled as a three-phase sinusoidal voltage source with time varying parameters, amplitude (V_m), angular frequency (ω), and phase angle (ϕ), described by:

$$V_{\text{grid}} [\text{V}] = V_m \sin(\omega t + \phi) \quad (3.15)$$

The grid's internal impedance is modeled as a series RL branch:

$$Z_{\text{source}} [\Omega] = R + j\omega L \quad (3.16)$$

Grid Strength and Short-Circuit Ratio (SCR)

Grid strength at the PCC is determined by the grid's Thevenin equivalent impedance (Z_{source}) [48]. A strong grid has low impedance, allowing it to maintain stable voltage under disturbances, while a weak grid has high impedance, making it more sensitive to power fluctuations [48].

A common metric for grid strength is the SCR, defined as [48]:

$$\text{SCR} = \frac{S_{\text{sc}}}{P_R} \quad (3.17)$$

where S_{sc} is the short-circuit capacity at PCC (VA), P_R is the rated capacity or injected power (W) from utility grid at the PCC [48].

For a Thevenin equivalent grid with voltage V_{grid} and impedance Z_{source} , the short circuit capacity is [48]:

$$S_{\text{sc}} = \frac{V_{\text{grid}}^2}{|Z_{\text{source}}|} \quad (3.18)$$

$$SCR = \frac{V_{\text{grid}}^2}{P_R \times |Z_{\text{source}}|} \quad (3.19)$$

Thus, SCR is inversely proportional to $|Z_{\text{source}}|$, as noted. However, SCR also depends on the inverter's rated power. Key classifications:

- **Strong grid:** $SCR > 3$ (low Z_{source}).
- **Weak grid:** $SCR < 3$ (high Z_{source}).

3.4.4 Energy Balance

Effective energy balancing depends on reliable energy generation and the reserve available to ensure supply and meet expected demand. The power flow in the microgrid is bi-directional depending on the power transfer to and from the main grid [12]. The utility grid supplements the microgrid to satisfy load demand such [12]:

$$P_L [\text{W}] = \eta_{\text{Inv}}(\eta_{pv}P_{pv} + \eta_B P_B ESS) + P_{\text{grid}} \quad (3.20)$$

Combining PV, and BESS for off-grid applications offer benefits such as grid stability and consistent power output [13]. Equation 3.21 and Equation 3.22 models the energy balance for on-grid and off-grid [13]:

$$\text{On-grid system: } P_{\text{grid}} [\text{W}] = P_{\text{load}} - (P_{PV} + P_{BESS}) \quad (3.21)$$

$$\text{Off-grid system: } P_{\text{load}} [\text{W}] = P_{PV} + P_{BESS} \quad (3.22)$$

3.4.5 Scenario

Loeriesfontein in South Africa's Northern Cape was an ideal location for a hybrid renewable microgrid due to its abundant solar, combined with its remote location and unreliable grid connection. The proposed microgrid integrates a solar PV, a battery energy storage system operating at 400V for local distribution with a grid-tied option. An intelligent Fuzzy Logic Controller (FLC) algorithm manages energy dispatch, prioritizing renewables while minimizing utility grid use and ensuring stable power supply. This system enhances energy independence, reduces costs, and supports rural electrification, aligning with South Africa's renewable energy goals while providing reliable electricity to the community.

3.4.6 Sizing of The Test Microgrid Components

The microgrid components were sized using mathematical models in section 3.4. The sizing references IEEE/IEC standards, with the load profile data in section 3.2 driving key assumptions. The microgrid is sized for standalone mode of operation, guided by IEEE Std 1547.4 (2011), that provides an overview of distribution secondary network systems design, components, and operation [49, p. 5].

Load

The load was modeled as a time-varying active power profile based on load data mentioned in section 3.2. [50] proposed a load profile of similar pattern to Figure 3.2b, however, the demand in the load profile in [50] was varying from 2600 kW to 4200 kW, representing a factory. Since Loeriesfontein is a small town, for the daily load profile in Figure 3.2b to match a small factory of 100 kW to 500 kW peak, the following scale was used:

The original data peaked in Figure 3.2b at 28.5 kW, scaling it to a small factory leads to

$$\text{Scaling Factor} = \frac{\text{Target Peak}}{\text{Original Peak}} = \frac{210}{28.5} = 7.36 \quad (3.23)$$

The scaling factor was then multiplied to all values sampled hourly from 00:00 to 23:00 to obtain a new peak of $28.5 \times 7.36 = 209.76$ kW and a new minimum of $20.8 \times 7.36 = 153.09$ kW.

The scaling factor of 8 converts the original profile into a small sized factory demand. The shape of the load profile is preserved, with the load type now similar to an agricultural processing factory such as small dairy, grain milling, or meat packaging.

The peak load was determined to be $P_{\text{peak load}} = 206.4$ kW. The daily energy demand was calculated by integrating the hourly load profile in Figure 3.2b considering the scale factor of 8 (see section C.1 ??):

$$E_{\text{Demand}} = \sum_{t=0}^{24} P_{\text{Load}}(t) \times \Delta t = 4326,42 \text{ kWh}$$

Solar PV

The PV was the priority renewable energy source in both grid-connected and standalone mode of operation. It was sized to meet the load demand fully and have excess power to charge the battery in both grid-connected and standalone mode. The sizing of the solar PV was based on IEC 62548 which sets out design requirements for PV, and IEC 62124 which verifies system design and performance of standalone PV systems.

After the total PV power generation was scaled from MW to kW as described in section 3.2, the PV power output model was used. Equation 3.24 accounts for irradiance and temperature losses. The parameters for G and T_{amb} were obtained in Table C.2. The total number of panels (N_{PV}) 1500, panel efficiency (η_{PV}) of 0.18 and panel area of 2000 m² were considered. These values were influenced by [51] for PV sizing. These parameters were applied to the hourly samples in Table C.2, a sample calculation was shown below Equation 3.25:

$$P_{pv} [\text{W}] = N_{pv} \times G \times A \times \eta \times [1 + \alpha(T_c - T_r)] \quad (3.24)$$

$$P_{pv} = 1500 \times 0.87267 \times 100 \times 0.30 \times [1 + (-3.7 \times 10^{-3})(24.32 - 25)] \quad (3.25)$$

$$P_{pv} = 472427.44 = 472.43 \text{ kW}$$

The total PV sizing was 472.43 kW, enough to meet the load demand and have surplus energy to charge the BESS.

BESS

As already covered in the chapter 2, the role of BESS was to provide power quality support, store excess PV, discharge to supply power during low generation and enable load shift.

Table 3.3 compared the BESS type available. The chosen BESS type was the Li-ion due to high cycle life and quick response.

Table 3.3: BESS Type and chemistry

Type	Energy Density	Cycle Life	Cost	Response
Lead-acid	Low	1500	Low	Slow
Li-ion	High	6000 and greater	Moderate	Fast
Flow Batteries	Medium	10000 and greater	High	Medium

The BESS must discharge when there is no PV power output or discharge along with PV to meet the load demand, from [Figure 3.3b](#), that occurred between times 00:00 to 05:00 and 18:00 to 23:00. The total number of hours where there is no solar PV power output were determined to be 9 hours. Hence, the BESS was sized to have enough capacity to support load demand for 9 hours. The BESS capacity [Equation 3.2](#) used an inverter efficiency (η_{inv}) of 0.95, accounting for a 5% energy loss during DC-AC conversion, as recommended by IEEE 1547-2018 for grid-tied inverters [52]. The BESS round-trip efficiency (η_{BESS}) of 0.96 reflected real-world losses from internal resistance and thermal dissipation during charge and discharge cycles, aligning with [IEEE SA - P3163](#) which sets the standards for Li-ion batteries. A depth of discharge (DOD) of 80% was adopted to balance usable capacity with battery lifespan, per [IEC 61427-1](#) guidelines. Autonomy day (A) value of 1 was chosen to satisfy TR06. These values ensured reliability across both grid-connected and standalone modes.

$$BESS_{cap} = \frac{A \times E_{Load}}{\eta_{inv} \times \eta_{BESS} \times DOD} = \frac{1 \times 1620}{0.95 \times 0.96 \times 0.80} = 2220.39 \text{ kWh}$$

E_{Load} considered the average daily load demand to be 180 kW, running for 9 hours due to solar PV intermittency, resulted to load energy demand of 1620 kWh. The energy battery energy storage needed to cover the full load for 1 day autonomy was determined to be 2220.39 kWh.

The power of the BESS was determined using [Equation 3.10](#). A worst case scenario of $P_{PV} = 0$ kW and $P_{Load} = \text{peak} = 206.4$ kW was considered:

$$P_{PV} + P_{BESS} = P_{Load} \implies 0 + P_{BESS} = 206.4 \text{ kW}$$

The BESS must also be able to absorb all surplus PV power after the load demand is met, hence, a values higher than 206 kW and 2220.39 kWh were chosen.

$$\therefore P_{BESS} = 300 \text{ kW}$$

The required discharge power is 300 kW, as a result the battery sizing is 300 kW/ 3000 kWh

Utility Grid

The utility grid serves as a backup power source when the microgrid operates in grid-connected mode. It provides additional power when PV and the BESS cannot meet load demand, however in this project it cannot charge the battery even when electricity prices are low to reduce utility grid energy costs. A balanced three-phase four-wire utility grid of 400 V, 50 Hz, was connected to the AC at the PCC, and provided voltage and frequency reference to for the microgrid system as per IEEE 1547 [27]. A low voltage was considered to ensure simple design that does not utilize a transformer for stepping down voltage, to also align with the TOU tariff used in [section 3.2](#). A study by [53] used a similar voltage of integration to the microgrid. The utility grid was sized with the maximum grid power import of 500 kW. This power import guaranteed the load demand was met, ensuring the utility grid can accommodate load expansion.

$$\text{Grid maximum import, } P_{\text{grid}} = 500 \text{ kW}$$

The values of R and L for source impedance were chosen as 0.08Ω and 6 mH , respectively as per IEC 60909-0. Using Equation 3.19, the SCR was determined to be:

$$SCR = \frac{V_{\text{grid}}^2}{P_R \times |Z_{\text{source}}|} = \frac{(400 \text{ V})^2}{500 \text{ kW} \times 0.0884 \Omega} = 3.62$$

A SCR of 3.62 indicated a strong grid.

3.5 Development of Intelligent Energy Management System Design

This section introduces the problem formulation that the IEMS needs to solve. It involves the objectives that must be achieved based on the problem formulation, lists the constraints, and develops the flowchart, showing the decisions that the IEMS must follow to achieve its objectives. [27] mentioned IEEE STD 2030.7 for the specification of microgrid controllers.

3.5.1 Problem Formulation

The growing need for sustainable and resilient energy solutions has driven the adoption of hybrid microgrids, integrating renewable energy sources, storage systems, and intelligent controls. However, ensuring cost-effectiveness and energy security in both standalone and grid-connected modes remains challenging due to fluctuating loads and renewable generation. This project focuses on designing and testing an intelligent energy management system (IEMS) that optimizes energy generation, storage, and grid interaction while minimizing Cost of Energy (COE) and maximizing Renewable Factor (RF).

Objective Function

The IEMS must demonstrate mode specific optimization behaviors. During grid-connected operation, the system minimizes total energy costs through an integrated strategy where solar PV generation receives highest priority, battery storage operates strategically (utilizing excess power from PV to charge if surplus power is available after load demand is met, and grid power in case of deficit power for load demand), while grid power imports are minimized, particularly during high tariff periods. This economic optimization occurs within reliability constraints including power supply stability and BESS degradation prevention.

In standalone mode, the optimization focus shifts to renewable energy maximization and backup resource conservation. PV system serve as the primary generation source, with battery storage providing supply-demand balancing. Both operational modes strictly maintain voltage and frequency stability while ensuring proper BESS discharging and charging patterns.

Constraints

The constraints are mathematical conditions used to define limitations and feasibility of the microgrid, and must be satisfied in an optimization problem. These constraints ensure that the microgrid operates efficiently, reliably, and within safe parameters [47]. The constraints are guided by IEEE Std 1547 and IEC 61851 [54]. The objective of this project was subject to the following constraints:

Power Balance Constraint:

$$P_{\text{gen}}(t) + P_{\text{grid}}(t) + P_{\text{BES}}(t) = P_{\text{load}}(t) \quad (3.26)$$

This ensured that power supply meets demand while accounting for system losses.

Renewable Factor (RF):

The RF was used to differentiate between the amount of power generated by the non-renewable resources, utility grid, and the renewable resources [55]. Expressed as a percentage, it gives a measure of the energy supplied by the renewable resources, and defined as follows [55]:

$$RF [\%] = \left(1 - \frac{\sum P_{grid}}{\sum P_{renewable\ resources}}\right) \times 100 \quad (3.27)$$

A desirable RF value of 100% means that the demand is fulfilled by the renewable resources [55].

Battery SOC:

$$SOC_{min} \leq SOC(t) \leq SOC_{max} \quad (3.28)$$

Battery SOC limits ensures the battery operates within safe limits, preventing degradation.

Voltage Limits:

$$\Delta V = \pm 10V \quad (3.29)$$

The chosen voltage limit was guided by the South African Grid Code (SAGC) [56], that stated the voltage at the POC is to be in the range -15% to +10% around the nominal voltage.

Frequency Limits in standalone:

$$49.5 \text{ Hz} \leq f(t) \leq 50.5 \text{ Hz} \quad (3.30)$$

Voltage and frequency limits ensure power quality at load terminals. Power quality indicators are specified in IEC 61000 and IEEE Std1159 [57]. The SAGC specifies minimum frequency operating range of 49.0 Hz to 51.0 Hz during a system frequency disturbance [56].

3.5.2 Algorithm Flowchart Design

The goal of the IEMS is to ensure the reliable, efficient, and cost-effective operation of a hybrid renewable energy system in both grid-connected and standalone modes. To structure and implement this control strategy, a decision-based flowchart was developed. The flowchart, as seen in Figure 3.5, provided a clear visual representation of the logical sequence of decisions made by the IEMS, including energy source prioritization, and BESS management. This approach ensured that complex operational conditions are handled systematically and consistently. The flowchart served as a critical tool for providing a high-level understanding of the microgrid and IEMS. Its clarity and modular structure also supported easier validation, debugging, and future scalability of the system.

Key points for grid-connected mode from the flowchart were:

- If the grid energy price TOU is below the threshold of R1.59/kWh, the microgrid is in grid-connected mode.
- The power balance is computed as the difference between the PV power generation and the load power demand. A decision then compares if the power balance is positive, PV meets load demand fully, or negative, the PV does not meet load demand.
- For positive power balance, a decision then compares the BESS SOC, if greater than maximum = 90%, the BESS idles and does not charge, if less than 90%, the final action is for PV to meet load demand and use surplus power to charge the BESS.
- For negative power balance, a decision then compares the BESS SOC, if less than minimum = 30%, the

utility grid is used to only meet the load demand, if more than 30%, the final action is use both PV and discharge BESS to meet load demand.

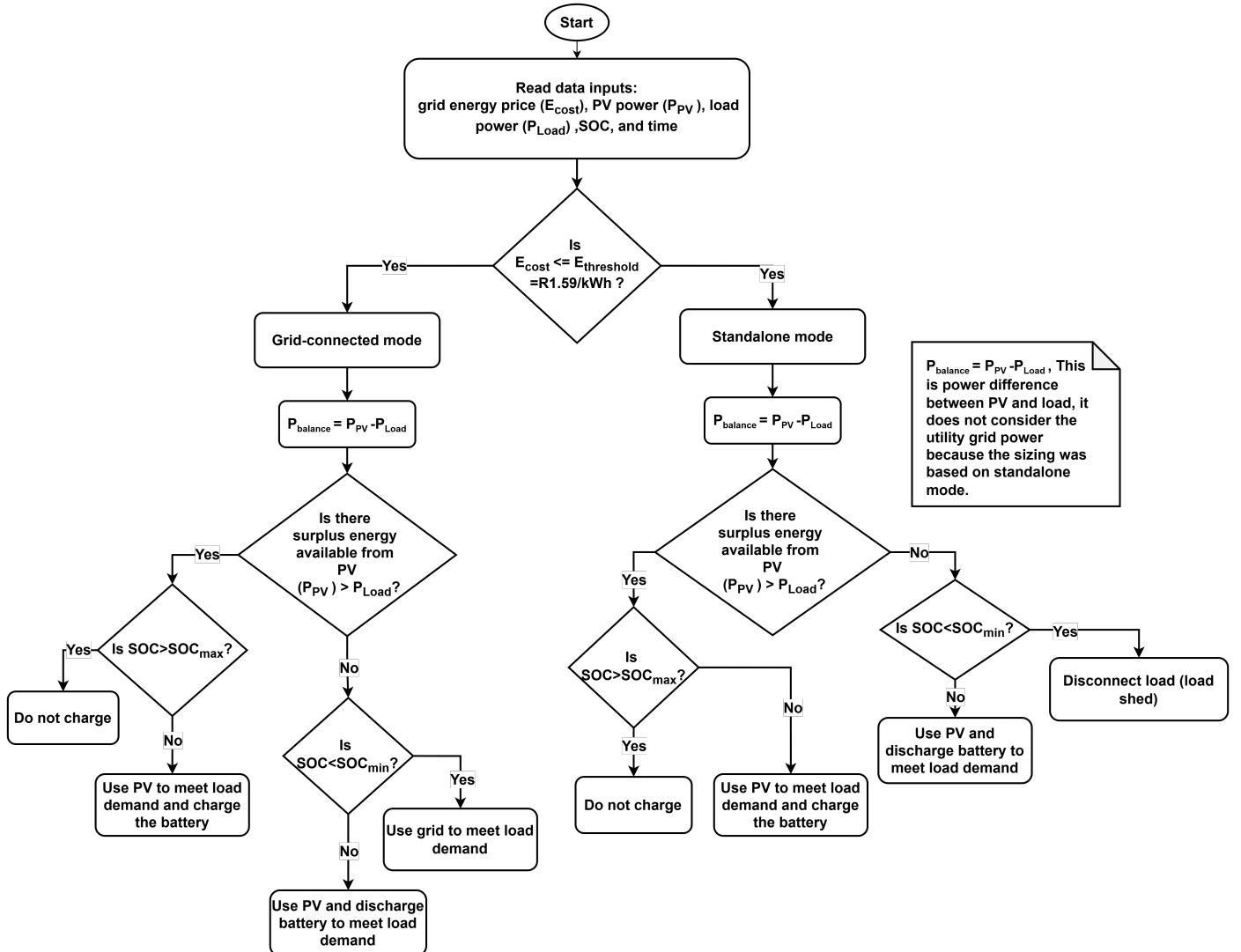


Figure 3.5: IEMS proposed flowchart

Key points for standalone mode from the flowchart are:

- If the grid energy price TOU is above the threshold of R1.59/kWh, the microgrid is in standalone mode.
- The power balance is computed and a decision then compares if the power balance is positive, PV meets load demand fully, or negative, the PV does not meet load demand.
- For positive power balance, a decision then compares the BESS SOC, if greater than maximum = 90%, the BESS idles and does not charge, if less than 90%, the final action is for PV to meet load demand and use surplus power to charge the BESS.
- For negative power balance, a decision then compares the BESS SOC, if less than minimum = 30%, the load is shed, if more than 30%, the final action is use both PV and discharge BESS to meet load demand.

3.5.3 FLC Design

Various intelligent control methods were considered for the IEMS in subsection 2.5.3, including FLC, ANN, MPC, and DL. ANN and DL require large labeled datasets and lack interpretability [58], while MPC involves complex real-time optimization and accurate modeling, making it less suitable for dynamic systems. FLC was selected for its simplicity, transparency, and ease of implementation.

Fuzzy logic addresses uncertainty in data and processes using linguistic terms for reasoning, allowing for the analysis of imprecise information and reducing the need for complex mathematical models [7]. Fuzzy Logic Control (FLC) extends this by providing a rule-based, intuitive framework that incorporates expert knowledge, handles uncertain inputs such as variable solar availability, and operates without the need for training data. These characteristics make FLC well-suited for the energy management strategy adopted in this project.

Based on the management algorithm that has been presented in Figure 3.5, a fuzzy logic controller is developed for the IEMS. The microgrid can operate in two modes, grid-connected mode when the grid energy price is cheap, and standalone mode when the grid energy prce is expansive. In both modes, the priority is PV, then BESS, and lastly the utility grid in grid-connected mode. In standalone mode, the priority is PV, then BESS, load shedding occurs when there is no enough power capacity from the PV and BESS to meet load demand, and the grid energy price is high, above the threshold of R1.59/kWh. The design of the fuzzy logic was separated into two sub-modules, one FLC that controls the switching of the microgrid modes from grid-connected to standalone mode and switching the load on or shedding the load. The other FLC was to control the scheduling of the BESS. Both the FL were created in using the Fuzzy Logic Designer app in MATLAB.

A FLC transforms precise inputs into intelligent control actions using linguistic reasoning. The high-level process consists of four key steps, illustrated in Figure 3.6:

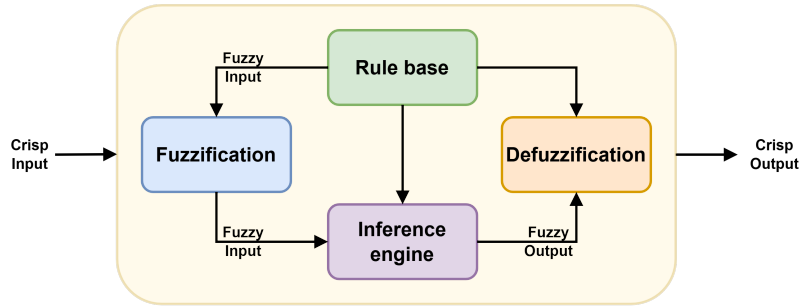


Figure 3.6: High level structure of the fuzzy inference system [6, 7].

1. Fuzzification converts crisp numerical inputs (measurements) into fuzzy linguistic variables using predefined membership functions. Each input is mapped to degrees of membership in overlapping fuzzy sets (e.g., ‘Low,’ ‘Medium,’ ‘High’), enabling graded interpretations.
2. Fuzzy rule base contains expert-defined ‘IF-THEN’ rules that encode the system’s behavior. These rules correlate input fuzzy sets to output fuzzy sets. The rule base complexity scales with the system’s requirements.
3. Inference engine evaluates the active rules by calculating each rule’s firing strength (degree of premise truth), and applying fuzzy operators (e.g., MIN/MAX) to infer output membership functions. The result is a composite fuzzy output representing the control action.

4. Defuzzification converts the fuzzy output into a crisp, executable value (a control signal) using methods like centroid or weighted average. This step ensures practical applicability.

3.5.4 FLC Design for BESS Control

A Mamdani FL was used for the design of BESS control. The design of the FLC for the BESS control was illustrated in [Figure 3.7](#).

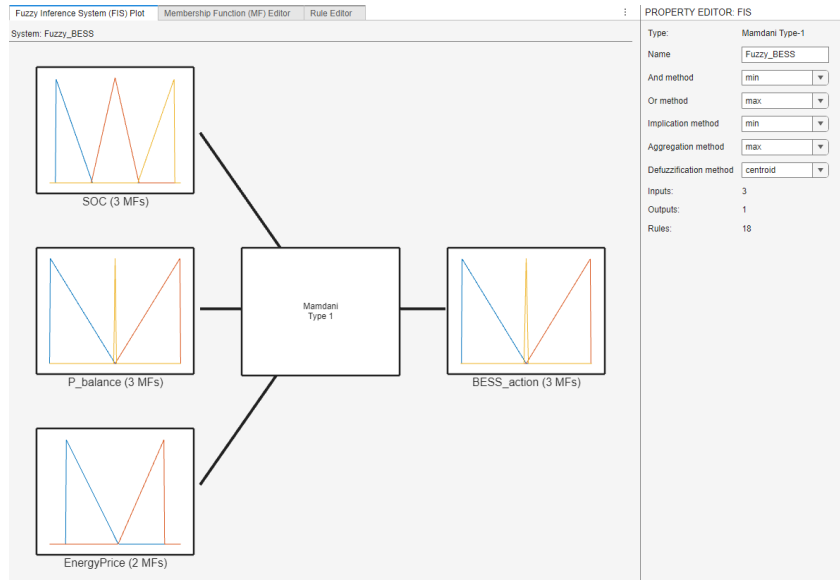


Figure 3.7: Fuzzy logic design for BESS action.

Step 1: Define Input and Fuzzification

This step involved identifying the input variables that affect the energy control in the system. These variables include factors such as grid energy price, power balance, and BESS SOC. The grid energy price was defined in linguistic terms to represent the membership function as low or high, power balance as negative, zero, or positive, and SOC as low, medium, high. The fuzzification of the inputs were presented in [Table 3.4](#).

Table 3.4: Defining fuzzy inputs.

Input	Description	Fuzzy Sets	Range
Grid energy price	Represents the current cost of electricity from the main grid, which drives operational mode decisions. Lower prices favor grid interactions while higher prices encourage PV and BESS optimum use.	Low, High	<ul style="list-style-type: none"> • Low (0 to R1.60/kWh) • High (1.59 to R3.00/kWh)
P _{balance}	Quantifies the instantaneous power mismatch between PV generation and load demand, defined in Equation 3.11 as $P_{balance} = P_{PV} - P_{Load}$. A key decision variable that indicates energy surplus or deficit conditions in the microgrid, directly influencing storage operation.	Positive, Zero, Negative	<ul style="list-style-type: none"> • Negative (-500 to 0 kW) • Zero (-10 to 10 kW) • Positive (0 to 500 kW)
SOC	Indicates the current energy level stored in the battery as a percentage of its total capacity. A critical constraint parameter that ensures battery longevity by preventing over-charging or deep discharging while utilizing available storage capacity.	Low, Medium, High	<ul style="list-style-type: none"> • Low (0 to 31%) • Medium (30 to 70%) • High (69 to 100%)

The membership functions for each input were carefully selected to balance precision, and computational efficiency. Triangular MFs were used for all input MFs for simplicity. Overlaps in fuzzy triangular membership

functions were crucial for enabling smooth interpolation between linguistic terms, activating multiple rules (see subsection C.3.1). Non-normalized ranges preserve physical interpretability for the design process [59, 60]. As seen in Table 3.4, the range of inputs used were real values instead of normalized values, this was to ensure no loss of physical meaning as normalized values may be less hard to interpret when debugging, for instance, a high grid energy cost being normalized 1 (R/kWh) instead of being a true value 2.304 (R/kWh).

Step 2: Identifying The Output Actions

After the fuzzification of inputs, the output actions were determined. The outputs are the actions that will be taken once the rules were created. The system has one output, the BESS action. Triangular MFs were used for the output for simplicity and computational efficiency. By computational efficiency, the rule evaluation is optimized because the fuzzy inference involves calculating the firing strength of rules by combining MF degrees ($\min()$ or $\prod()$ operations), thus triangular MFs simplify these operations due to their piecewise linearity [59, 61]. Table 3.5 details the MFs that make up the output BESS actions.

Table 3.5: Defining fuzzy outputs.

MF Name	Description	Range
Discharge	Represents the action of releasing stored energy from the battery to the grid or local load. The triangular MF peaks at maximum discharge rate with gradual decrease toward idle state, ensuring smooth transitions. Positive values indicate power flowing out of the battery.	0 to 300 kW
Idle	Represents a neutral state where the battery neither charges nor discharges significantly. This narrow band around zero accommodates minimal power flow to maintain system stability and prevents rapid switching between charge and discharge states.	-10 to 10 kW
Charge	Represents the action of storing energy in the battery from the grid or local generation. The triangular MF peaks at maximum charging rate with gradual increase from idle state, ensuring smooth transitions. Negative values indicate power flowing into the battery.	-300 to 0 kW

Step 3: Formulate Fuzzy Rules

A comprehensive set of fuzzy rules were developed to map the input variables to the output variable. These rules evaluate specific combinations of grid energy price, power balance ($P_{balance}$), and the SOC to determine appropriate BESS actions, as detailed in Table 3.6. The Mamdani Fuzzy Inference System (FIS) employed in this design relied on collective evaluation of all applicable rules to derive control decisions. The complete rule base consists of 18 rules, calculated by multiplying the membership functions of each input, 3 MFs for $P_{balance}$, 2 MFs for grid energy price, and 3 MFs for SOC, resulting in $3 \times 2 \times 3 = 18$ possible combinations. The rule base implemented a strategic energy management approach with three primary operational objectives:

1. For maximum PV utilization when positive $P_{balance}$ (surplus power), the BESS charges regardless of price or SOC, defined by rules 1 to 6, to maximize consumption of surplus PV power.
2. During balanced conditions (zero $P_{balance}$), the system remains idle, defined by rules 7 to 12, to minimize battery cycling.
3. For intelligent discharge, during negative $P_{balance}$ (deficit), the system discharges when grid energy prices are high regardless of SOC, except for $SOC < 30\%$ defined by rules 13 to 15, protects battery health by

remaining idle when grid prices are high but SOC is low, defined by rule 16, and lastly discharges to avoid expensive grid imports when prices are high with adequate SOC, defined by rules 17 to 18 in [Table 3.6](#).

Triangular MFs were adopted for their numerical simplicity and interpretability. Their piecewise linear form allows straightforward calculations of membership degrees during simulation, reducing computational overhead while maintaining smooth transitions between linguistic terms, for example, $P_{balance}$ transitioning between zero and negative. While trapezoidal or Gaussian MFs could offer marginally smoother transitions, triangular MFs strike a practical balance between precision and computational cost for simulations, as demonstrated in [\[60\]](#) for isolated multi-microgrid systems.

The maximum (max) method aggregates rule outputs, preserving the strongest contribution when multiple rules fire simultaneously for example, $P_{balance}$ transitioning between zero and negative. This approach, combined with overlapping triangular MFs, ensures smooth control behavior without abrupt switching. For instance, if $P_{balance}$ is slightly negative, SOC is medium, and the grid energy price is high, both Rules 16 (idle) and 17 (discharge) may activate. The max method prioritizes the rule with the highest firing strength, for example, favoring discharge over idle if SOC is sufficient. Similar aggregation strategies have been adopted in energy management systems, as demonstrated by [\[62\]](#) for FLC design and implementation.

In summary, the maximum method was used for rule aggregation, preserving the strongest rule contributions when multiple rules fire simultaneously. This approach, combined with overlapping triangular MFs, created smooth transitions between operating modes as input conditions gradually change. The complete rule base was systematically organized in [Table 3.6](#).

Table 3.6: Fuzzy rules for BESS action.

$P_{balance} = P_{PV} - P_{Load}$	Grid energy price	SOC	BESS Action	Rule
Positive	Low	Low	Charge	1
		Medium	Charge	2
		High	Charge	3
	High	Low	Charge	4
		Medium	Charge	5
		High	Charge	6
Zero	Low	Low	Idle	7
		Medium	Idle	8
		High	Idle	9
	High	Low	Idle	10
		Medium	Idle	11
		High	Idle	12
Negative	Low	Low	Idle	13
		Medium	Discharge	14
		High	Discharge	15
	High	Low	Idle	16
		Medium	Discharge	17
		High	Discharge	18

The original 18 rule set was reduced to 8 rules by eliminating redundant conditions where inputs had no impact on outputs. All positive $P_{balance}$ scenarios now trigger BESS action charge to prioritizing full utilization of surplus PV power after it has met the load demand. Zero $P_{balance}$ cases default to BESS action idle to minimizing battery cycling. Negative $P_{balance}$ rules were selectively kept, using grid energy price and SOC to decide between

discharging for cost savings and idling for BESS. This maintains system objectives while improving computational efficiency. The final rules are presented in [Table 3.7](#).

Table 3.7: Optimized fuzzy rules for BESS action.

$P_{\text{balance}} = P_{\text{PV}} - P_{\text{Load}}$	Grid energy price	SOC	BESS Action	Rule
Positive	-	-	Charge	1
Zero	-	-	Idle	2
Negative	Low	Low	Idle	3
Negative	Low	Medium	Discharge	4
Negative	Low	High	Discharge	5
Negative	High	Low	Idle	6
Negative	High	Medium	Discharge	7
Negative	High	High	Discharge	8

Step 4: Defuzzification

The final stage of the fuzzy decision-making process is defuzzification, which converts the aggregated fuzzy output into a single crisp control value. This process begins with the combination of all truncated output membership functions from the aggregation step, weighted by their respective rule firing strengths. The resulting aggregated membership function represents the overall fuzzy inference output.

To obtain a precise control action for the BESS, we apply the centroid (center of gravity) method, which calculates the defuzzified output y^* as:

$$y^* = \frac{\int y \cdot \mu(y) dy}{\int \mu(y) dy} \quad (3.31)$$

where $\mu(y)$ is the aggregated membership degree at output level y . Compared to alternatives like bisector or mean-of-maxima, the centroid method provides smoother output transitions particularly suited for BESS control while maintaining computational efficiency [63]. This ensures precise and stable control signals within the IEMS, as illustrated in the FLC structure diagram ([Figure 3.7](#)).

The piecewise linear nature of our triangular membership functions (from Step 3) enables efficient centroid calculation through geometric decomposition, requiring minimal computational resources for real-time implementation. This approach aligns with successful applications in fuzzy logic-based EMS documented in [64, 63].

3.5.5 FLC Design for Operation Mode and Load Control

A Sugeno fuzzy inference system (FIS) was designed for mode switching and load control due to its computational efficiency and precise binary output capabilities, making it more suitable than Mamdani systems for this application [6]. The defuzzification method, weighted average (wtaver) was selected for its simplicity in aggregating rule outputs.

System Structure

As seen in [Figure 3.8](#), there are three inputs namely grid energy price in R/kWh, power balance ($P_{\text{balance}} = P_{\text{PV}} - P_{\text{Load}}$) in kW and BESS SOC in (%)



Figure 3.8: Input membership functions (shared with Mamdani FLC) and structure of the Sugeno FLC.

There are two outputs of binary format namely PCC command (PCC_{cmd}) for switching between grid-connected (0) and standalone (1) modes, and load command ($Load_{cmd}$) for load disconnection, load shed (0) and maintaining load connection (1).

Membership Functions

The input membership functions use the same triangular forms as the Mamdani FLC defined in [Table 3.4](#) for design consistency, however, the outputs are constant MFs (0 or 1) replacing Mamdani's fuzzy outputs for structural efficiency

Rule Base

The system evaluates 18 rules as presented in [Table 3.8](#), adapted from Mamdani rule logic but optimized for binary outputs.

Key priorities include:

- Load connection is always maintained at when the grid energy price is low.
- Load is shedding under critical conditions (High grid energy price, negative $P_{balance}$ and low SOC)

The original 18 rule set in [Table 3.8](#) was optimized to 6 rules presented in [Table 3.9](#) through logical aggregation of cases with identical outputs. This preserves all system functionality while improving computational efficiency. The critical load shedding condition (high grid energy price, negative $P_{balance}$, low SOC) remains isolated as Rule 3 to ensure fail-safe operation.

The load connected is kept on when the $P_{balance}$ is zero because the transition is quick, hence, the load is kept on to prevent a spike or dip in the power profile of the load, as a result, the equilibrium state ($P_{balance}$) represents ideal zero power flow.

Table 3.8: Rules based on grid energy price, power balance, SOC, and commands

Grid energy price	P _{balance}	SOC	PCC_cmd	Load_cmd	Rule
Low	Positive	Low	Grid-connected	Load on	1
		Medium	Grid-connected	Load on	2
		High	Grid-connected	Load on	3
	Negative	Low	Grid-connected	Load on	4
		Medium	Grid-connected	Load on	5
		High	Grid-connected	Load on	6
	Zero	Low	Grid-connected	Load on	7
		Medium	Grid-connected	Load on	8
		High	Grid-connected	Load on	9
High	Positive	Low	Standalone	Load on	10
		Medium	Standalone	Load on	11
		High	Standalone	Load on	12
	Negative	Low	Standalone	Load shed	13
		Medium	Standalone	Load on	14
		High	Standalone	Load on	15
	Zero	Low	Standalone	Load on	16
		Medium	Standalone	Load on	17
		High	Standalone	Load on	18

Table 3.9: Optimized 6 rule Sugeno FLC

Grid energy price	P _{balance}	SOC	PCC	Load	Rule
Low	-	-	Grid-connected	Load on	1
High	Positive	-	Standalone	Load on	2
High	Zero	-	Standalone	Load on	3
High	Negative	Low	Standalone	Load shed	4
High	Negative	Medium	Standalone	Load on	5
High	Negative	High	Standalone	Load on	6

3.6 Simulation Model for Test Microgrid and IEMS

This section outlines the simulation model used for the test microgrid. It further provides the simulation approach followed, and lastly integrates the test microgrid with the FLC.

3.6.1 Simulation Model

The simulation model was developed using standard components from the MATLAB Simulink Simscape library [65]. The grid connection was modeled using a three-phase voltage source paired with a three-phase circuit breaker, representing the point of common coupling (PCC) as illustrated in Figure 3.9. This setup ensures stable power supply integration with the microgrid components.

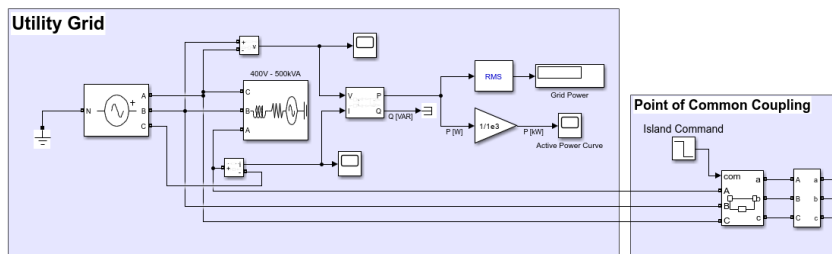


Figure 3.9: Utility grid simulation model.

The PV system was implemented using a three-phase dynamic load block [Figure 3.10a](#). PV data obtained from sizing was directly fed into this subsystem, allowing the simulation to accurately reflect the output without requiring data type conversions.

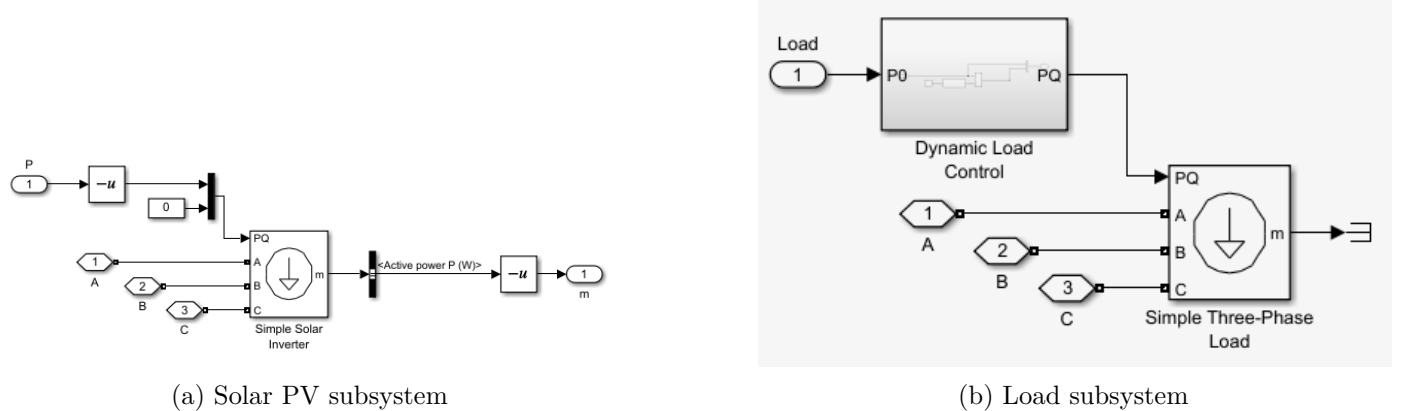


Figure 3.10: Simulation models.

A variable three-phase dynamic load was employed to model the consumer demand profile [Figure 3.10b](#). The dynamic load control accepts raw load profile data from MATLAB workspace. This approach simplifies integration without additional data pre-processing.

The BESS model in [Figure 3.11a](#) regulates battery current through a controlled variable load. Key configurable parameters include SOC limits for charge and discharge control, initial SOC, power rating (kW), and energy capacity (kWh), charge/discharge efficiency and rate constraints. This flexible design allows precise tuning of storage behavior under different operating conditions.

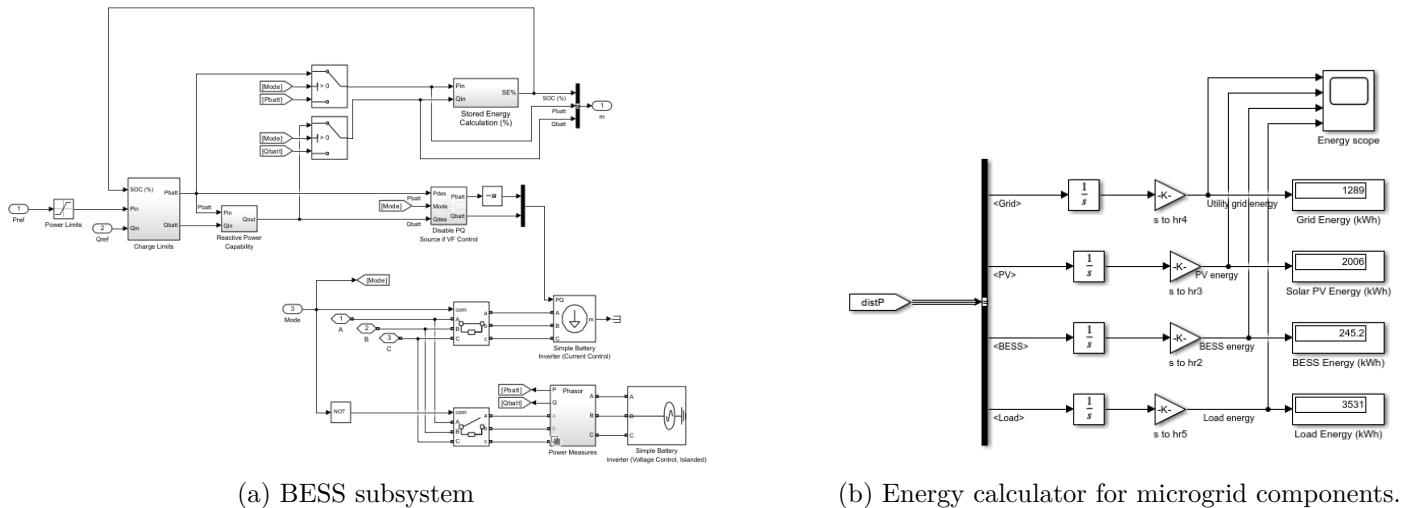


Figure 3.11: Simulation models.

[Figure 3.11b](#) used the power signal output from each component, and integrated each one of them to determine the energy. A gain block was used to convert the seconds to hours to achieve consistent energy units of kWh.

[Figure 3.12](#) used from tags taken from the measurement ports of the microgrid components. The from tags such as Vgrid, Igrid, Vload, Iload were fed into the Phasor Sequence Analyzer to determine the real power of the

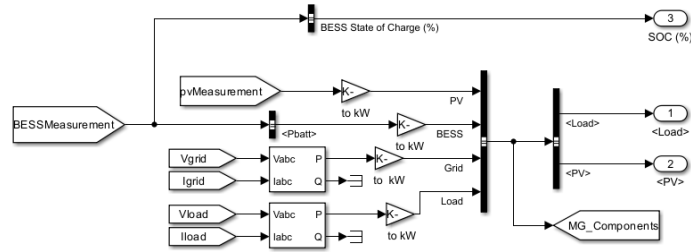


Figure 3.12: Microgrid measurement signals.

utility grid and load. The load voltage is measured using the 3 phase measurement. A bus creator was used to combine the signals for PV, BESS, Grid, Load into a goto tag call MG_Components.

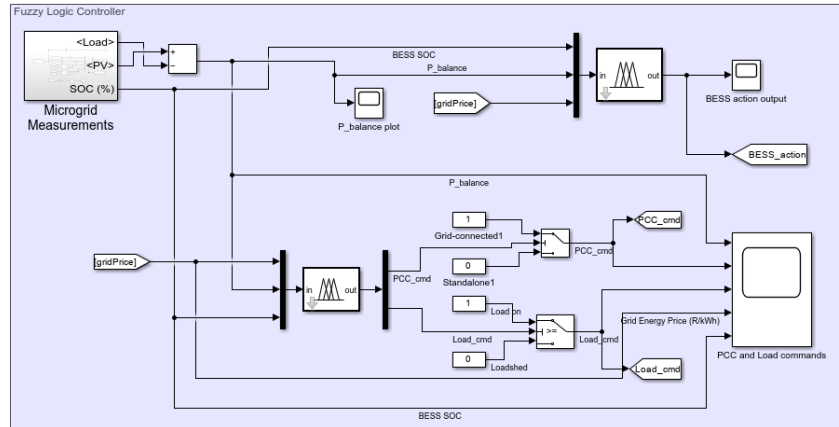


Figure 3.13: Fuzzy logic simulink model.

Figure 3.13 illustrates the FLC model. From the microgrid measurements subsystem, the signals are Load, PV and SOC. The PV and Load signals passed through the subtract block to obtain $P_{balance}$, the difference between PV power and load power. A mux block was used to combine all the $P_{balance}$, SOC and grid energy price signals into one signal which were fed to the FLC blocks. The output of the Mamdani FLC is BESS_action, the Sugeno FLC output went through a demux block to obtain PCC_cmd and Load_cmd. These two signals were then fed into switch blocks, this was done to ensure the return either 0 or 1.

3.6.2 Simulation Approach

The simulation approach involved several steps. Initially, the data were obtained from section 3.2 and sizing data from subsection 3.4.6. The data were processed by standardizing it and was imported into MATLAB workspace as arrays. A test microgrid was developed using MATLAB-Simulink. Mamdani's and Sugeno's Fuzzy Inference System (FIS) were adopted for designing the IEMS using the MATLAB FL Designer. The IEMS was then implemented on the test microgrid in MATLAB-Simulink. The process is summarized in Figure 3.14

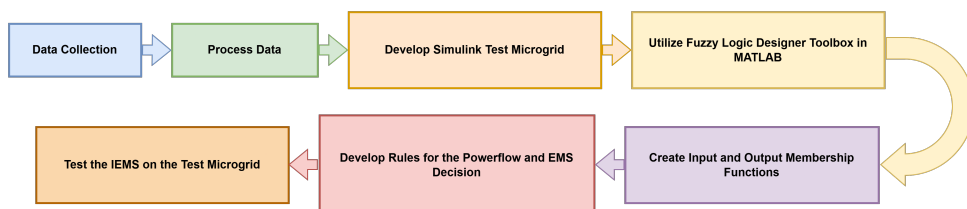


Figure 3.14: Overall simulation steps and approach

3.6.3 Integration of Test Microgrid and IEMS

Figure 3.15 shows an integration diagram of the FLC with the microgrid. The figure also annotates the interconnection of the microgrid and FLC. Raw data flow is the data obtained inputted from excel. Power flow is the direction of power within the microgrid. PV, BESS and utility power the load, while BESS absorbs power from PV to charge. Lastly, the simulation data flow is the connection of the Simulink signals with the rest of the subsystems. The FLC IEMS tracks the BESS SOC, grid energy price and the difference between PV generation and load demand to perform its decisions.

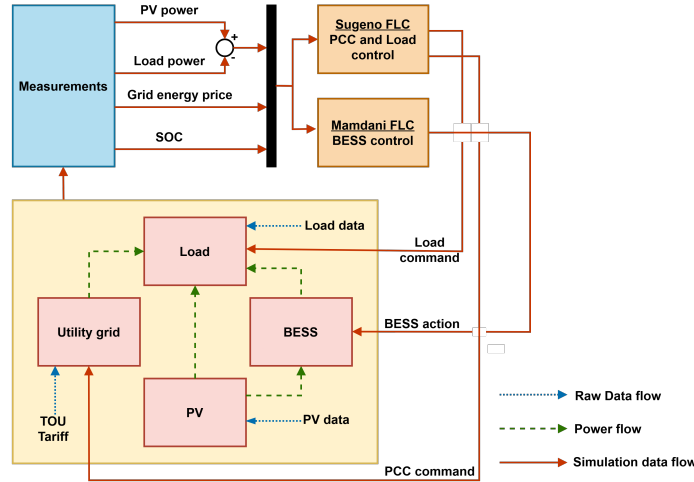


Figure 3.15: Test microgrid with FLC integration.

The final simulation integrated all subsystems, illustrated in Figure 3.16.

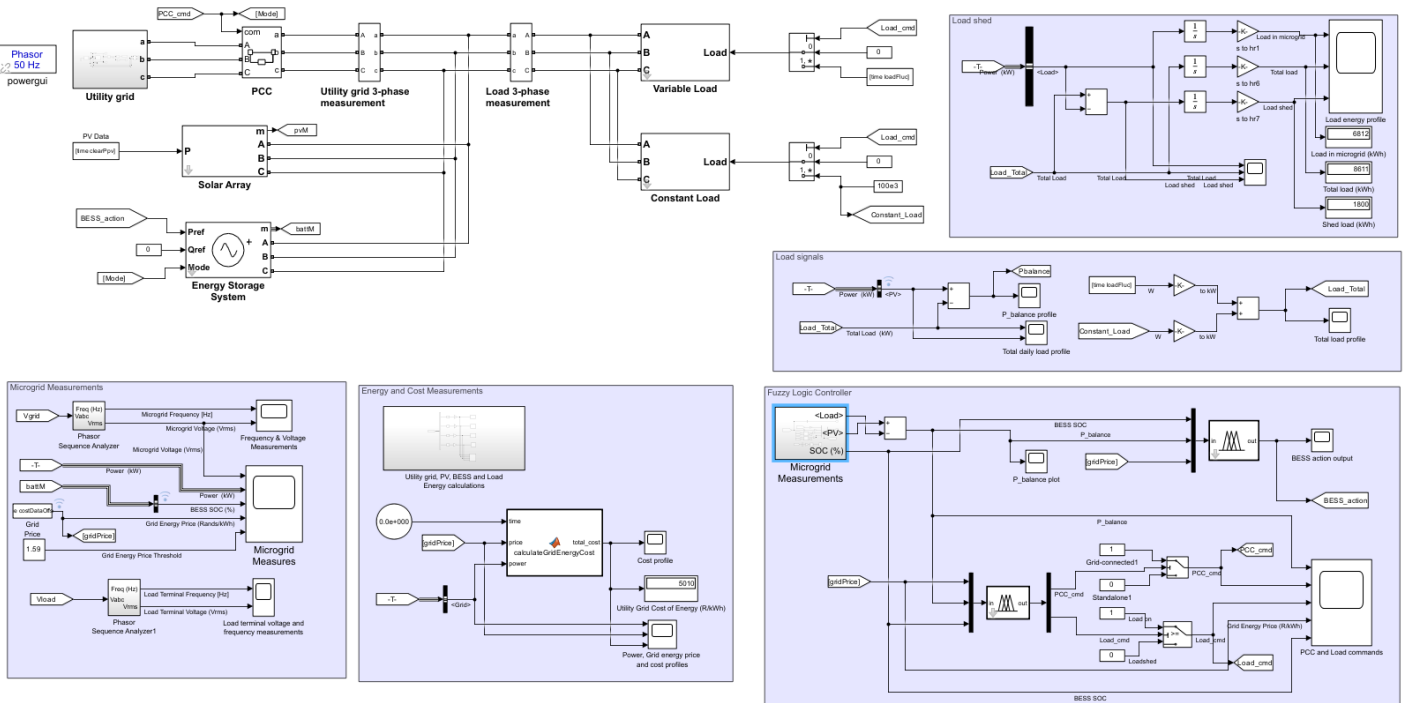


Figure 3.16: Microgrid model with fuzzy logic.

The microgrid model was implemented in phasor mode to enable computationally efficient long-term analysis.

Phasor representation eliminates the need to simulate instantaneous AC waveforms by modeling sinusoidal quantities as rotating vectors with magnitude and phase components. This approach reduced computational complexity while maintaining accuracy for steady-state power flow analysis, voltage regulation analysis, and energy management optimization.

As a result, the 86400 second (24 hour) simulation duration was achieved through variable time-step integration and averaged component models. The simulation uses adaptive time stepping, taking larger steps during steady-state conditions and smaller steps only during system transients. Component models are PQ simulation (Power Quality simulation) focusing on the steady-state performance of the power grid, instead of EMT simulation (Electromagnetic Transient simulation) which focuses on the dynamic behavior of the grid, particularly during transient events like switching. Thus, this enables long simulations for microgrid and IEMS performance evaluation.

3.7 Case Study Development

This subsection presents a structured set of case studies developed to evaluate the operational performance and decision-making capabilities of the proposed IEMS under various scenarios. Each case study is designed to simulate specific operating conditions of a hybrid microgrid, enabling targeted analysis of system responses such as power source coordination, cost analysis, and power quality at load terminals under dynamic load changes. The case studies to be investigated and their objectives are listed as follows:

3.7.1 Case 1: Base Model with no BESS and FLC

This case study will investigate the baseline performance without integration of FLC and BESS. This case study will observe the power flow of the utility grid and PV. Metrics such as the Renewable Factor (RF) and cost profile of the utility grid will be investigated. The significance of this study to highlight the need of battery storage.

3.7.2 Case 2: Modified Base Case without FLC IEMS

This case study will investigate a modified model of the microgrid with BESS, with no FLC integration. This is to evaluate the how the sources manage power flow without any intelligent algorithm. The metrics that will be observed are the BESS charging and discharging patterns without the energy management, RF, and the cost profile of the utility grid. This is to highlight the need for an intelligent EMS to manage BESS charging and discharging to improve cost-effectiveness of utilizing the grid under low TOU tariff.

3.7.3 Case 3: Operation Mode Selection on TOU with Varying Load

This case study will evaluate the FLC IEMS performance under microgrid sizing conditions. Key analysis will be to observe the effectiveness of the microgrid mode of operation transition, renewable energy prioritization, BESS SOC management, the RF and the cost profile of the utility grid with FLC integrated. The significance of this study to highlight the benefits of an intelligent algorithm for energy management.

3.7.4 Case 4: Operation Mode Selection on TOU with Varying Load and Constant Load

This case study will evaluate the FLC IEMS performance under additional load conditions. Key analysis will be to observe load shedding implementation, and power sharing under constrained resources. Furthermore, the RF and the cost profile will be analyzed. The power quality will be investigated when loads are disconnected.

Table 3.10 presents a summary of the case study providing the evaluation matrix.

Table 3.10: Case study evaluation summary.

Case	Conditions	Key Metrics	Evaluation Focus
1	No BESS, no FLC	Grid dependence, RF, costs	Baseline establishment
2	BESS, no FLC	SOC management, degradation risks	Uncontrolled storage behavior
3	Standard operation	Mode transitions, TOU response, power quality, cost savings	Core FLC performance
4	Increased load	Load shedding, resource allocation	System capacity limits

Chapter 4

Results and Analysis

This section evaluates the function of the fuzzy logic controller (FLC) intelligent management system (IEMS) through a series of case studies. Four cases were presented and each of them analyze the performance of the FLC IEMS in terms of power flow of the microgrid components, BESS SOC dynamics, power quality at load terminals, and energy calculations. An evaluation of the FLC IEMS was made, highlighting its strengths and weaknesses in the context of this project, and whether it met the technical requirements. The results are in the form of plots and calculations. Each plot was plotted against time in hours, covering 24 hours. The time axis was real numbers with long decimals. The whole number represented hours and the decimal part was converted to minutes by multiplying by it 60.

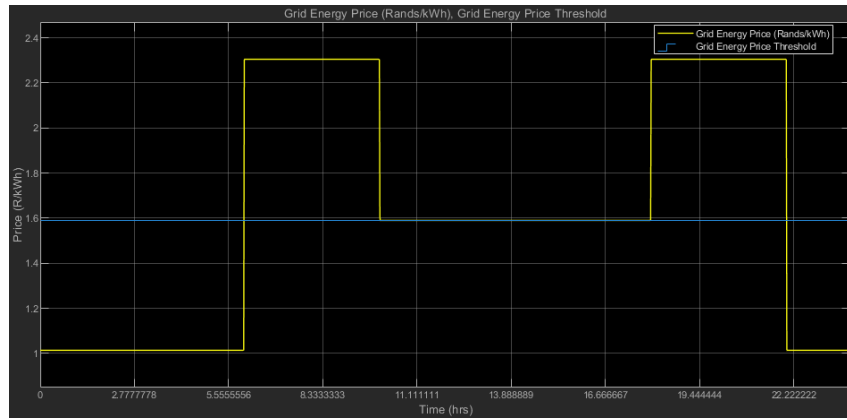


Figure 4.1: Grid energy price TOU scheme.

All case studies used the same TOU tariff as illustrated in [Figure 4.1](#). This figure shows a grid energy price profile with the threshold energy price set at R1.59/kWh. The ToU tariffs in [Figure 4.1](#) showed two peak periods from 06:00 to 10:00 and 18:00 to 22:00, two off peak periods from 00:00 to 06:00 and 22:00 to 00:00, and a standard period from 10:00 to 18:00.

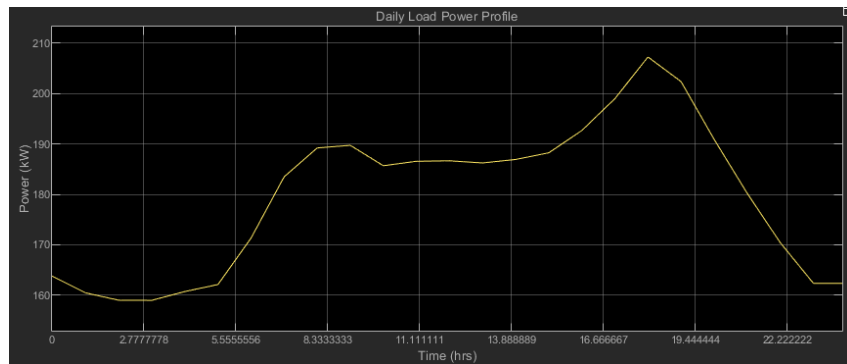


Figure 4.2: Daily load profile.

[Figure 4.2](#) illustrates the daily load profile with low peaks at 02:42 of size 159 kW. High peaks were observed at

08:36 of size 189.5 kW and 18:00 of size 207.1 kW, the load profile was from the load sizing in [subsection 3.4.6](#).

4.1 Case 1: Base Case without FLC IEMS and Battery Storage

4.1.1 Objective

The objective of this case study was to evaluate the power flow, power quality, and energy calculations when the FLC IEMS and BESS was not implemented. The purpose is to establish a baseline performance of the microgrid system operating without intelligent energy management and battery storage, which will serve as a reference point for comparison with subsequent cases where the FLC IEMS and BESS are integrated. This baseline assessment focuses on capturing system behavior under standard operating conditions, including load variation, renewable energy intermittency, utility grid utilization pattern. The analysis aims to identify potential inefficiencies, cost issues, and energy utilization metrics that could potentially be improved through intelligent control strategies in later case studies.

4.1.2 Simulation Setup

The simulation was ran for 86400 seconds to model a full day. The microgrid components were connected without the FLC IEMS and BESS integration, as a results only three components were connected, utility grid, PV, and load. The microgrid was set to be always grid-connected during all TOU tariff periods.

The BESS parameters were as follows:

- Rated Power: 0 kW, to model no contribution of BESS.

4.1.3 Power Flow Analysis

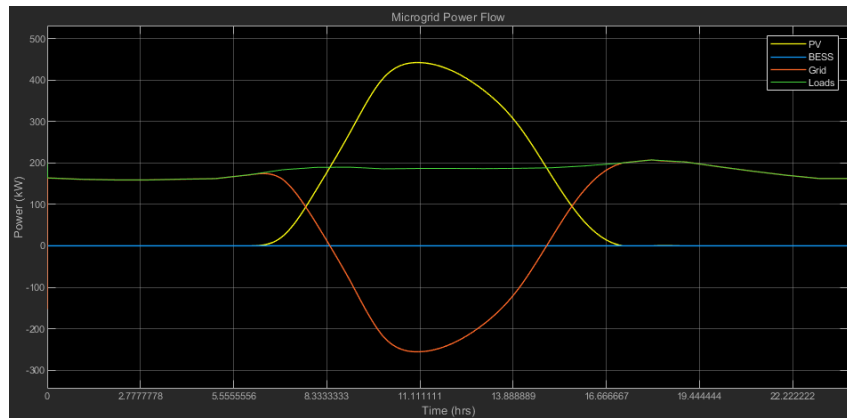


Figure 4.3: Microgrid power profiles.

The power flow plot's significance in [Figure 4.3](#) was to illustrate the microgrid's operation under the ToU tariff without battery storage. From 00:00 to 06:24, the grid supplied the entire load since PV generation was unavailable. Despite the tariff shifting to peak at 06:00, the grid remained the sole power source until PV generation begins at 06:24.

At 08:26, PV generation matched the load demand (intersection point), and surplus was exported to the grid, causing the utility profile to drop below zero. This export continued until 14:53, when PV generation decreased, requiring grid support again. After 17:10, with no PV generation, the grid supplied the entire load, including during peak tariff hours from 18:00 to 22:00.

Since the grid and PV met all the load demand, no load shedding occurred under this case study. However, this case results in higher electricity costs during peak hours, to be later discussed in the energy calculations section.

4.1.4 Power Quality Analysis

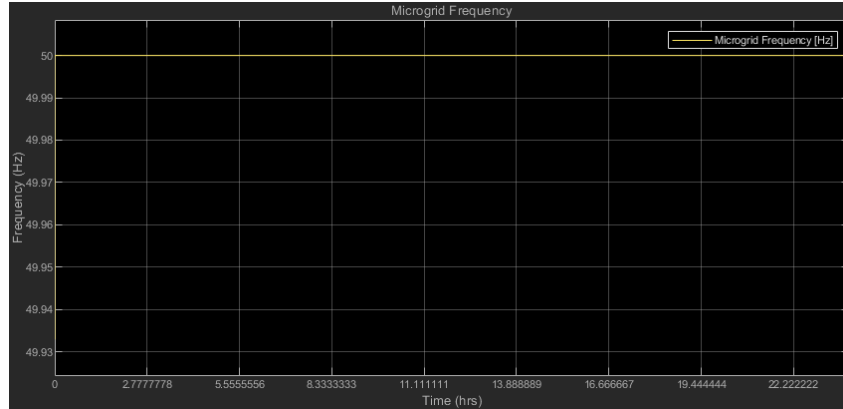


Figure 4.4: Microgrid frequency profile.

The frequency profile in figure 4.4 remained constant at 50 Hz as a result of seamless DER power sharing. A stable constant frequency profile indicated a good power quality as there was zero frequency fluctuations, keeping within the frequency limits stated in Equation 3.30 of 49.5 Hz to 50 Hz.

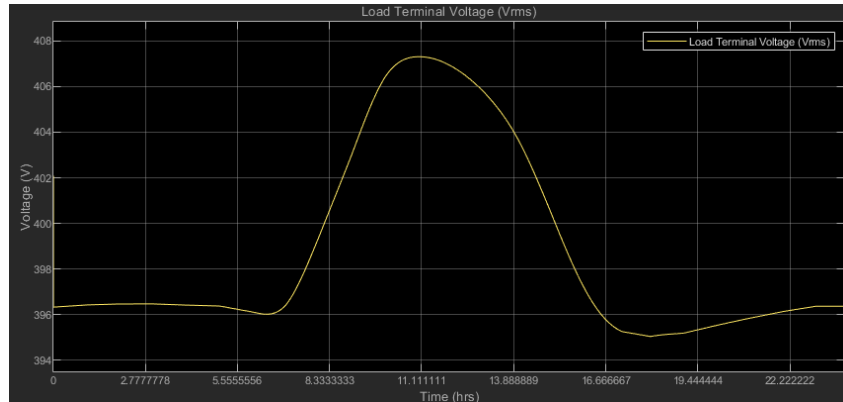


Figure 4.5: Load terminal voltage profile under varying PV generation conditions.

The nominal voltage of the microgrid and the load was set to 400 V. As shown in Figure 4.5, the voltage exhibited fluctuations due to PV power variations. The maximum voltage of 407.3 V occurred at 10:46, corresponding to a +7.3 V deviation from the nominal value. Conversely, the minimum voltage of 395.1 V was recorded at 18:16, resulting in a -4.9 V deviation. The total voltage fluctuation range was determined to be $407.3 - 400 = 7.3$ V, and was within permissible limits of ± 10 V as defined by Equation 3.29.

The voltage profile exhibited a swell-like characteristic, closely following the PV power generation pattern. This correlation indicated that PV injection directly influenced the voltage regulation, with higher solar generation increased voltage due to reduced grid dependency, while lower generation periods lead to voltage dips. As a result of the total voltage fluctuation was within ± 10 V, this case was complaint with the SAGC.

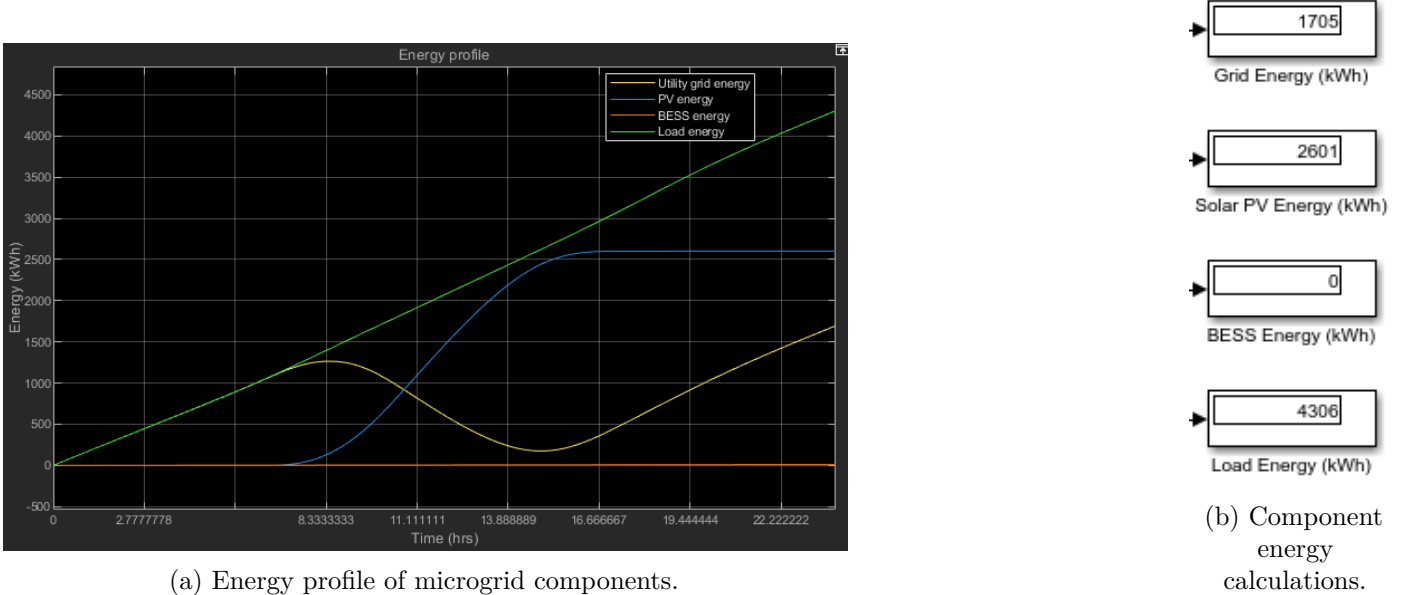


Figure 4.6: Energy profiles and calculations.

4.1.5 Energy Calculations

Figure 4.6a shows the energy profile of each component in the microgrid. The significance of this plot was to show the total accumulated energy consumption of the load compared to the energy of the utility grid, and PV.

The total energy supplied from the utility grid was 1705 kWh, 2601 kWh for PV, 0 kWh for BESS, with the load energy demand at 4306 kWh as seen in figure 4.6b. The total combined energy supply was 4306 kWh, matching the load demand. PV contributed 60.40% to the load demand, BESS 0%, and the utility grid 39.60%. This resulted in 60.40% of the load demand being met by PV only

Figure 4.6b presented the energy calculations of each microgrid component, which were significant in evaluating renewable utilization such as Renewable Factor (RF) metric defined in Equation 3.27. The RF quantifies the proportion of the electricity demand met by the renewable sources such as PV and BESS, offering critical insights as to how much demand is fulfilled by the renewable sources

Using Equation 3.27

$$RF(\%) = \left(1 - \frac{\sum P_{grid}}{\sum P_{renewable}}\right) \times 100$$

Values from Figure 4.6b were substituted

$$RF = \left(1 - \frac{1705}{2601 + 0}\right) \times 100 = 34.45\%$$

A desirable value of RF was 100%, however this case achieved a RF of 34.45%, indicating that 34.45% of the total energy supply was renewable, with 65.55% reliance on the utility grid.

Figure 4.7 correlated the grid cost profile to the TOU tariff with grid power usage. Higher cost periods (morning and evening peaks) align with increased grid dependency. From Figure 4.7, the cost profile increased from 00:00 until 08:00 in a linearly pattern due to power import from the utility grid. It remained flat from 08:00 to 15:09 due to the utility grid absorbing excess power from the PV. After 15:09, the cost profile increased in a linearly pattern, indicating import of power from the utility grid. The total cost of energy for utility grid usage was R4437.00.

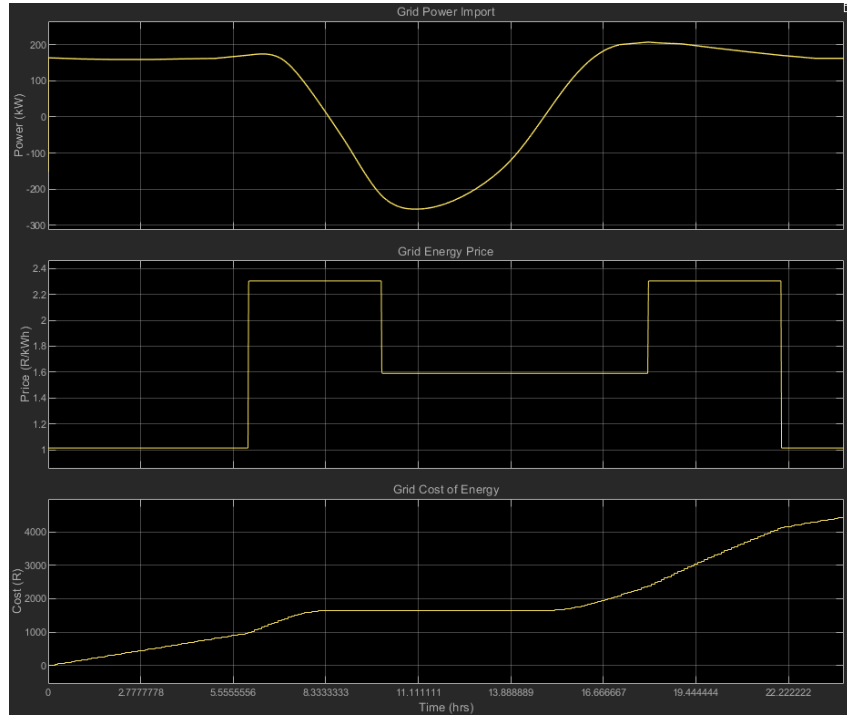


Figure 4.7: Grid power, TOU tariff, and utility grid cost profile.

4.1.6 Evaluation of Base Case

The base case simulation without the FLC IEMS provided key insights into the microgrid's default operation over a 24-hour period.

Key findings from the power flow indicated that the microgrid remained grid-connected throughout, with the utility grid supplying power during non-PV generation hours. Excess PV power from 08:26 to 14:53 was exported to the grid rather than stored. The microgrid maintained acceptable power quality with frequency stable at 50 Hz and voltage fluctuations within limits, with total deviation of 12.2 V from the nominal voltage of 400 V (Vrms).

The energy distribution indicated that the load demand was 4306 kWh, PV contribution was 2601 kWh (60.40%), and the utility grid contribution was 1695 kWh (39.36%), with an achieved renewable factor (RF) of 34.45%. From the economic performance, the total energy cost of the utility grid was R4426.00, without economic optimization during the peak TOU periods.

Major inefficiencies included no BESS usage as the excess PV energy exported instead of stored. There was a high grid dependency during costly peak TOU periods. Lastly, the a low RF was achieved, as a result poor renewable utilization without storage and intelligent algorithm.

This baseline case demonstrates the need for an IEMS to improve operational efficiency, increase renewable energy utilization, and reduce costs. The FLC IEMS implementation in subsequent cases should address these identified inefficiencies by strategically controlling BESS operation, and optimizing power flow during different TOU periods.

4.2 Case 2: Modified Base Case without FLC IEMS

4.2.1 Objective

The objective of this case study was to evaluate the power flow, BESS SOC dynamics, power quality, and energy calculations when the FLC IEMS was not implemented. The purpose was to establish a baseline performance of the microgrid system operating without intelligent energy management, which will serve as a reference point for comparison with subsequent cases where the FLC IEMS was integrated. This baseline assessment focuses on capturing microgrid behavior under standard operating conditions from the microgrid sizing in [subsection 3.4.6](#), including load variation, renewable energy intermittency, and battery storage utilization pattern. The analysis aims to identify potential inefficiencies, power quality issues, and energy utilization metrics that could potentially be improved through intelligent control strategies in later case studies.

4.2.2 Simulation Setup

The simulation was ran for 86400 seconds to model a full day. The microgrid components including BESS were connected without the FLC IEMS integration. The microgrid was set to be always grid-connected during peak TOU tariff periods.

The BESS parameters were as follows:

- Initial SOC: 50%
- Minimum SOC Limit: 30%
- Maximum SOC Limit: 90%
- Rated Power: 300 kW, obtained from BESS sizing.
- Rated Capacity: 3000 kWh, obtained from BESS sizing.

4.2.3 Power Flow Analysis

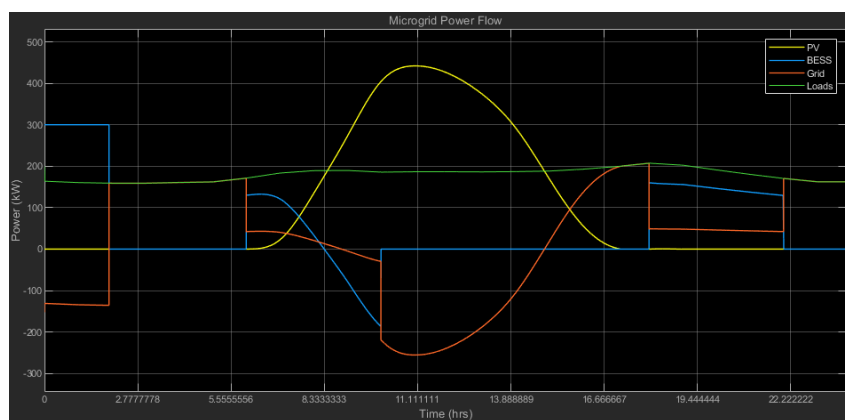


Figure 4.8: Microgrid power flow profiles showing contributions from PV, BESS, grid, and loads.

The power flow in [Figure 4.8](#) is analyzed as follows:

- 00:00 to 02:00: The BESS discharged to power the loads while exporting excess energy to the grid as the grid power flow was negative. After 02:00, the BESS stopped discharging, and the grid became the sole power source until 06:00.

- 06:00 to 08:30: PV generation began, supplementing the grid and BESS to meet load demand. The BESS reduced its discharge as PV output increases, transitioning to charging at 08:20. The grid's power import decreased until 08:45, when it started absorbing surplus PV power (grid power flow becomes negative).
- 08:30 to 10:00: PV generation fully met the load at 08:25, after which excess PV power charged the BESS and was exported to the grid. At 10:00, the BESS stopped charging (power drops to 0 kW), causing the grid to absorb more PV power as the utility grid power drops to -219.9 kW.
- 10:00 to 14:50: The grid absorbed surplus PV power. After 14:50, PV generation no longer met the load demand, and the grid resumed importing power to supplement the PV.
- 17:30 to 18:00: PV generation stopped, leaving the grid as the sole power source. From 18:00 to 22:00, the BESS discharged again, reducing grid reliance. After 22:00, the BESS stopped discharging, and the grid met the entire load.

The key observations were that the BESS prioritized load powering and excess export during low PV generation. PV surplus was first used to charge the BESS, then exported to the grid.

4.2.4 BESS SOC Dynamics

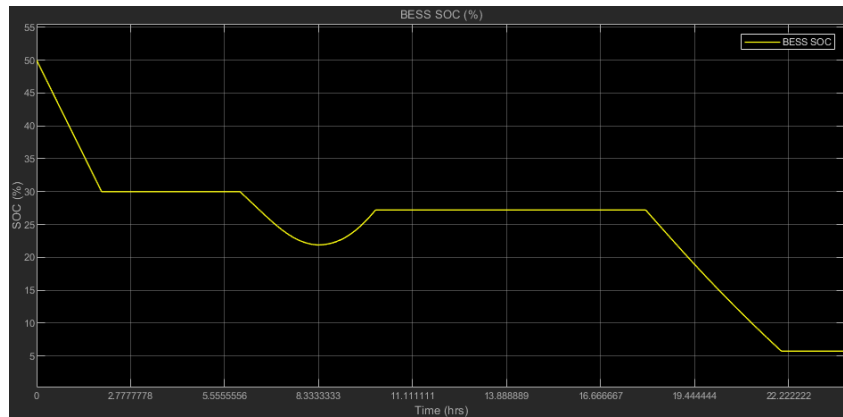


Figure 4.9: BESS SOC profile.

In figure 4.9, the BESS SOC linearly decreased from its initial SOC from 50% to its minimum limit 30% from 00:00 to 01:56, and remained idle until 06:00. From 06:00 to 08:23, it discharged from 30% to 22%, and began charging from 22% to 27% from 08:23 till 10:00 as seen in figure 4.9. The SOC profile then remained constant at 27% from 10:00 to 18:00, indicating that the BESS was not charging. From 18:00 to 22:00, the SOC decreased linearly, indicating the BESS discharged from 27% until 5.71%, and then remained constants at 5.71% from 22:00 onward as illustrated in figure 4.9.

Key observations:

- Uncontrolled discharge patterns with multiple deep discharge cycles
- More aggressive energy depletion during off peak hours

4.2.5 Power Quality Analysis

There was a frequency dip at 01:54 of size 49.945 Hz. A frequency spike occurred at 06:00 of size 50.035 Hz. Another frequency spike occurred at 10:00 with a magnitude on 50.046 Hz. Another frequency spike was recorded

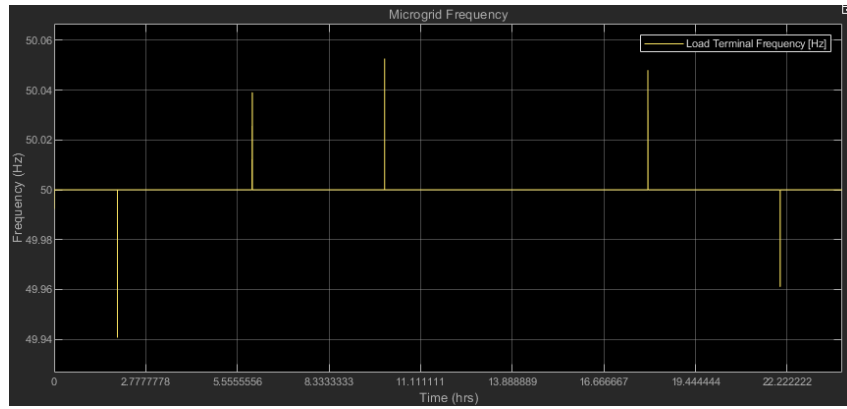


Figure 4.10: Microgrid frequency profile.

at 18:00 of size 50.043. Lastly, a frequency dip of 49.958 occurred at 22:00 as seen in [Figure 4.10](#). The frequency dips were due to the utility grid importing power to the microgrid, the the spikes were due to the it absorbing power from the BESS or reducing the grid power import. As a result, the minimum frequency fluctuation was $50 - 49.945 = 0.055$ Hz, and the maximum frequency fluctuation was $50.046 - 50 = 0.046$ Hz.

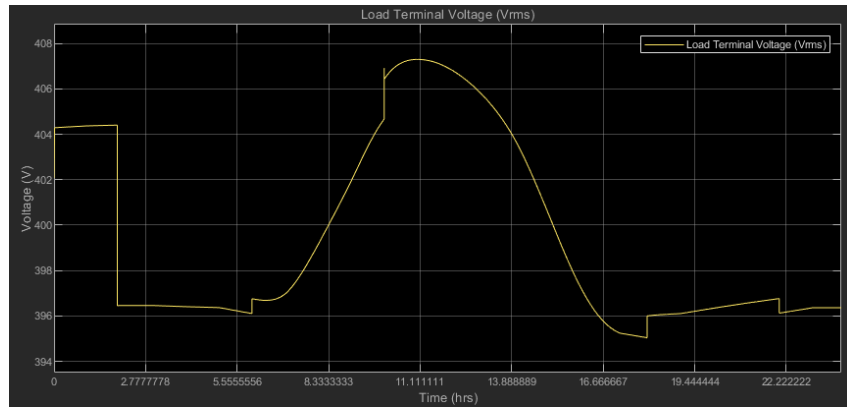


Figure 4.11: Load terminal voltage profile.

The load terminal voltage profile in [Figure 4.11](#) showed significant fluctuations around the nominal voltage of 400 V. At 00:00, the voltage started at 402.1 V, slightly above nominal, and quickly rose to 404.3 V. By 01:54, it peaked at 404.4 V before sharply dropping to 396.5 V, due to power sharing by the BESS and utility grid. During the early morning (01:54 to 06:00), the voltage remained below nominal, hovering around 396.1 V to 396.7 V, due to utility grid supply solely supplying the load. At 10:00 to 11:00 overvoltage conditions occurred, with the voltage climbing from 404.6 V to 406.5 V and peaking at 407.3 V by 11:00, likely due to peak power injection from PV. In the evening (18:00 to 22:00), the voltage dipped to its lowest point of 395 V at 18:00 before a slight recovery to 396 V, reflecting high evening demand. By 22:00, another drop occurs from 396.8 V to 396.1 V, further highlighting instability during peak periods. Total voltage fluctuation were $407.3 - 400 = 7.3$ V, within the voltage limits defined in [Equation 3.29](#), hence, this case was compliant with the SAGC.

4.2.6 Energy Calculations

The energy flow dynamics of the microgrid are analyzed in this section, with key observations from [Figure 4.12](#). The utility grid exhibited bidirectional energy flow throughout the day:

- 00:00 to 03:32: Energy values below zero indicated power absorption from the BESS.
- 03:32 to 12:00: Positive energy values showed power import to the load.

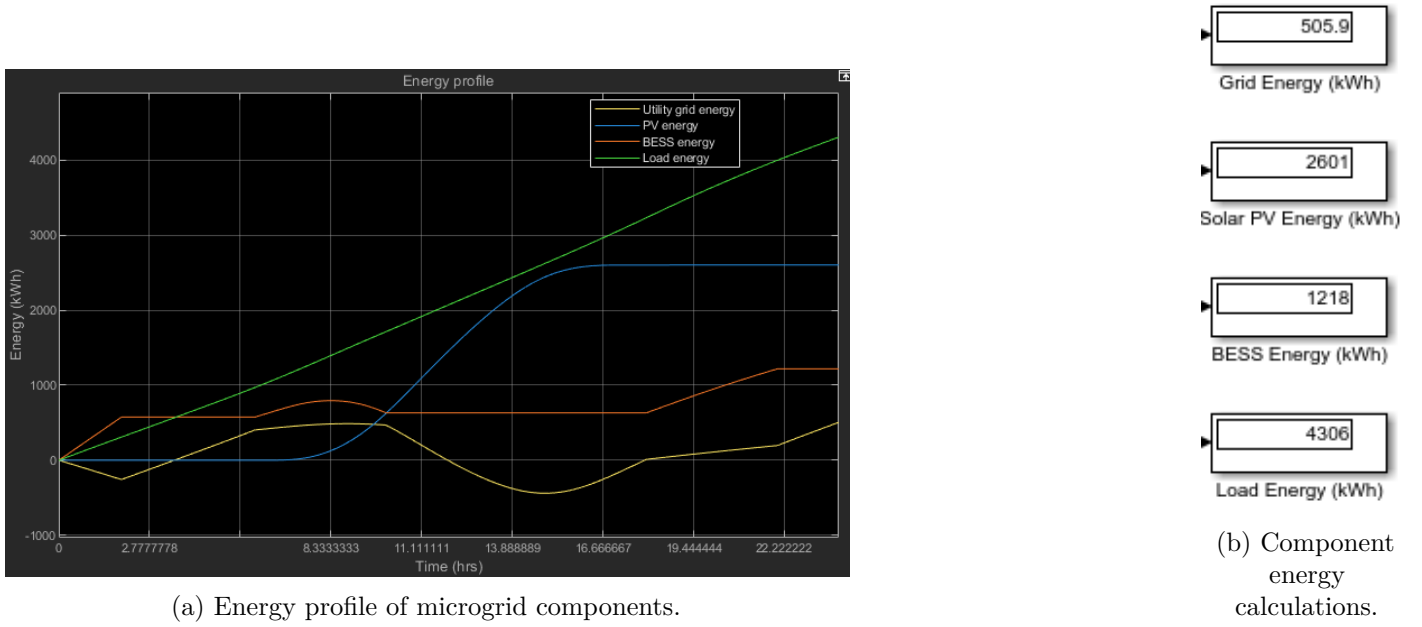


Figure 4.12: Energy profiles and calculations for the base case.

- 12:00 to 18:00: The grid absorbed surplus PV energy, followed by power export to the microgrid from 14:49 to 8:00.
- After 18:00: Linear energy increase demonstrated grid support for evening demand.

The total energy contributions from the utility grid was 505.9 kWh (11.75% of load demand), PV system was 2601 kWh (60.40%) and BESS was 1218 kWh (28.29%). The total energy supply of 4324.9 kWh exceeded the load demand of 4306 kWh by 18.9 kWh, with PV and BESS collectively meeting 88.69% of the demand.

The Renewability Factor (RF) was calculated as:

$$RF(\%) = \left(1 - \frac{\sum P_{\text{grid}}}{\sum P_{\text{renewable}}}\right) \times 100 = \left(1 - \frac{505.9}{2601 + 1218}\right) \times 100 = 86.75\%$$

While the 86.75% RF suggested strong renewable penetration, this value was exaggerated by the abnormal BESS discharging patterns. Firstly, the BESS operation exceeded its safe limitations of 30%, and secondly, it discharged to the grid instead of the load only.

From Figure 4.13, the cost profile was constant from 00:00 until 01:57 since the cost function considers power grid power. Power export to the grid have different tariffs to the one the study uses. Ultimately, the goal of the report was to determine cost related to using the utility grid, not cost benefits of exporting to the utility grid. At 01:57, it increased in a linearly pattern, indicating grid power import to the microgrid. It then curved and remained flat until 15:00 indicating there was power export to the utility grid. After 15:00, it increased until 24:00. The total cost of energy for utility grid usage was R2317.00

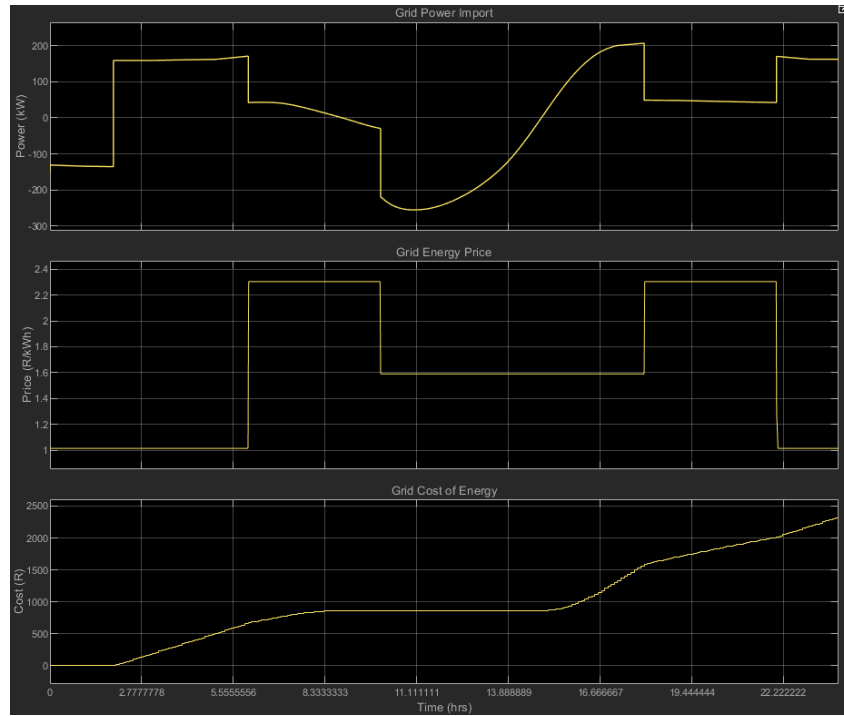


Figure 4.13: Grid power, grid energy price and cost of energy profile.

4.2.7 Evaluation of Modified Base Case

The microgrid successfully maintained power supply using PV, BESS, and grid support. PV contributed 60.4% of total demand, demonstrating strong renewable integration. The BESS provided 28.3% of energy, reducing grid reliance.

The shortfalls of this case was the BESS management, where it discharged below the 30% SOC limit, reaching 5.71%, risking damage. The charging was insufficient, leaving SOC at only 27% despite available PV surplus. Even though the cost of utilizing the grid was low relative to case 1, this was due to the BESS power being absorbed by the utility grid, displaying poor discharging due to the absence of the FLC IEMS. The calculated RF of 86.75% was misleading due to excessive BESS discharge to the grid rather than load support.

This modified case demonstrates the need for an IEMS to improve operational efficiency, increase renewable energy utilization, and reduce costs. The FLC IEMS implementation in subsequent cases should address these identified inefficiencies by strategically controlling BESS operation, and optimizing power flow during different TOU periods.

4.3 Case 3: Mode Selection on a TOU tariff with Varying Load

4.3.1 Objective

The objective of this case study was to evaluate the performance of the FLC in selecting the correct mode of operation for the microgrid based on ToU grid energy pricing scheme, and scheduling the DERs to meet load demand with PV meeting most of the load demand. The type of load assessed in this case study is a varying load of a small factory as described in chapter 3.

4.3.2 Simulation Setup

The simulation was ran for 86400 seconds to model a full day. A varying load type was connected. The FLC was connected to the PCC for selecting the mode of the microgrid, it was also connected at the load side to select whether the load is shed or not, and also connected at the BESS power input to schedule it charging or discharging.

The BESS parameters were as follows:

- Initial SOC: 50%
- Minimum SOC Limit: 30%
- Maximum SOC Limit: 90%
- Rated Power: 300 kW, obtained from BESS sizing.
- Rated Capacity: 3000 kWh, obtained from BESS sizing.

4.3.3 Power Flow Analysis

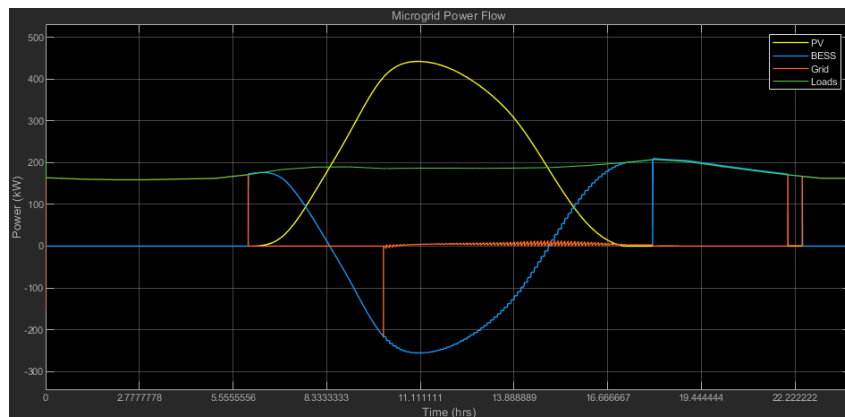


Figure 4.14: Microgrid power profiles.

The purpose of [Figure 4.14](#) was to illustrate the power profiles of all microgrid components under the Time-of-Use (ToU) tariff and to analyze the power flow behavior in each component. From 00:00 to 06:00, the utility grid alone supplied the load demand because the photovoltaic (PV) system did not generate power during this period. The Battery Energy Storage System (BESS) remained idle, neither charging nor discharging. During this interval, the microgrid operated in grid-connected mode under the off-peak ToU tariff of R1.014/kWh.

At 06:00, the ToU tariff shifted to peak pricing, prompting the utility grid to disconnect. The microgrid transitioned to standalone mode, which was evident from the instantaneous drop in the utility grid's power to 0 kW in [Figure 4.14](#). In standalone mode, the PV system began generating power but could not fully meet the load demand. As a result, the BESS started discharging at 06:00, indicated by a positive power flow in the figure. From 06:00 to 08:26, the load demand was jointly met by the PV system and the BESS.

At 08:26, the load profile intersected the PV profile, resulting in a power balance ($P_{\text{balance}} = P_{\text{PV}} - P_{\text{Load}}$) of zero. At this point, the BESS power flow reversed polarity from positive (discharging) to negative (charging). From 08:26 to 14:53, the PV system alone satisfied the load demand, with surplus power charging the BESS. The BESS power profile closely followed the PV profile, confirming that all excess power was directed to the BESS.

At 10:00, the microgrid reverted to grid-connected mode when the ToU tariff reached the standard pricing threshold. This reconnection caused a brief dip in the utility grid's power profile. However, since the PV system was already meeting the load, the utility grid's power spiked momentarily before returning to 0 kW.

From 15:00 to 18:00, the BESS discharged again (positive power profile), working alongside the PV system to supply the load. After 18:00, PV generation ceased, leaving the BESS as the sole power source until 22:24, as shown in [Figure 4.14](#).

At 22:00, the utility grid's power profile spiked, marking the microgrid's transition back to grid-connected mode. By 22:24, the BESS was fully depleted, and with no PV generation, the utility grid supplied the load until 24:00 under the off peak tariff.

The load profile in [Figure 4.14](#) confirmed that the load was continuously met throughout the day, demonstrating proper sizing of the microgrid components and zero load shedding.

4.3.4 BESS SOC Dynamics

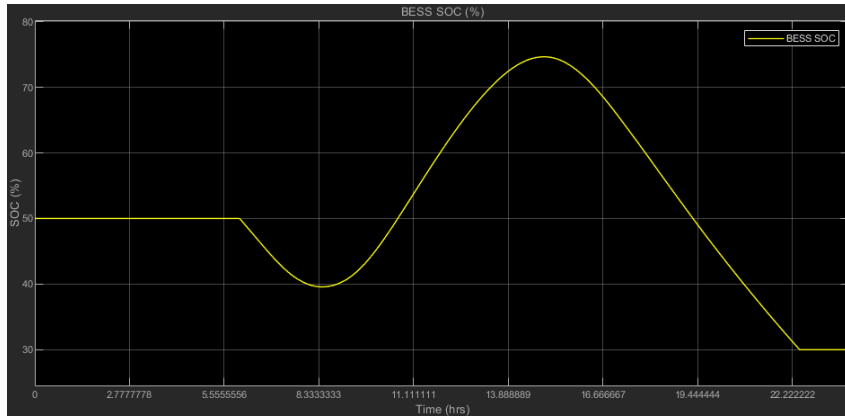


Figure 4.15: BESS SOC profile.

The BESS SOC was initially at 50% from 00:00 to 06:00, indicating that it was idle as observed in [Figure 4.15](#) as the utility grid was the only DER to meet the load demand. From 06:00 to 08:26, the BESS discharged, indicated by the SOC profile decreasing from 50% to 39% in [Figure 4.15](#). From 08:26 to 14:53, the BESS charged and reached a peak of 74.6% as seen in [Figure 4.15](#). From 14:53 to 22:24, the BESS discharged from 74.6% to its lowest limit of 30%, and did not further discharge from there as the BESS SOC remained constant at 30% from 22:24 to 00:00 as seen in [Figure 4.15](#).

4.3.5 Power Quality Analysis

[Figure 4.16](#) shows the microgrid frequency as the microgrid transitioned from grid-connected mode to standalone mode. The key points that were observed was when the microgrid transitioning modes. At 06:00, the microgrid transitioned from grid-connected mode to standalone mode, and a frequency spike was observed as seen in [Figure 4.16](#). The frequency fluctuation was determined to be $\Delta f = 50.055 - 50 = 0.055$ Hz.

At 10:00, the microgrid transitioned from standalone mode to grid-connected mode, and a frequency spike was observed as seen in [Figure 4.16](#). The frequency fluctuation was determined to be $\Delta f = 50.045 - 50 = 0.045$ Hz.

At 22:00, the microgrid transitioned from standalone mode to grid-connected mode, and a frequency spike occurred, as a result, the frequency fluctuation was determined to be $\Delta f = 50 - 49.987 = 0.013$ Hz.

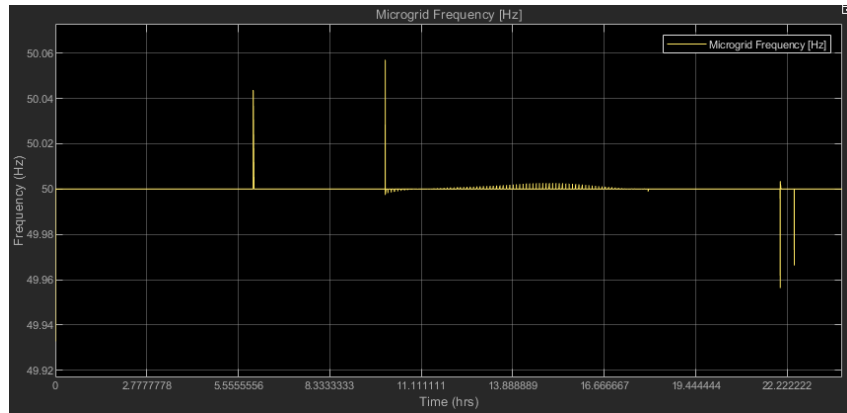


Figure 4.16: Microgrid frequency profile.

Lastly at 22:24, when the utility grid met the load demand as seen in [Figure 4.14](#), there was a frequency spike as seen in [Figure 4.16](#). The fluctuation was determined to be $\Delta f = 50.001 - 49.958 = 0.043$ Hz. As a result, during these transitions, the frequency fluctuations were within the limits specified in [Equation 3.30](#) of $49.5 \text{ Hz} \leq f(t) \leq 50.5 \text{ Hz}$.

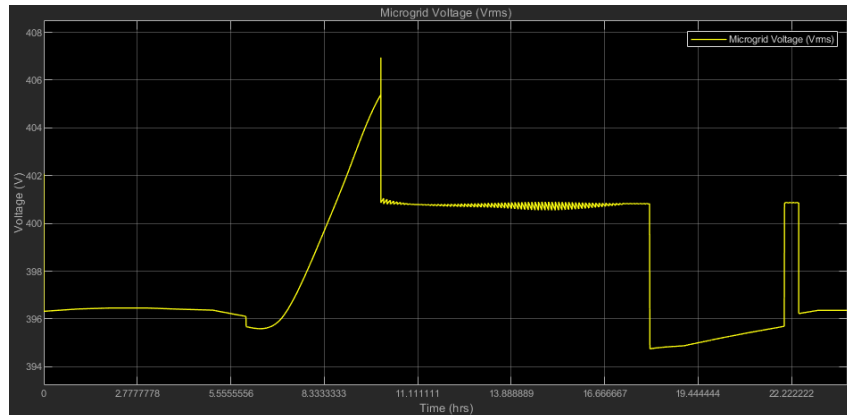


Figure 4.17: Microgrid voltage profile.

From [Figure 4.17](#), the voltage fluctuated based on the switching of the DERs and the transition of microgrid from grid-connected to standalone mode. Similar to frequency analysis, the voltage fluctuations were analyzed at critical points at 06:00, 10:00, 18:00, 22:00 and 22:24. The voltage fluctuations were as follows:

- 06:00, $396.1 - 395.7 = 0.4$ V
- 10:00, $407 - 401 = 6$ V
- 18:00, $400 - 394 = 6$ V
- 22:00, $400 - 395.7 = 4.3$ V
- 22:10, $400.9 - 396.2 = 4.7$ V

Even though voltage fluctuations were within the limits of ± 10 V as specified in [Equation 3.29](#), because the simulation was ran in phasor mode, the voltage profile was supposed to be in steady state, without excessive fluctuations. As a result, the FLC underperformed in keeping the voltage profile constant through out mode transitions and DER power sharing. The total voltage fluctuation was determined to be 6 V, which was within the voltage limits on ± 10 V, consequently, this case complied with the SAGC.

4.3.6 Energy Calculations

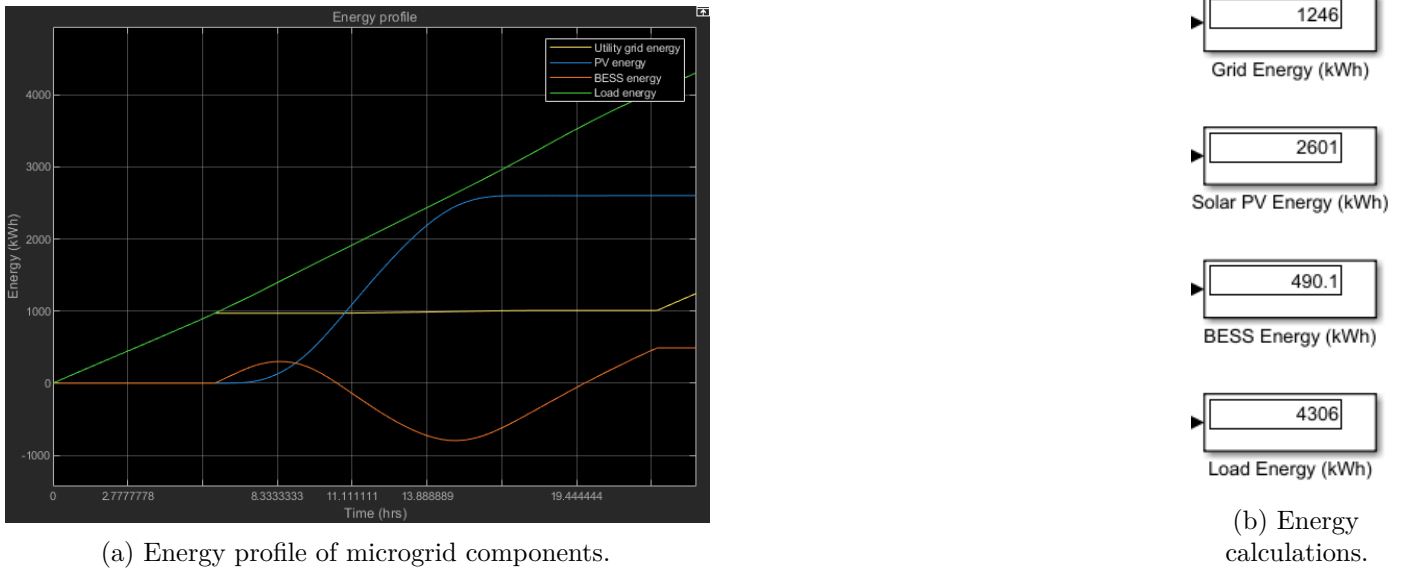


Figure 4.18: Energy profiles and calculations.

The total energy supply from the utility grid was 1246 kWh, 2601 kWh for PV, and 490.1 kWh for BESS, while the load energy demand was 4306 kWh as seen in Figure 4.18b. The total combined energy supply was 4337.1 kWh, confirming that the DERs collectively met the load energy demand, with a marginal surplus of 31.1 kWh. The PV system dominated the supply, aligning with the objective of being the priority primary renewable energy source. The contributions of each component to the load demand were determined as follows:

- PV contribution to load demand: $\frac{2601}{4306} \times 100 = 60.40\%$
- BESS contribution to load demand: $\frac{490.1}{4306} \times 100 = 11.38\%$
- Utility grid contribution to load demand: $\frac{1246}{4306} \times 100 = 28.94\%$

The energy supplied by renewable sources, PV and BESS amounted to 71.78%

Using Equation 3.27

$$RF(\%) = \left(1 - \frac{\sum P_{grid}}{\sum P_{renewable}}\right) \times 100 = \left(1 - \frac{1246}{2601 + 490.1}\right) \times 100 = 59.69\%$$

A desirable value of RF was 100%, however the FLC IEMS achieved a RF of 59.68%, indicating that 59.69% of the total energy supply is renewable, with 40.31% reliance on the utility grid. The RF highlighted opportunities to further reduce utility grid dependence by:

- Increase BESS capacity to store excess PV generation, at the same time increase PV capacity.
- Consider using lower limits of SOC, 10% instead of 30%.

The bottom plot in Figure 4.19 shows the grid cost of energy profile, revealing key insights into how the FLC responds to pricing signals and power import decisions. From 00:00 to 06:00, the cost rises linearly, corresponding to grid power import as already discussed in the power flow analysis subsection. When the grid tariff changed from off peak to standard peak and peak TOU from 06:00 to 22:24, the cost profile remained flat, indicating

that the utility was off, because of the standalone mode or the PV and BESS meeting the load demand. After 22:24, the cost profile increases linearly, indicating resumed utility grid action by FLC. The total cost of energy from the grid was obtained to be R1312.00.

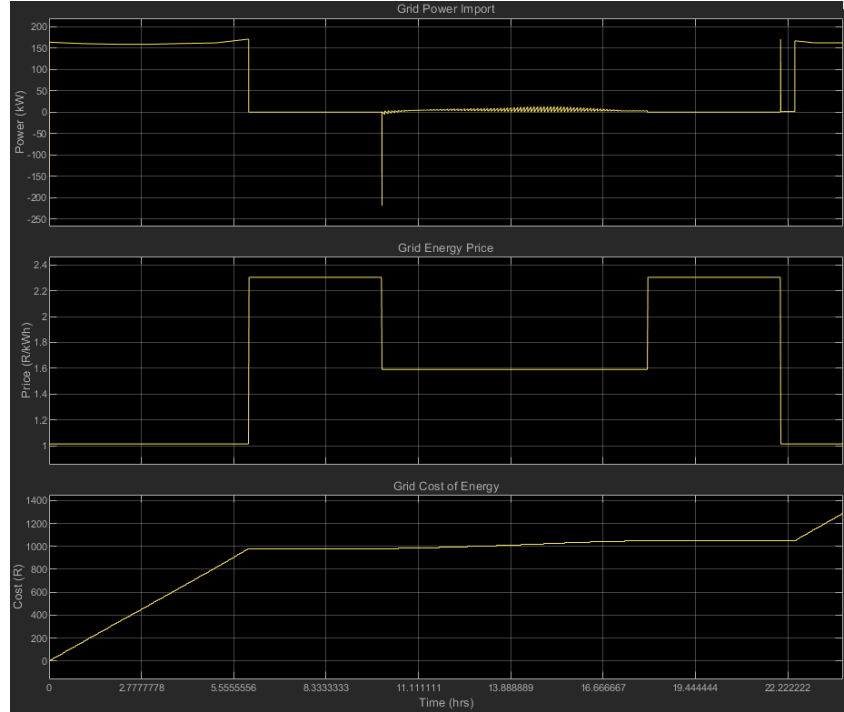


Figure 4.19: Grid power, grid energy price and cost of energy profile.

The cost profile in Figure 4.19 confirmed the FLC minimized utility grid activities by using it to import power primarily during low tariff periods, and avoiding grid usage during high tariff periods. As a result, this reflected the efficacy of the FLC to be cost-effective during gird-connected mode.

4.3.7 Evaluation of FLC IEMS and Summary of IEMS Function

The FLC based IEMS demonstrated effective performance in achieving its primary objectives of minimizing cost of energy drawn from the utility grid and optimizing microgrid resource utilization across different operating modes. The evaluation of the FLC IEMS revealed several key performance aspects:

Cost Minimization and Grid Interaction Strategy

The FLC IEMS successfully implemented a good grid interaction strategy that prioritized cost-effectiveness. The controller demonstrated intelligent decision making by:

- Restricting grid power imports to low tariff periods (00:00 to 06:00 and 22:24 to 24:00), when the ToU tariff was at off-peak rates (R1.014/kWh).
- Disconnecting from the utility grid at 06:00 when tariffs switched to peak rates, transitioning the microgrid to standalone mode.
- Reconnecting to the grid at 10:00 when tariffs returned to standard rates, but maintaining zero grid imports due to sufficient renewable generation.

- Maintaining standalone operation during high tariff periods and only resuming grid imports at 22:24 when both tariffs were low and renewable resources were depleted.
- The utility grid does not charge the BESS even on low tariff periods, indicating the FLC in only utilizing the grid to meet the load demand.

This strategic grid interaction resulted in a total grid energy cost of only R1290.00 despite importing 1246 kWh, 28.94% of total load, demonstrating the cost-effectiveness of the FLC IEMS. The flat cost profile between 06:00 to 22:24 visible in [Figure 4.19](#) serves as strong evidence of the controller's ability to avoid grid imports during high tariff periods.

Renewable Resource Optimization

The FLC IEMS effectively maximized renewable energy utilization through intelligent scheduling of the DERs:

- PV generation was consistently prioritized as the primary energy source, contributing 60.40% (2601 kWh) of the total load demand.
- The BESS was intelligently scheduled to:
 - Discharge during peak tariff periods, 06:00 to 08:26, to complement rising PV generation.
 - Charge during midday hours, 08:26 to 14:53, when PV generation exceeded load demand.
 - Discharge during evening hours, 14:53 to 22:24, to compensate for declining PV generation.
- The controller maintained BESS operation within safe operational limits, between 30% to 90% SOC, reaching a peak SOC of 74.6% and never falling below the 30% threshold
- Combined renewable contribution (PV + BESS) reached 71.78% of total load demand, with a Renewable Factor (RF) of 59.68%

The FLC IEMS resource scheduling demonstrated good decision making, as evidenced by the fast transitions between energy sources and the absence of any load shedding throughout the 24 hour period.

Operational Stability and Power Quality Management

A critical aspect of microgrid management is maintaining power quality during mode transitions and varying load conditions. The FLC IEMS demonstrated fairly good performance in this area:

- Frequency stability was maintained throughout all mode transitions, with maximum deviations of just 0.055 Hz, well within the acceptable range of 49.5 - 50.5 Hz.
- Voltage fluctuations during critical switching events remained within ± 6 V, significantly below the ± 10 V limit. However, the voltage profile did not remain constant as expected of a vrm analysis, this indicated poor system voltage regulation by the FLC IEMS.
- Seamless mode transitions were executed at four critical times, 06:00, 10:00, 22:00, and 22:24 without disruption to load service.
- The energy balance was precisely maintained, with total supply of 4337.1 kWh, closely matching the total demand 4306 kWh, indicating minimal energy waste.

These metrics validated the controller's ability to maintain operational stability while executing energy management strategies.

The FLC IEMS demonstrated adaptability to changing conditions throughout the day and successfully managed the varying load profile of a small factory without load shedding. The FLC IEMS also adjusted operational modes in response to ToU tariff changes, prioritizing cost savings, scheduled the BESS charging and discharging based on power balance conditions and lastly maintained power quality despite multiple transitions between grid-connected and standalone modes.

4.4 Case 4: Operation Mode Selection on a TOU tariff with Varying Load and Constant Load

4.4.1 Objective

The objective of this case study was to evaluate the performance of the FLC in selecting the correct mode of operation for the microgrid based on ToU grid energy pricing scheme, and scheduling the DERs to meet load demand with PV meeting most of the load demand. The type of load assessed in this case study was a varying load of a small factory as described in [chapter 3](#) and an additional constant load.

4.4.2 Simulation Setup

The simulation was ran for 86400 seconds to model a full day. A varying load type was connected, and a constant load was also connected. This load type modeled an industrial motor rated at 100 kW. The FLC was connected to the PCC for selecting the mode of the microgrid, it was also connected at the load side to select whether the load is shed or not, and also connected at the BESS power input to schedule charging or discharging. The varying load added an offset of 100 kW, with the new peak at 306 kW.

The BESS parameters were as follows:

- Initial SOC: 50%
- Minimum SOC Limit: 30%
- Maximum SOC Limit: 90%
- Rated Power: 300 kW, obtained from BESS sizing.
- Rated Capacity: 3000 kWh, obtained from BESS sizing.

Switching signals based on the TOU can be observed in appendix D in figure [D.3](#).

4.4.3 Power Flow Analysis

The utility grid supplied the load demand from 00:00 to 06:00 when no PV power was generated and the BESS neither charged nor discharged, as the system operated under the off-peak time-of-use (TOU) tariff. During this period, the microgrid remained in grid-connected mode. At 06:00, when the TOU tariff transitioned from off-peak to peak periods, the BESS discharged alongside PV generation to meet the load demand. The microgrid switched to standalone mode, and the utility grid was deactivated, as shown in Figure [4.20](#). However, minor ripples in the utility grid power were observed, ranging from -15 kW to 5 kW, indicating that the grid was not entirely

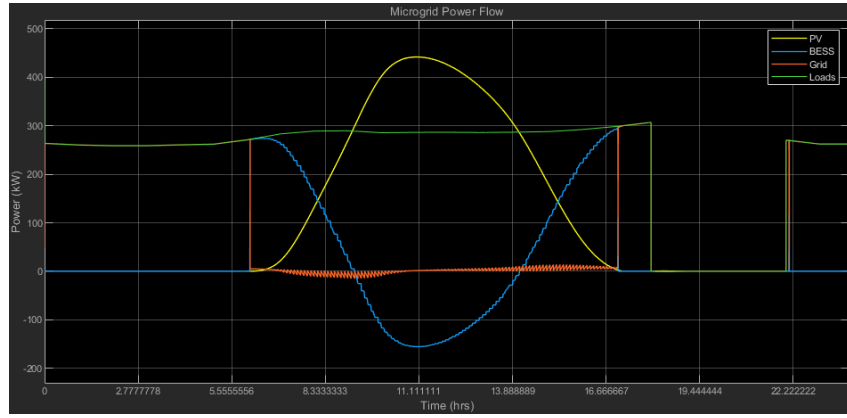


Figure 4.20: Power flow profiles for each microgrid component.

disconnected (see Figure ?? in Appendix D). Despite these ripples, the fuzzy logic controller (FLC) successfully suppressed grid power import, as PV and BESS fully met the load demand, rendering the fluctuations negligible.

At 10:00, the TOU tariff prompted the microgrid to transition back to grid-connected mode. Although the utility grid was reconnected, no power was imported, as PV and BESS continued to satisfy the load demand. Minor ripples continued but remained within a marginal range of 0 to 15 kW.

By 17:00, the BESS power output dropped to zero, and the FLC activated the utility grid to import power to meet the load demand (Figure 4.20). This occurred during the standard TOU tariff period, justifying the grid's utilization.

At 18:00, the TOU tariff shifted to peak periods, triggering the microgrid to revert to standalone mode and disconnect the utility grid. As depicted in Figure 4.20, the load was shed due to the high grid energy price during peak hours, a negative power balance ($P_{\text{balance}} = P_{\text{PV}} - P_{\text{Load}}$), and the BESS state of charge (SOC) reaching its minimum threshold of 30% (fully discharged). This aligned with Rule ? in ?. Load shedding began from 18:00 to 22:00. After 22:00, the TOU tariff reverted to off peak, and the utility grid resumed power import, restoring the load until 00:00 (Figure 4.20).

4.4.4 BESS SOC Dynamics

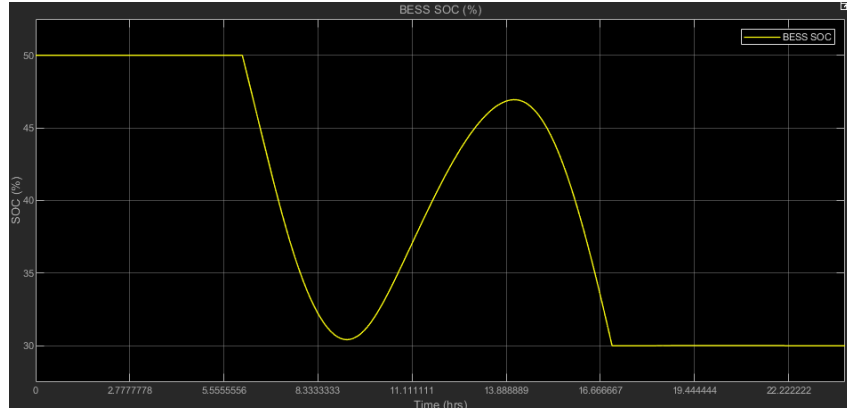


Figure 4.21: BESS SOC profile.

In figure 4.21, the SOC was initially 50% from 00:00 to 06:00, indicating the BESS was idle since the utility grid was meeting the load demand during the low period TOU tariff. From 06:00 to 09:12, the BESS discharged, resulting in the SOC decreasing from 50% to 30.44%. This was during the time where both PV and BESS met

the load demand.

From 09:12 to 14:10, the BESS increased from 30.44% to 46.94% as an indication that it was charging using the surplus power from PV after the load demand was met as seen in figure 4.21. From 14:10 to 17:06, the SOC decreased, as an indication of the BESS discharging to meet the load demand along with PV. At 17:06, the BESS SOC reached the SOC limit of 30%, and the BESS remained idle from 17:06 until 00:00.

4.4.5 Power Quality Analysis

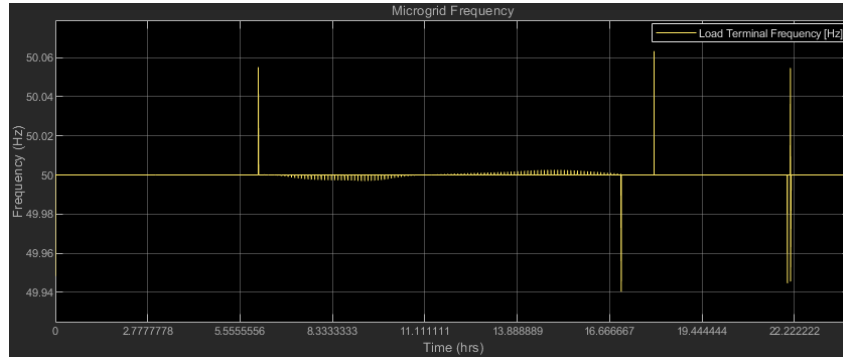


Figure 4.22: Microgrid frequency profile.

In figure 4.22, frequency spikes occurred at 06:00, 18:00, and at 22:06. These instances were when the utility grid was switch off and resumed back on as a result of the microgrid transitioning between the two modes of operation. The maximum spike was recorded at 18:00, and the fluctuation was $\Delta f = 50.065 - 50 = 0.065$ Hz. The frequency dips occurred at 17:00, 22:00 and 22:06. The frequency fluctuations were within the South African Grid Code operating range of 48.9 Hz to 51.0 Hz.

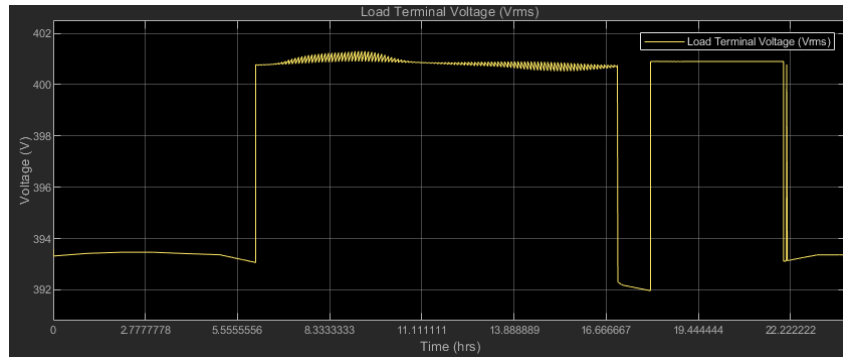


Figure 4.23: Load terminal voltage.

The nominal voltage of the load and the microgrid was 400 V, and from figure 4.23, the maximum voltage was recorded to be 401.2 V and the minimum to be 392 V. As a result, the voltage fluctuation recorded was $\Delta V = 401.2 - 392 = 9.2$ V. The voltage this voltage fluctuation is the result of the utility grid switching on and off as per mode of operation transition rules, and also due to the load shedding that occurred. The voltage profile remained flat after each transition, however due to the FLC ability to not fully switch off the grid at peak periods, the flat regions after each transition were due to the utility providing reference voltage.

Both frequency and voltage fluctuation are within allowable limits as the the IEC, IEEE and South African Grid Code.

4.4.6 Energy Calculations

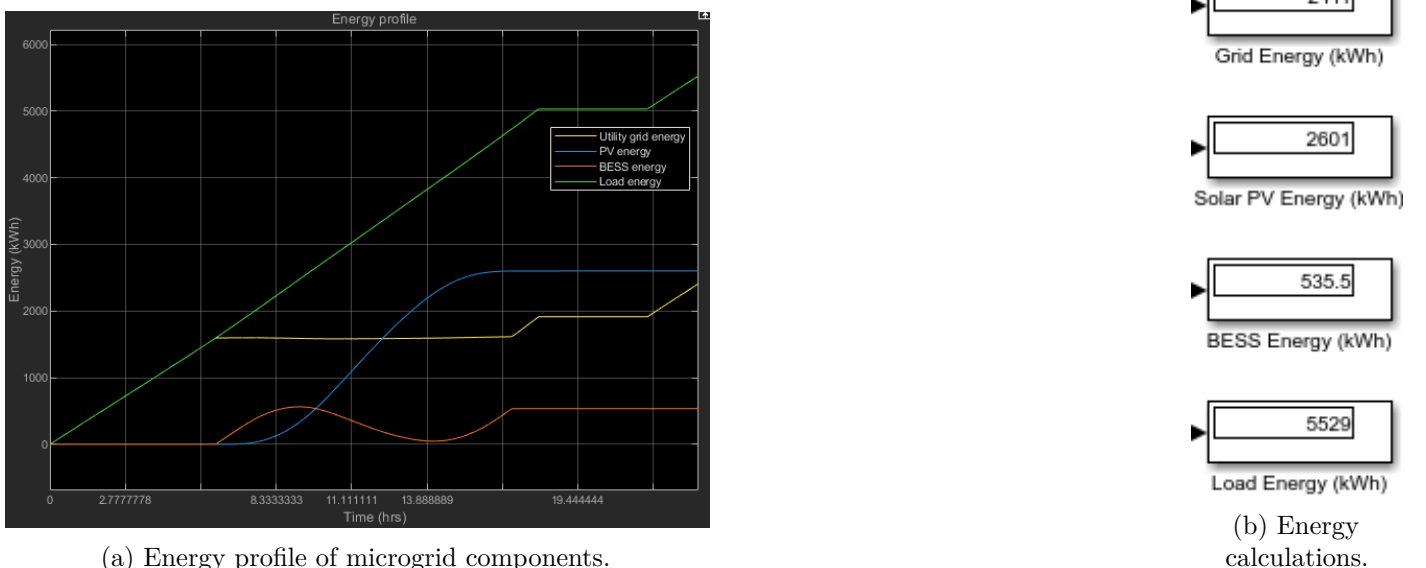


Figure 4.24: Energy profiles and calculations.

In Figure 4.24a, the critical periods that were investigated were at 18:00 to 22:00, when the load was shed. It can be observed in figure 4.24a that between these times, the load energy profile and the grid energy profile remained constant, as a result of no energy demand and no energy import. The total load shed was 1165 kWh for 4 hours, illustrated in Figure D.6 (see load profile in section D.2 Figure D.5).

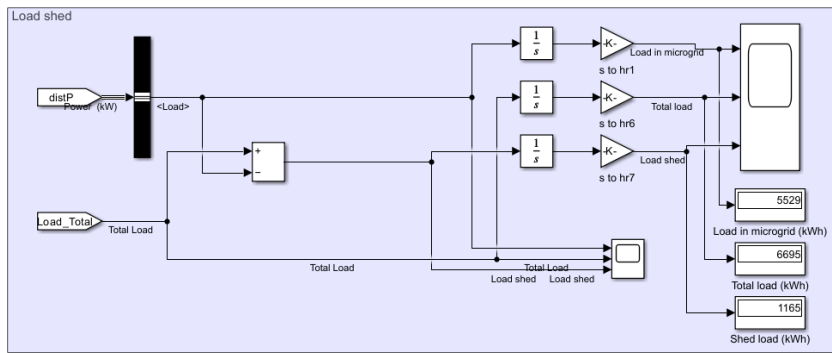


Figure 4.25: Load shed calculations.

The total energy supply from the utility grid was 2411 kWh, 2601 kWh for PV, and 535.5 kWh for BESS, with the load energy demand being 5529 kWh as seen in Figure 4.24b. The total combined energy supply was 5547.5 kWh, with surplus energy being to 18.5 kWh. PV contributed 47.04% to the load demand, BESS 9.69%, and the utility grid 43.60%. This resulted in 56.73% of the demand being met by PV and BESS.

The RF was determined to be:

$$RF = \left(1 - \frac{2411}{2601 + 535.5}\right) \times 100 = 23.13\%$$

A desirable RF was 100%, however the FLC achieved 23.13%, indicating that 23.13% of the total energy supply is renewable, with 76.87% reliance on the utility grid. This huge reliance in the grid was due to the added load

of 100 kW, as this load was not accounted for in the sizing of PV and BESS.

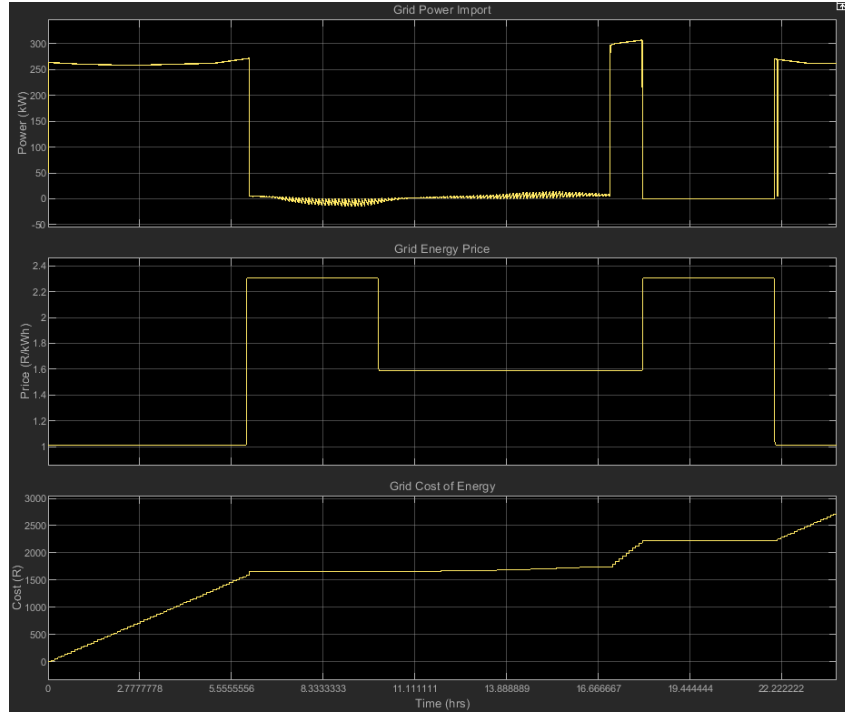


Figure 4.26: Grid power, grid energy price and cost of energy profile.

From Figure 4.26, the cost profile remained constant from 06:00 to 17:07 due to utility grid being off. It remained constant again from 18:00 to 22:00 due to load shedding, and the microgrid being in standalone mode. The total cost of energy from the grid amounted to R2711.00.

The FLC IEMS was effective in minimizing cost of energy from the grid during periods where PV and BESS met the load demand, and during grid import at off peak TOU tariff periods, at an expense of load shedding.

4.4.7 Evaluation of FLC IEMS Performance

The FLC based IEMS demonstrated effective performance in achieving its primary objectives of minimizing cost of energy drawn from the utility grid and optimizing microgrid resource utilization across different operating modes. The evaluation of the FLC IEMS revealed several key performance aspects:

Cost Minimization and Grid Interaction Strategy

The FLC based IEMS demonstrated effective cost minimization by leveraging TOU tariff dynamics and prioritizing renewable resources during peak periods. Key observations were:

- The FLC successfully avoided grid power import during peak TOU periods from 06:00 to 10:00 and 18:00 to 22:00 by relying on PV and BESS, reducing energy costs. Minor grid ripples (-15 kW to 15 kW) were negligible (see Figure D.4).
- During evening peak (18:00–22:00), the FLC (rule 4) enforced load shedding to prevent expensive grid imports (Figure D.6), sacrificing 1,165 kWh demand coverage. This resulted in grid energy costs totaling R2711.00.

The limitation of this case was that the 76.87% grid reliance was a result of undersized PV/BESS for the 100 kW added load. Sizing adjustments could further reduce costs.

Renewable Resource Optimization

The FLC IEMS effectively maximized renewable energy utilization through intelligent scheduling of the DERs:

- PV Utilization: Contributed 47.04% of demand (2,601 kWh), with surplus charging BESS from 09:12 to 14:10.
- BESS Coordination: Achieved 9.69% demand coverage with SOC maintained at 30 to 50%, but evening depletion required load shedding.
- Renewable Factor: RF of 23.13% (56.73% PV+BESS) was suboptimal due to grid dependence.

A future improvement opportunity would be to adjust the SOC minimum limits from 30% to 10%, to allow the BESS to discharge further to meet the load demand.

Operational Stability and Power Quality

A critical aspect of microgrid management is maintaining power quality during mode transitions and varying load conditions. The FLC IEMS demonstrated fairly good performance in this area:

- Frequency Stability: Transient spikes ($\Delta f = 0.065$ Hz at 18:00) during mode transitions complied with grid codes (48.9 to 51.0 Hz).
- Voltage Regulation: Fluctuations ($\Delta V = 9.2$ V, 392 to 401.2 V) were within IEEE 1159 and the South African Grid Code, $\pm 10\%$ limits. The flat regions after mode transition and load events indicated a fair voltage stability, largely due to the utility grid providing the reference.
- Load Shedding Impact: Voltage dips during 18:00 to 22:00 did not violate thresholds but affected reliability.

Chapter 5

Discussion

5.1 Summary of FLC IEMS Function

The Fuzzy Logic Controller based Intelligent Energy Management System (FLC IEMS) demonstrated effective microgrid management across two case studies with varying configurations. The FLC IEMS primary functions included:

- Mode Selection: Automatically switching between grid-connected and standalone modes based on Time-of-Use (TOU) tariff periods, avoiding grid usage during peak pricing (06:00 to 10:00 and 18:00 to 22:00).
- DER Scheduling: Prioritizing PV generation as the primary energy source while intelligently managing BESS charging and discharging cycles. The controller maintained BESS SOC between 30-90% in normal operation.
- Cost Optimization: Minimizing energy costs by strategically limiting grid imports to off peak periods (00:00 to 06:00 and 22:00 to 00:00) when tariffs were lowest (R1.59/kWh).
- Power Quality Maintenance: Keeping frequency fluctuations within 49.95 to 50.5 Hz and voltage variations within ± 10 V, complying with South African Grid Code standards.
- Load Management: Implementing load shedding (Case 4) when renewable resources were insufficient during peak tariff periods to avoid costly grid imports.

5.2 Comparative Performance Metrics

Table 5.1 presents the key metrics achieved in each case study.

Table 5.1: Performance comparison across case studies

Metric	Case 1 (No IEMS/BESS)	Case 2 (No IEMS)	Case 3 (IEMS)	Case 4 (IEMS + Extra Load)
Grid Energy (kWh)	1705 (39.60%)	505.9 (11.75%)	1246 (28.94%)	2411 (43.60%)
PV Energy (kWh)	2601 (60.40%)	2601 (60.40%)	2601 (60.40%)	2601 (47.04%)
BESS Energy (kWh)	0 (0%)	1218 (28.29%)	490.1 (11.38%)	535.5 (9.69%)
Renewable Factor	34.45%	86.75%	59.69%	23.13%
Total Cost (R)	4437.00	2317.00	1312.00	2711.00
Load Shed (kWh)	0	0	0	1165
Max Freq. Fluctuation	0	0.055 Hz	0.055 Hz	0.065 Hz
Max Volt. Fluctuation	7.3 V	7.3 V	6 V	9.2 V

Key observations:

- The IEMS (Cases 3 and 4) significantly reduced costs compared to uncontrolled operation (Cases 1 and 2).
- Case 2 showed misleadingly high RF (86.75%) due to abnormal BESS discharge patterns.

- Case 4 performance suffered due to undersized PV and BESS for the additional 100 kW load.
- Power quality remained within standard limits across all cases, with great quality observed in case 3 due to correct matching of DER sources and load. Furthermore, FLC IEMS handling power sharing effectively, allowing the frequency and voltage to remain within standard limits.

5.3 Limitations and Challenges

Several aspects did not perform as intended: **BESS Management Issues:**

- Without IEMS (Case 2), the BESS discharged excessively to 5.71% SOC, risking battery damage.
- The IEMS's conservative 30% SOC minimum limit led to load shedding in Case 4 when slightly deeper discharge could have prevented it.
- In case 3, the voltage profile was reference to the power profile of the PV due to its high power injection compared to the utility grid.

Renewable Utilization:

- The 60.4% PV contribution ceiling in all case studies suggested static PV sizing, as a result, case 4 displayed under-sizing of PV and BESS for higher loads.

Load Shedding:

- The 4 hour load shedding in Case 4 (1165 kWh) indicated inadequate capacity planning.
- The FLC lacked predictive capabilities to anticipate and prevent this situation.

Grid Interaction:

- Small power ripples (-15 to 15 kW) occurred during standalone mode (Case 4).
- No revenue generation from exported PV surplus was implemented.

5.4 Achievement of IEMS Objectives

The FLC IEMS successfully achieved its primary technical objectives:

Cost Minimization:

- Reduced grid energy costs by $\frac{R4437.00 - R1312}{R4437} \times 100 = 70.43\%$ in Case 3 compared to the baseline (Case 1) through strategic TOU tariff response.

Renewable Optimization:

- PV generation was fully utilized by the BESS for charging, indicating the execution of the Mamdani FLC rule set properly ([Table 3.7](#)).

Power Quality:

- All cases maintained stable frequency despite spikes and dips. These spike and dips did not extend for more than 0.01 seconds. This indicated that good power sharing across DERs, especially in case 3 and 4, where BESS charging and discharging was scheduled by the FLC IEMS.

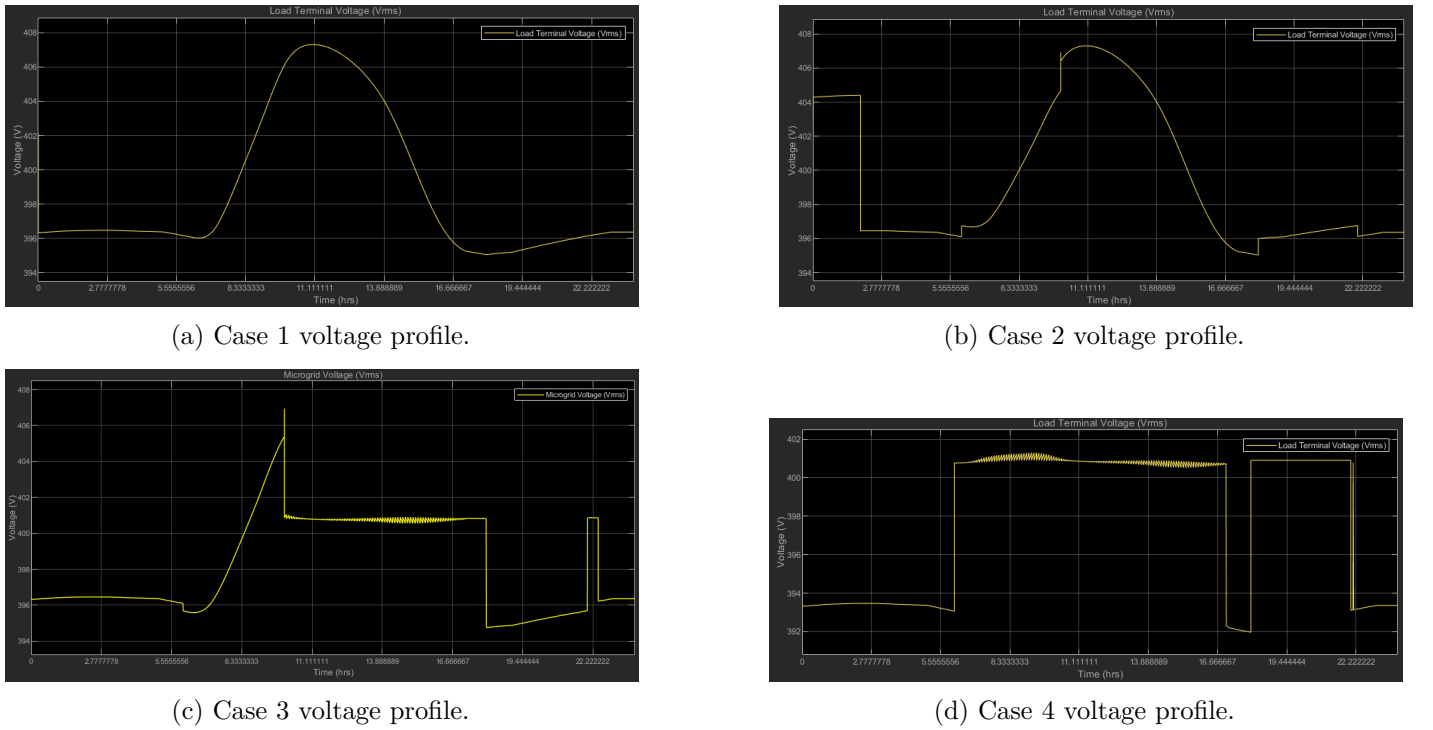


Figure 5.1: Voltage profiles across case studies.

- From Figure 5.1, case 3 and case 4 had fair voltage stability plots, due to the presence of the FLC IEMS. The flat regions in Figure 5.1c was due to the utility grid during grid-connected mode, providing reference voltage. Similar to Figure 5.1d, the flat region were better managed compared to case 3. From these plots, it can be concluded that the reference voltage was provided by the utility grid, and the FLC IEMS fell short to maintain the voltage at nominal value of 400 V during standalone mode.

Operational Modes:

- FLC IEMS correctly implemented mode switching at tariff transition points (06:00 to 10:00 and 18:00 to 22:00), indicating correct rule firing from the Sugeno FLC rule set from (Table 3.9).

However, the FLC IEMS showed limitations when faced with undersized components (Case 4) and could benefit from:

- Adaptive SOC limits based on forecasted conditions
- Larger PV/BESS capacity for expanded loads
- Predictive control elements to anticipate energy needs
- Introduce curtailment and peak shaving algorithms for further IEMS robustness

The design of the microgrid and the FLC IEMS satisfied the technical requirements TR01 to TR06 from Table 3.1. Furthermore, the FLC IEMS effectively met its core design requirements and its major objectives of minimizing the overall cost of energy drawn from the grid under grid-connected mode and ensured optimum utilization of microgrid generators under standalone mode, with a major drawback of load shedding during the standalone mode.

Chapter 6

Conclusions

This research successfully designed and implemented an intelligent energy management system (IEMS) for a hybrid microgrid with battery storage, addressing the critical need for cost-effective and reliable distributed energy systems. Through a comprehensive literature review of classical, heuristic, and intelligent algorithms, fuzzy logic control (FLC) was identified as the optimal approach, balancing computational efficiency with implementation simplicity.

The microgrid architecture was strategically designed for dual mode operation (grid-connected and standalone) using data from open source websites including Eskom for load profiles, PV generation data, and NASA for weather datasets. The system comprised of solar PV as the primary energy source, battery energy storage system (BESS) for excess energy absorption, and utility grid backup, integrated at 400V AC in Loeriesfontein. MATLAB Simulink provided the simulation platform for comprehensive system modeling and validation.

The Sugeno FLC based IEMS demonstrated superior performance in power flow management and seamless mode transitions, with Mamdani FLC demonstrating good BESS charging and discharging patterns. Under optimal conditions, the system achieved a renewable factor of 59.69% with grid energy costs of only R1312.00, validating the economic benefits of intelligent energy management. The modular FLC design enabled easy scalability and parameter tuning, while efficient BESS scheduling maximized renewable energy utilization and minimized grid dependence.

Comprehensive case studies revealed the system's adaptability to varying load conditions. However, performance degradation was observed under increased load scenarios, where the renewable factor dropped significantly to 23.13% with corresponding grid costs rising to R2711.00. This highlights the importance of proper system sizing and load forecasting in microgrid design.

This work contributes to the field by providing a practical framework for intelligent microgrid energy management that balances cost optimization with energy security. The research demonstrates that FLC based systems can effectively manage complex energy flows while maintaining system stability across different operating conditions. The comprehensive performance analysis under varying load and resource conditions provides valuable insights for future microgrid implementations.

The research successfully demonstrates that intelligent energy management systems using fuzzy logic control can significantly enhance microgrid performance, achieving substantial cost savings and renewable energy integration. The developed IEMS provides a good foundation for sustainable energy systems, contributing valuable insights to the advancement of smart grid technologies and distributed energy resource management.

Chapter 7

Recommendations

This project successfully demonstrated the potential of intelligent energy management systems for hybrid microgrids in reducing grid energy costs and optimizing renewable energy utilization while maintaining power quality at load terminals. The fuzzy logic controller achieved a renewable factor of 59.69% with grid energy costs of R1312.00 under optimal conditions, validating the economic and technical benefits of intelligent energy management. However, due to time constraints and scope limitations, several areas require further investigation to enhance system performance and practical implementation.

The current FLC implementation relied on pre-defined rules that lack predictive capabilities and demonstrated sensitivity to load variations, as evidenced by the significant performance degradation when additional loads were introduced, the renewable factor dropped to 23.13% with grid costs increasing to R2711.00. Future research should prioritize implementing Adaptive Neuro-Fuzzy Inference Systems (ANFIS) using the successful Case 3 results as training data, combining fuzzy logic interpretability with neural network learning capabilities. Integration of machine learning algorithms would enhance predictive load forecasting, solar irradiance prediction, and dynamic battery optimization with real-time parameter adaptation to varying operating conditions.

Component sizing emerged as a critical factor affecting system performance, particularly under increased load scenarios. While this research focused on mathematical calculations for solar PV and battery energy storage system sizing based on load requirements, future studies should investigate intelligent optimization algorithms for microgrid component sizing that account for economic constraints, reliability requirements, and scalability considerations. Additionally, the analysis of power quality, limited to RMS voltage and frequency fluctuations against nominal values, requires expansion to include comprehensive power quality assessment methods such as total harmonic distortion analysis, voltage sag/swell evaluation, and transient response characterization. Economic analysis incorporating lifecycle costs, grid export tariffs, curtailment and peak shaving algorithms would strengthen efficacy of the intelligent energy management system.

By addressing these recommendations, future research can build upon the findings of this project and contribute significantly to advancing intelligent energy management systems for hybrid microgrids. The demonstrated effectiveness of the FLC based approach provides a solid foundation for developing more sophisticated, adaptive, and commercially viable energy management solutions that can accelerate the transition to sustainable distributed energy systems.

Bibliography

- [1] A. R. Battula, S. Vuddanti, and S. R. Salkuti, “Review of energy management system approaches in microgrids,” *Energies*, vol. 14, no. 17, 2021. [Online]. Available: <https://www.mdpi.com/1996-1073/14/17/5459>
- [2] M. Uddin, H. Mo, D. Dong, S. Elsawah, J. Zhu, and J. M. Guerrero, “Microgrids: A review, outstanding issues and future trends,” *Energy Strategy Reviews*, vol. 49, p. 101127, 2023. [Online]. Available: <https://www.sciencedirect.com/science/article/pii/S2211467X23000779>
- [3] G. Shahgholian, “A brief review on microgrids: Operation, applications, modeling, and control,” *International Transactions on Electrical Energy Systems*, vol. 31, no. 6, p. e12885, 2021. [Online]. Available: <https://onlinelibrary.wiley.com/doi/abs/10.1002/2050-7038.12885>
- [4] K. Cabana-Jiménez, J. E. Candelo-Becerra, and V. Sousa Santos, “Comprehensive analysis of microgrids configurations and topologies,” *Sustainability*, vol. 14, no. 3, 2022. [Online]. Available: <https://www.mdpi.com/2071-1050/14/3/1056>
- [5] A. Elmouatamid, R. Ouladsine, M. Bakhouya, N. El Kamoun, M. Khaidar, and K. Zine-Dine, “Review of control and energy management approaches in micro-grid systems,” *Energies*, vol. 14, no. 1, 2021. [Online]. Available: <https://www.mdpi.com/1996-1073/14/1/168>
- [6] MathWorks, “Fuzzy inference process,” <https://www.mathworks.com/help/fuzzy/fuzzy-inference-process.html>, 2024, accessed: May 23, 2025.
- [7] R. Saatchi, “Fuzzy logic concepts, developments and implementation,” *Information*, vol. 15, no. 10, 2024. [Online]. Available: <https://www.mdpi.com/2078-2489/15/10/656>
- [8] A. Shufian and N. Mohammad, “Modeling and analysis of cost-effective energy management for integrated microgrids,” *Cleaner Engineering and Technology*, vol. 8, p. 100508, 2022. [Online]. Available: <https://www.sciencedirect.com/science/article/pii/S2666790822001136>
- [9] R. P. K. K. V. Subudhi, Bidyadhar, “Introduction to smart grids and microgrids,” 2025. [Online]. Available: <https://app.knovel.com/hotlink/khtml/id:kt01417AZ8/control-communication/background>
- [10] M. G. M. Almihat, “An overview of ac and dc microgrid energy management systems,” *AIMS Energy*, vol. 11, no. 6, pp. 1031–1069, 2023. [Online]. Available: <https://www.aimspress.com/article/doi/10.3934/energy.2023049>
- [11] S. Saponara, R. Saletti, and L. Mihet-Popa, “Hybrid micro-grids exploiting renewables sources, battery energy storages, and bi-directional converters,” *Applied Sciences*, vol. 9, no. 22, 2019. [Online]. Available: <https://www.mdpi.com/2076-3417/9/22/4973>
- [12] “Optimizing microgrid integration of renewable energy for sustainable solutions in off/on-grid communities,” *Journal of Electrical Systems and Information Technology*, vol. 11, no. 1, p. 61, 12 2024, copyright - Copyright Springer Nature B.V. Dec 2024; Last updated - 2024-12-18; SubjectsTermNotLitGenreText -

- Egypt; Iran; Gulf of Suez. [Online]. Available: <http://ezproxy.uct.ac.za/login?url=https://www.proquest.com/scholarly-journals/optimizing-microgrid-integration-renewable-energy/docview/3145924338/se-2>
- [13] Q. Hassan, S. Algburi, A. Z. Sameen, H. M. Salman, and M. Jaszczur, “A review of hybrid renewable energy systems: Solar and wind-powered solutions: Challenges, opportunities, and policy implications,” *Results in Engineering*, vol. 20, p. 101621, 2023. [Online]. Available: <https://www.sciencedirect.com/science/article/pii/S259012302300748X>
- [14] I. Rai and S. C, “Microgrid and grid synchronization: A critical analysis of challenges and opportunities,” *Electric Power Systems Research*, vol. 242, p. 111434, 2025. [Online]. Available: <https://www.sciencedirect.com/science/article/pii/S0378779625000276>
- [15] J. Hmad, A. Houari, A. E. M. Bouzid, A. Saim, and H. Trabelsi, “A review on mode transition strategies between grid-connected and standalone operation of voltage source inverters-based microgrids,” *Energies*, vol. 16, no. 13, 2023. [Online]. Available: <https://www.mdpi.com/1996-1073/16/13/5062>
- [16] C. Zhang, W. Lin, D. Ke, and Y. Sun, “Smoothing tie-line power fluctuations for industrial microgrids by demand side control: An output regulation approach,” *IEEE Transactions on Power Systems*, vol. 34, no. 5, pp. 3716–3728, 2019.
- [17] F. Agha Kassab, R. Rodriguez, B. Celik, F. Locment, and M. Sechilariu, “A comprehensive review of sizing and energy management strategies for optimal planning of microgrids with pv and other renewable integration,” *Applied Sciences*, vol. 14, no. 22, 2024. [Online]. Available: <https://www.mdpi.com/2076-3417/14/22/10479>
- [18] S. K. Panda and B. Subudhi, “A review on robust and adaptive control schemes for microgrid,” *Journal of Modern Power Systems and Clean Energy*, vol. 11, no. 4, pp. 1027–1040, 2023.
- [19] M. Hemmati, B. Mohammadi-Ivatloo, M. Abapour, and A. Anvari-Moghaddam, “Optimal chance-constrained scheduling of reconfigurable microgrids considering islanding operation constraints,” *IEEE Systems Journal*, vol. 14, no. 4, pp. 5340–5349, 2020.
- [20] T. S. Tran, D. T. Nguyen, and G. Fujita, “The analysis of technical trend in islanding operation, harmonic distortion, stabilizing frequency, and voltage of islanded entities,” *Resources*, vol. 8, no. 1, 2019. [Online]. Available: <https://www.mdpi.com/2079-9276/8/1/14>
- [21] S. Punitha, N. P. Subramaniam, and P. A. D. Vimal Raj, “A comprehensive review of microgrid challenges in architectures, mitigation approaches, and future directions,” *Journal of Electrical Systems and Information Technology*, vol. 11, no. 60, 2024. [Online]. Available: <https://doi.org/10.1186/s43067-024-00188-4>
- [22] A. S. Satapathy, S. Mohanty, A. Mohanty, R. K. Rajamony, M. E. M Soudagar, T. Y. Khan, M. Kalam, M. M. Ali, and M. N. Bashir, “Emerging technologies, opportunities and challenges for microgrid stability and control,” *Energy Reports*, vol. 11, pp. 3562–3580, 2024. [Online]. Available: <https://www.sciencedirect.com/science/article/pii/S2352484724001732>
- [23] R. Upadhyay and P. K. Rathore, “A review on optimal sizing, stability control and energy management techniques for pv and wind (hybrid) ac/dc microgrids,” *International Journal of Trend in Scientific Research and Development (IJTSRD)*, vol. 5, no. 4, pp. 709–715, June 2021. [Online]. Available: <https://www.ijtsrd.com/papers/ijtsrd42404.pdf>

- [24] M. S. Bakare, A. Abdulkarim, A. N. Shuaibu, and M. M. Muhamad, “Energy management controllers: strategies, coordination, and applications,” *Energy Informatics*, vol. 7, no. 1, p. 57, 12 2024, copyright - © The Author(s) 2024. This work is published under <http://creativecommons.org/licenses/by/4.0/> (the “License”). Notwithstanding the ProQuest Terms and Conditions, you may use this content in accordance with the terms of the License; Last updated - 2024-10-03; SubjectsTermNotLitGenreText - Economic. [Online]. Available: <http://ezproxy.uct.ac.za/login?url=https://www.proquest.com/scholarly-journals/energy-management-controllers-strategies/docview/3082448188/se-2>
- [25] R. G. Allwyn, A. Al-Hinai, and V. Margaret, “A comprehensive review on energy management strategy of microgrids,” *Energy Reports*, vol. 9, pp. 5565–5591, 2023. [Online]. Available: <https://www.sciencedirect.com/science/article/pii/S2352484723007230>
- [26] O. Chekira, Y. Boujoudar, H. El Moussaoui, A. Boharb, T. Lamhamdi, and H. El Markhi, “An improved microgrid energy management system based on hybrid energy storage system using ann narma-l2 controller,” *Journal of Energy Storage*, vol. 98, p. 113096, 2024. [Online]. Available: <https://www.sciencedirect.com/science/article/pii/S2352152X24026823>
- [27] S. Ahmad, M. Shafiullah, C. B. Ahmed, and M. Alowaifeer, “A review of microgrid energy management and control strategies,” *IEEE Access*, vol. 11, pp. 21 729–21 757, 2023. [Online]. Available: <https://ieeexplore.ieee.org/stamp/stamp.jsp?tp=&arnumber=10050868>
- [28] M. Shafiullah, A. M. Refat, M. E. Haque, D. M. H. Chowdhury, M. S. Hossain, A. G. Alharbi, M. S. Alam, A. Ali, and S. Hossain, “Review of recent developments in microgrid energy management strategies,” *Sustainability*, vol. 14, no. 22, 2022. [Online]. Available: <https://www.mdpi.com/2071-1050/14/22/14794>
- [29] T. Pippia, J. Sijs, and B. De Schutter, “A single-level rule-based model predictive control approach for energy management of grid-connected microgrids,” *IEEE Transactions on Control Systems Technology*, vol. 28, no. 6, pp. 2364–2376, 2020.
- [30] S. Iqbal, M. Nasir, M. F. Zia, K. Riaz, H. Sajjad, and H. A. Khan, “A novel approach for system loss minimization in a peer-to-peer energy sharing community dc microgrid,” *International Journal of Electrical Power Energy Systems*, vol. 129, p. 106775, 2021. [Online]. Available: <https://www.sciencedirect.com/science/article/pii/S0142061521000156>
- [31] G. Liu, M. F. Ferrari, and Y. Chen, “A mixed integer linear programming-based distributed energy management for networked microgrids considering network operational objectives and constraints,” *IET Energy Systems Integration*, vol. 5, no. 3, pp. 320–337, 2023. [Online]. Available: <https://ietresearch.onlinelibrary.wiley.com/doi/abs/10.1049/esi2.12103>
- [32] K. Parvin, M. S. H. Lipu, M. A. Hannan, M. A. Abdullah, K. P. Jern, R. A. Begum, M. Mansur, K. M. Muttaqi, T. M. I. Mahlia, and Z. Y. Dong, “Intelligent controllers and optimization algorithms for building energy management towards achieving sustainable development: Challenges and prospects,” *IEEE Access*, vol. 9, pp. 41 577–41 602, 2021.
- [33] E. Kabalci, “3.5.3.1 multiobjective gray wolf optimization algorithm,” 2021. [Online]. Available: <https://app.knovel.com/mlink/khtml/id:kt012LAQ65/hybrid-renewable-energy/multiobjective-gray-wolf>
- [34] K. M. Singh and S. Gope, “Renewable energy integrated multi-microgrid load frequency control using grey wolf optimization algorithm,” *Materials Today: Proceedings*, vol. 46, pp. 2572–2579, 2021, international

- Conference on Smart and Sustainable Developments in Materials, Manufacturing and Energy Engineering. [Online]. Available: <https://www.sciencedirect.com/science/article/pii/S2214785321010956>
- [35] Z. Ullah, S. Wang, J. Lai, M. Azam, F. Badshah, G. Wu, and M. R. Elkadeem, "Implementation of various control methods for the efficient energy management in hybrid microgrid system," *Ain Shams Engineering Journal*, vol. 14, no. 5, p. 101961, 2023. [Online]. Available: <https://www.sciencedirect.com/science/article/pii/S2090447922002726>
- [36] S. E. Eyimaya and N. Altin, "Review of energy management systems in microgrids," *Applied Sciences*, vol. 14, no. 3, 2024. [Online]. Available: <https://www.mdpi.com/2076-3417/14/3/1249>
- [37] F. Vivas, F. Segura, and J. Andújar, "Fuzzy logic-based energy management system for grid-connected residential dc microgrids with multi-stack fuel cell systems: A multi-objective approach," *Sustainable Energy, Grids and Networks*, vol. 32, p. 100909, 2022. [Online]. Available: <https://www.sciencedirect.com/science/article/pii/S2352467722001588>
- [38] T. A. Nakabi and P. Toivanen, "Deep reinforcement learning for energy management in a microgrid with flexible demand," *Sustainable Energy, Grids and Networks*, vol. 25, p. 100413, 2021. [Online]. Available: <https://www.sciencedirect.com/science/article/pii/S2352467720303441>
- [39] Eskom Holdings SOC Ltd, *Eskom Digital Tariff Booklet 2024*, South Africa, May 2024, accessed: 2025-04-16. [Online]. Available: https://www.eskom.co.za/distribution/wp-content/uploads/2024/05/ESK114-Eskom-Digital-Tariff-Booklet-2024_Final.pdf
- [40] J. Warner, J. Sexauer, W. V. den Broeck, B. P. Kinoshita, J. Balinski, C. Clauss, twmeggs, alexsavio, A. Unnikrishnan, M. Miretti, G. Castelão, F. A. Pontes, T. Uelwer, phme283, pd2f, laurazh, F. Batista, moetayuko, alexbuy, W. Song, T. Ni, T. G. Badger, R. A. M. Pérez, N. Muoh, J. F. Power, H. Mishra, G. O. Trullols, A. Hörteborn, and T. Germer, "Jdwarner/scikit-fuzzy: Scikit-fuzzy 0.5.0," Aug. 2024, available at Zenodo. [Online]. Available: <https://doi.org/10.5281/zenodo.802396>
- [41] HOMER Energy by UL, "Homer pro - microgrid optimization software," 2024, accessed: 2025-04-16. [Online]. Available: <https://www.homerenergy.com/products/pro/index.html>
- [42] DIgSILENT GmbH, "Digsilent powerfactory - renewables," 2024, accessed: 2025-04-16. [Online]. Available: <https://www.digsilent.de/en/renewables.html>
- [43] S. Upadhyay, I. Ahmed, and L. Mihet-Popa, "Energy management system for an industrial microgrid using optimization algorithms-based reinforcement learning technique," *Energies*, vol. 17, no. 16, 2024. [Online]. Available: <https://www.mdpi.com/1996-1073/17/16/3898>
- [44] The MathWorks, Inc., "Matlab - data analysis," 2024, accessed: 2025-04-16. [Online]. Available: <https://www.mathworks.com/products/matlab/data-analysis.html>
- [45] M. M. Kamal, I. Ashraf, and E. Fernandez, "Planning and optimization of standalone microgrid with renewable resources and energy storage," *Energy Storage*, vol. 5, no. 1, p. e395, 2023. [Online]. Available: <https://onlinelibrary.wiley.com/doi/abs/10.1002/est2.395>
- [46] H. R. E. H. Bouchekara, Y. A. Sha'aban, M. S. Shahriar, S. M. Abdullah, and M. A. Ramli, "Sizing of hybrid pv/battery/wind/diesel microgrid system using an improved decomposition multi-objective evolutionary algorithm considering uncertainties and battery degradation," *Sustainability*, vol. 15, no. 14, 2023. [Online]. Available: <https://www.mdpi.com/2071-1050/15/14/11073>

- [47] M. Bilal, P. N. Bokoro, and G. Sharma, "Hybrid optimization for sustainable design and sizing of standalone microgrids integrating renewable energy, diesel generators, and battery storage with environmental considerations," *Results in Engineering*, vol. 25, p. 103764, 2025. [Online]. Available: <https://www.sciencedirect.com/science/article/pii/S2590123024020073>
- [48] M. Maharjan, A. Ekic, M. Beedle, J. Tan, and D. Wu, "Evaluating grid strength under uncertain renewable generation," *International Journal of Electrical Power Energy Systems*, vol. 146, p. 108737, 2023. [Online]. Available: <https://www.sciencedirect.com/science/article/pii/S0142061522007335>
- [49] T. Basso, "Ieee 1547 and 2030 standards for distributed energy resources interconnection and interoperability with the electricity grid," National Renewable Energy Laboratory (NREL), Golden, CO, Technical Report NREL/TP-5D00-63157, December 2014, contract No. DE-AC36-08GO28308. [Online]. Available: <https://www.nrel.gov/publications/>
- [50] M. Mirzaei and B. Vahidi, "Feasibility analysis and optimal planning of renewable energy systems for industrial loads of a dairy factory in tehran, iran," *Journal of Renewable and Sustainable Energy*, vol. 7, p. 063114, 11 2015.
- [51] F. J. Fernández, F. Segura, J. Andujar Marquez, A. Palacio, J. Saenz, F. Isorna, and E. López, "Multi-objective fuzzy logic-based energy management system for microgrids with battery and hydrogen energy storage system," *Electronics*, vol. 9, p. 1074, 06 2020.
- [52] J. Shi, L. Ma, C. Li, N. Liu, and J. Zhang, "A comprehensive review of standards for distributed energy resource grid-integration and microgrid," *Renewable and Sustainable Energy Reviews*, vol. 170, p. 112957, 2022. [Online]. Available: <https://www.sciencedirect.com/science/article/pii/S1364032122008383>
- [53] J. Jayaram, M. Srinivasan, N. Prabaharan, and T. Senju, "Design of decentralized hybrid microgrid integrating multiple renewable energy sources with power quality improvement," *Sustainability*, vol. 14, no. 13, 2022. [Online]. Available: <https://www.mdpi.com/2071-1050/14/13/7777>
- [54] D. Rebollal, M. Carpintero-Rentería, D. Santos-Martín, and M. Chinchilla, "Microgrid and distributed energy resources standards and guidelines review: Grid connection and operation technical requirements," *Energies*, vol. 14, no. 3, 2021. [Online]. Available: <https://www.mdpi.com/1996-1073/14/3/523>
- [55] H. R. E.-H. Bouchekara, M. S. Javaid, Y. A. Shaaban, M. S. Shahriar, M. A. M. Ramli, and Y. Latreche, "Decomposition based multiobjective evolutionary algorithm for pv/wind/diesel hybrid microgrid system design considering load uncertainty," *Energy Reports*, vol. 7, pp. 52–69, 2021. [Online]. Available: <https://www.sciencedirect.com/science/article/pii/S2352484720315274>
- [56] South African Grid Code Secretariat, "Grid connection code for renewable power plants (rpps) connected to the electricity transmission system (ts) or the distribution system (ds) in south africa," National Energy Regulator of South Africa (NERSA), Tech. Rep., January 2022, administered by the SA Grid Code Secretariat. Contact: Mr. T. Mchunu, System Operator, Eskom Transmission Division, P.O Box 103, Germiston 1400, South Africa. Tel: +27 (0)11 871 3076. Email: mchunut@eskom.co.za. [Online]. Available: <https://www.sseg.org.za/grid-connection-code-for-renewable-power-plants-connected-to-the-electricity-transmission-system-or-the-distributi>
- [57] G. Van den Broeck, J. Stuyts, and J. Driesen, "A critical review of power quality standards and definitions applied to dc microgrids," *Applied Energy*, vol. 229, pp. 281–288, 2018. [Online]. Available: <https://www.sciencedirect.com/science/article/pii/S0306261918310869>

- [58] S. Mischos, E. Dalagdi, and D. Vrakas, “Intelligent energy management systems: a review,” *Artificial Intelligence Review*, vol. 56, pp. 11635–11674, 2023. [Online]. Available: <https://doi.org/10.1007/s10462-023-10441-3>
- [59] A. Sadollah, *Introductory Chapter: Which Membership Function is Appropriate in Fuzzy System?*, 10 2018.
- [60] M. Rodriguez, D. Arcos-Aviles, and F. Guinjoan, “Simple fuzzy logic-based energy management for power exchange in isolated multi-microgrid systems: A case study in a remote community in the amazon region of ecuador,” *Applied Energy*, vol. 357, p. 122522, 2024. [Online]. Available: <https://www.sciencedirect.com/science/article/pii/S030626192301886X>
- [61] M. A. Alghassab, “Fuzzy-based smart energy management system for residential buildings in saudi arabia: A comparative study,” *Energy Reports*, vol. 11, pp. 1212–1224, 2024. [Online]. Available: <https://www.sciencedirect.com/science/article/pii/S2352484723016311>
- [62] A. Chojecki, M. Rodak, A. Ambroziak, and P. Borkowski, “Energy management system for residential buildings based on fuzzy logic: design and implementation in smart-meter,” *IET Smart Grid*, vol. 3, no. 2, pp. 254–266, 2020. [Online]. Available: <https://ietresearch.onlinelibrary.wiley.com/doi/full/10.1049/iet-stg.2019.0005>
- [63] E. Q. M. Julin, V. Subramanian, V. Bereznychenko, and R. Narayananamoorthi, “Cognitive fuzzy logic-integrated energy management for self-sustaining hybrid renewable microgrids,” *Scientific Reports*, vol. 15, no. 1, p. 9915, 2025. [Online]. Available: <https://doi.org/10.1038/s41598-025-94077-z>
- [64] E. Nivolianiti, Y. L. Karnavas, and J.-F. Charpentier, “Fuzzy logic-based energy management strategy for hybrid fuel cell electric ship power and propulsion system,” *Journal of Marine Science and Engineering*, vol. 12, no. 10, 2024. [Online]. Available: <https://www.mdpi.com/2077-1312/12/10/1813>
- [65] J. LeSage, “Microgrid energy management system (ems) using optimization,” <https://github.com/jonlesage/Microgrid-EMS-Optimization/releases/tag/v19.1.0>, 2025, retrieved April 6, 2025.

Appendix A

AI Prompts Documentation

Citation and Reference Check

- **Tool used:** DeepSeek
- **Purpose:** To verify citation, formating and completeness according to IEEE standard.
- **Prompt used:**

Review my citations and references as per the IEEE standard. Also check for completeness in the reference section.

Figure A.1: Snippet of the prompt used.

Latex figures and table formatting

- **Tool used:** DeepSeek
- **Purpose:** To ensure the figures and tables I used stay where they are originally placed.
- **Prompt used:**

The figures and tables don't stay in the place I originally put them in when running the document in latex, which command can i use to fix this

Figure A.2: Snippet of the prompt used.

Appendix B

Ethics Clearance



PRE-SCREENING QUESTIONNAIRE OUTCOME LETTER

STU-EBE-2025-PSQ001550

2025/04/07

Dear Ntokozo Radebe,

Your Ethics pre-screening questionnaire (PSQ) has been evaluated by your departmental ethics representative. Based on the information supplied in your PSQ, it has been determined that you do not need to make a full ethics application for the research project in question.

You may proceed with your research project titled:

Intelligent Energy Management System for a Hybrid Microgrid with Renewables and Battery Storage

Please note that should aspect(s) of your current project change, you should submit a new PSQ in order to determine whether the changed aspects increase the ethical risks of your project. It may be the case that project changes could require a full ethics application and review process.

Regards,

Faculty Research Ethics Committee

Figure B.1: Ethics clearance outcome.

Appendix C

Methodology Additional Content

Link to the [github](#) repo for simulation files.

C.1 Data Collections and Preparation

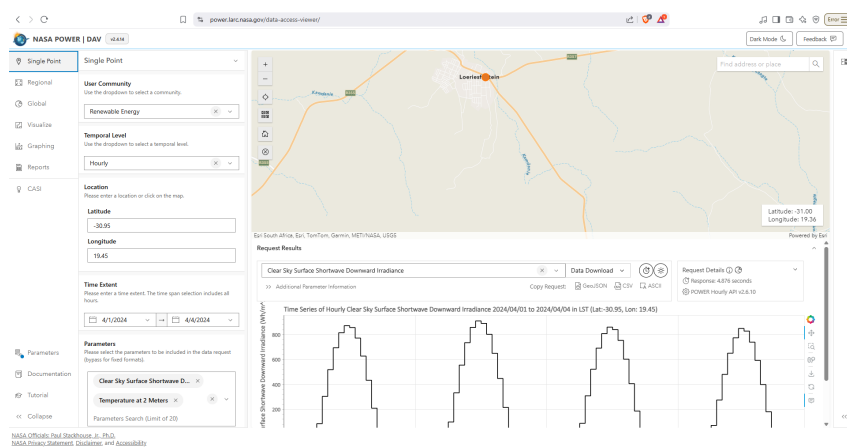


Figure C.1: NASA data viewer website.

C.2 Microgrid Component Sizing

C.2.1 Load Data

This was the original load data.

Table C.1: Original load data from [section 3.2](#)

Time	Power [kW]
00:00	189,4289
01:00	187,1185
02:00	187,3415
03:00	189,985
04:00	198,6374
05:00	207,3186
06:00	217,7941
07:00	226,5231
08:00	189,4289
09:00	187,1185
10:00	187,3415
11:00	189,985
12:00	198,6374
13:00	207,3186
14:00	217,7941
15:00	226,5231
16:00	189,4289
17:00	187,1185
18:00	187,3415
19:00	189,985
20:00	198,6374
21:00	207,3186
22:00	217,7941
23:00	226,5231

C.2.2 Solar PV Data

This was the original PV data.

Table C.2: Original PV data from section 3.2

Time	PV Power [kW]	Irradiance [W/m ²]	Temperature [°C]
00:00	0	0	14,89
01:00	0	0	14,62
02:00	0	0	14,28
03:00	0	0	13,99
04:00	0	0	13,75
05:00	0	0	13,47
06:00	0,005327	84,47	13,78
07:00	0,208969	303,83	15,52
08:00	0,737112	518,6	17,93
09:00	1,142367	694,95	20,25
10:00	1,476158	815,55	22,41
11:00	1,529217	872,67	24,32
12:00	1,498532	857,55	25,62
13:00	1,45999	772,83	26,16
14:00	1,386243	627,97	25,86
15:00	1,143442	433,75	24,81
16:00	0,779349	208,95	23
17:00	0,35168	20,3	20,38
18:00	0,019597	0	18,26
19:00	0	0	16,66
20:00	0	0	15,23
21:00	0	0	13,99
22:00	0	0	12,97
23:00	0	0	12,09

C.3 FLC Design

C.3.1 Membership Function

An essential component of FLC design is the membership function, which defines how each input is mapped to a degree of membership within a fuzzy set. One of the most commonly used types is the triangular membership function due to its simplicity and ease of computation [7]. As shown in Figure C.2, this function is characterized by three parameters: a , b , and c , where $a < b < c$. Parameters a and c represent the start and end points of the triangle's base, while b corresponds to the peak value where the membership degree is 1.

The triangular membership function can be symmetric or asymmetric, and its shape defines how input values are fuzzified. It is mathematically expressed as:

$$\mu_{\text{triangular}}(x) = \max \left(\min \left(\frac{x-a}{b-a}, \frac{c-x}{c-b} \right), 0 \right) \quad (\text{C.1})$$

Figure C.2 illustrates a symmetric triangular membership function for the set Medium SOC with $a = 30$, $b = 50$, and $c = 70$. For instance, to determine the degree of membership for $x = 40$, the following steps are used:

$$\begin{aligned} \mu_{\text{triangular}}(20) &= \max \left(\min \left(\frac{40-30}{50-30}, \frac{70-40}{70-50} \right), 0 \right) \\ &= \max \left(\min \left(\frac{10}{20}, \frac{30}{20} \right), 0 \right) \\ &= \max (\min (0.5, 1.5), 0) \\ &= \max (0.5, 0) = 0.5 \end{aligned}$$

This approach allows for a gradual transition between membership levels, which is essential for managing the uncertainty and imprecision in real-world systems.

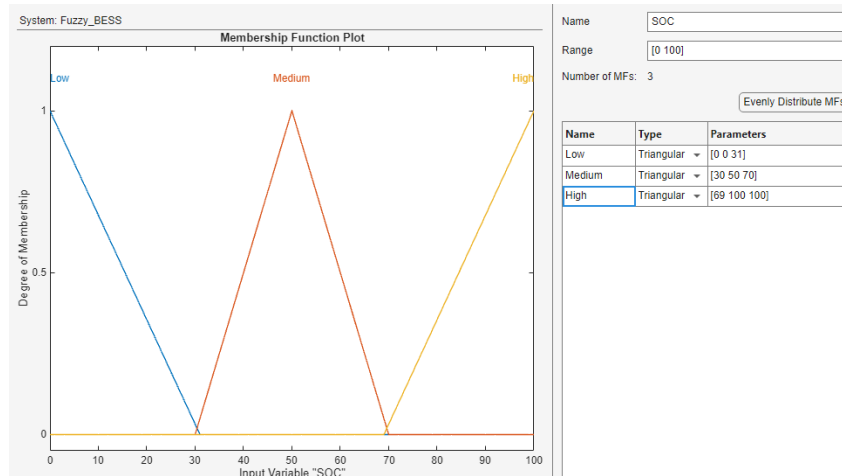


Figure C.2: A triangular membership function.

Appendix D

Results Additional Content

D.1 Cost of Energy Calculations

Figure D.1 is the implemented MATLAB function used to calculate the cost of energy from the grid.

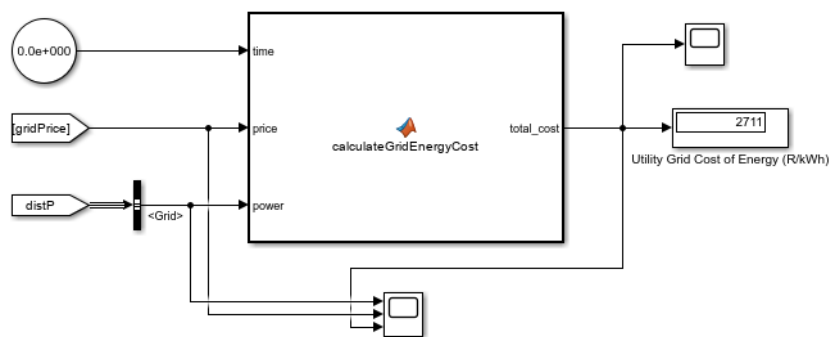


Figure D.1: Matlab function implementation for cost of energy calculations.

Figure D.2 is the code sample used to determine the cost of energy from the grid.

D.2 Case 4: Operation Mode Selection on a TOU tariff with Varying Load and Constant Load

Figure D.3 shows the switching command of at the point of common coupling (PCC) for case 4.

Figure D.4 is the zoomed in plot of Figure 4.20, showing the grid power profile ripples due to being on, but not importing any power.

Figure D.5 shows the load profile of the total load and the shed load.

Figure D.6 shows the Simulink blocks used to calculate the shed load.

```

function total_cost = calculateGridEnergyCost(time, price, power)
% Inputs:
%   time - Current simulation time (s)
%   price - Current electricity price ($/kWh)
%   power - Current grid import power (kW) (positive = importing)

% Output:
%   total_cost - Running total of energy costs ($)

persistent cumulative_cost;
persistent last_time;

% Initialize
if isempty(cumulative_cost)
    cumulative_cost = 0;
    last_time = 0;
end

% Calculate time step in hours
dt = (time - last_time)/3600;

% Only calculate if time has advanced
if dt > 0
    % Cost = power (kW) * time (h) * price (R/kWh)
    % Only count positive power (importing)
    if power > 0
        cumulative_cost = cumulative_cost + power * dt * price;
    end
end

% Update time for next step
last_time = time;

% Output the total
total_cost = cumulative_cost;
end

```

Figure D.2: Cost of energy code snippet.

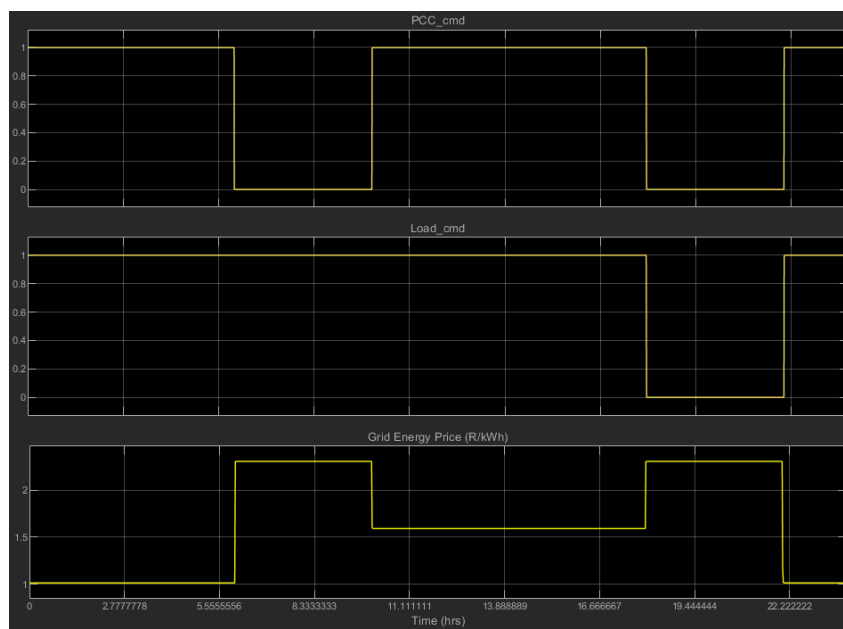


Figure D.3: PCC and load switching signals.

D.2. Case 4: Operation Mode Selection on a TOU tariff with Varying Load and Constant Load

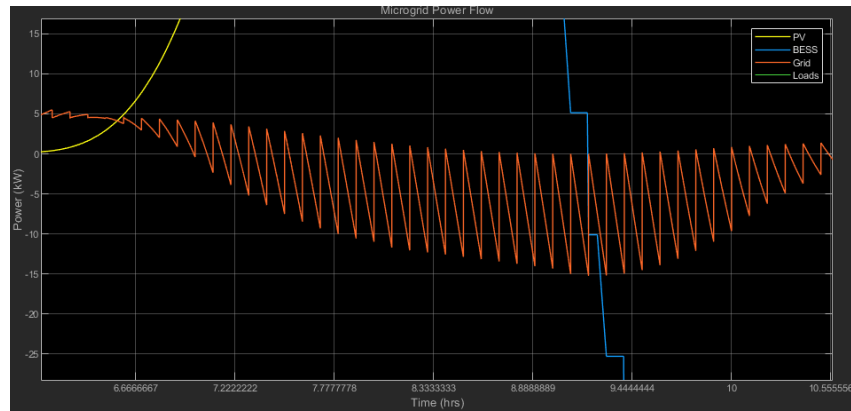


Figure D.4: Utility grid power profile ripples.

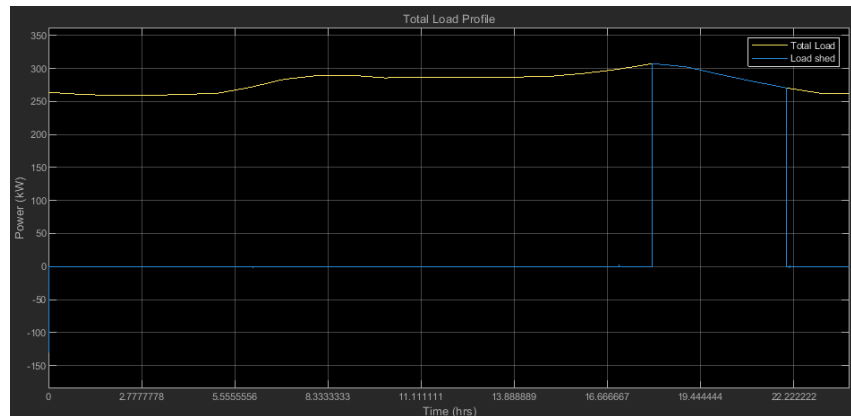


Figure D.5: Total load and shed load profile.

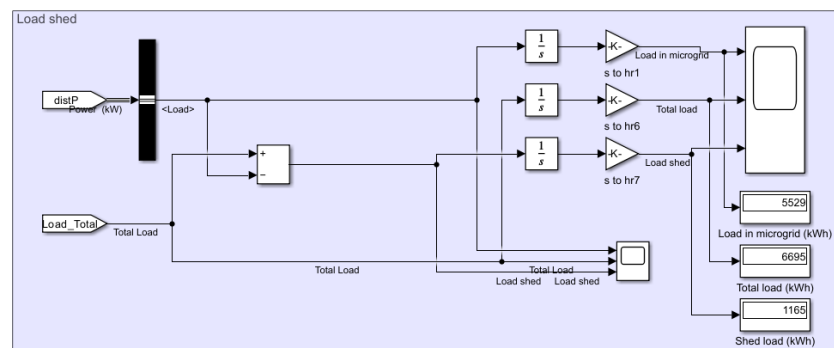


Figure D.6: Load shed calculations.

Appendix E

GA Table

Table E.1: GA tracking table

GA	Requirement	Justification and section in the report
1	Problem-solving	Problem-solving is demonstrated in chapter 3 . The main focus of this project is developing an intelligent energy management system for a microgrid. To do achieve this, research was conducted to decide on an intelligent algorithm/controller to design. Furthermore, an understanding was required to model a microgrid in which the intelligent energy management system was going to be tested on.
4	Investigations, experiments and data analysis	The investigations were proposed in chapter 3 , and experiments were presented in chapter 4 . The experiments in a form of simulations were conducted to model real-world parameters, and standards were used to verify the design of the intelligent energy management system. Data analysis if found in chapter 4 , were plots are evaluated and conclusions are drawn from the based on analysis of calculations and plots.
5	Use of engineering tools	The use of engineering tools is presented in chapter 3 and chapter 4 . MATLAB Simulink was the simulation tool of choice after a detailed research on the available simulation tools available.
6	Professional and technical communication (Long report)	The extensive research about the topic investigated was presented in a format that can be understood by both engineering professionals and other non-technical audience, this is evident in chapter 2 . The report was written according to the academic and professional standard. It utilized technical language for in-depth analysis, and provided visual aids to explain processes for better understanding. This is evident in chapter 3
8	Individual work	The research was carried out independently throughout the entire project. Additional help was requested through the approval of the supervisor. Online resources such as databases including IEEE, Science Direct and Research Gate were consulted for additional input and were cited accordingly. Progress was monitored by the supervisor and updates were communicated with the supervisor to ensure timely completion of the project. Individual work was maintained in chapter 1 , chapter 2 , chapter 3 , chapter 4 , and chapter 6 .
9	Independent learning ability	Independent learning was demonstrated in chapter 3 , where engineering principles of design were applied to develop the intelligent algorithm, the Fuzzy Logic Controller. Further independent learning was demonstrated in performing simulations in MATLAB Simulink, using self-taught knowledge and online boot camp learning. Complex processes involving creating subsystems in MATLAB Simulink were understood and the process of Fuzzy Inference System was learned by independently by consulting online resources.